UCRL 2560

UNIVERSITY OF CALIFORNIA

Radiation Laboratory

BERKELEY, CALIFORNIA

UCRL-2560
Unclassified-Chemistry Distribution

UNIVERSITY OF CALIFORNIA

Radiation Laboratory

Contract No. W-7405-eng-48

STUDIES IN THE NUCLEAR CHEMISTRY OF PLUTONIUM, AMERICIUM, AND CURIUM AND THE MASSES OF THE HEAVIEST ELEMENTS

Richard Alois Glass
Thesis

April 20, 1954

Berkeley, California

STUDIES IN THE NUCLEAR CHEMISTRY OF PLUTONIUM, AMERICIUM, AND CURIUM AND THE MASSES OF THE HEAVIEST ELEMENTS

By

Richard Alois Glass
B.S. (University of Notre Dame) 1950

DISSERTATION

Submitted in partial satisfaction of the requirements for the degree of

DOCTOR OF PHILOSOPHY

in

Chemistry

in the

GRADUATE DIVISION

of the

UNIVERSITY OF CALIFORNIA

Approved:

Professor Glenn Theodore Seaborg, Chairman, ...

Assistant Professor Owen Chamberlain, ...

Professor Gerhard Krohn Rollefson. .....

Committee in Charge

Deposited in the University Library. .....
Date Librarian

TABLE OF CONTENTS

TABLE OF CONTENTS (Cont'd)

LIST OF ILLUSTRATIONS

LIST OF ILLUSTRATIONS (Cont'd)

LIST OF ILLUSTRATIONS (Cont'd)

STUDIES IN THE NUCLEAR CHEMISTRY OF PLUTONIUM, AMERICIUM, AND CURIUM AND THE MASSES OF THE HEAVIEST ELEMENTS

Richard Alois Glass
Radiation Laboratory and Department of Chemistry
University of California, Berkeley, California

April 20, 1954

ABSTRACT

Ion exchange column elution methods for the separation of americium and curium using tartrate and lactate solutions have been developed which are superior to citrate elutions. Tartrate elutions are suitable for slow separations and lactate elutions are satisfactory for general use where rapid separations are required.

Fission and spallation products were isolated from Pu^{239} targets which had been bombarded with alpha particles of 21 to 37 Mev energy. Fission yield curves as well as fission and spallation excitation functions are presented and discussed in terms of odd-even and Z^2/A effects. The high cross sections observed for the $(\alpha, 2n)$ and $(\alpha, p2n)$ reactions were surprising results from this investigation. In the course of the Pu^{239} bombardments, studies of the decay schemes of Am^{240}, Cm^{240}, and Cm^{241} were undertaken.

Decay energy and half-life information on all of the trans-mercury nuclides has been collected and systematized. Trends on the energy surface for alpha energies, beta energies, nucleon binding energies, and Bohr-Wheeler parameters are presented. These energy systematics have led to a complete tabulation of the masses of the isotopes of the elements above mercury. Predictions of nuclear properties are included for some isotopes of elements 99 through 103.

STUDIES IN THE NUCLEAR CHEMISTRY OF PLUTONIUM, AMERICIUM, AND CURIUM AND THE MASSES OF THE HEAVIEST ELEMENTS

Richard Alois Glass
Radiation Laboratory and Department of Chemistry
University of California, Berkeley, California

April 20, 1954

I. GENERAL INTRODUCTION

A large number of radioactive nuclides are produced in the bombardments of heavy elements in charged particle accelerators such as the cyclotron. The induced nuclear reactions as well as the products can be studied if the radioactive isotopes of each element are isolated after bombardment. By the counting of radioactivity the amounts of the nuclides produced under a given intensity and duration of bombardment and the cross sections or probabilities of the reactions forming them can be calculated. These in turn allow some conclusions to be drawn about the mechanisms of reaction. At the same time the radioactive decay of the nuclides can also be studied to determine alpha, beta and gamma energies and half-lives. The decay energies can be correlated to give a picture of the energy surface made up of the masses or total energies of all the nuclides. The above two aspects can be considered under the classifications of induced nuclear reactions and spontaneous nuclear reactions. A third, practical aspect, the isolation of the bombardment products, is a problem in radiochemistry; that is, it involves the chemical separations of minute (tracer) quantities of the elements and the detection of their radioactivity. Since the chemical aspect is necessary for the nuclear studies the whole problem becomes one in nuclear chemistry.

The following sections of the present work present data in these three aspects of the study of radioactive isotopes of the heaviest elements. The next section deals with the chemical separation of americium and curium using ion exchange resins and organic chelating agents. Results of this study are employed in the separation of (α, xn) and (α, pxn) products from the bombardments of plutonium for the determination of cross sections described in the third section. The preparation of plutonium targets and the isolation of fission products are further chemical problems related to this study. Excitation functions are presented there for the production of spallation and fission products from low energy, alpha-particle bombardments of Pu^{239}. The fourth section treats decay energy data among the heaviest elements. Decay energies, not only of the isotopes studied in the previous sections, but of all of the elements above mercury, are collected and analyzed for systematic trends and then used to calculate masses and nucleon binding energies of the nuclides. Data from naturally occurring and artificially produced radioactive isotopes are employed. Empirical correlations of half-lives as well as energies are made.

The material from the last two sections can be analyzed in the terms of the statistical model (liquid drop) of the nucleus. For example, the compound nucleus theory can be used to interpret the fission and spallation results from the cross section studies, since the bombarding alpha-particles had less than 50 Mev energy. In addition, the mass equation terms, e.g., volume, surface and coulomb energy, and the derived Bohr-Wheeler parameters referred to in the last section can be used to describe the general trends of the energy surface.

II. CHELATING AGENTS APPLIED TO ION EXCHANGE SEPARATIONS OF AMERICIUM AND CURIUM

A. Introduction

The importance of chelating agents in the cation exchange column separations of the tripositive rare earths and actinides has been firmly established.[1-13] For the rare earths, with the exception of cerium and europium, for which other methods of separation exist, and also for the actinides, americium, curium, berkelium, californium, and elements 99 and 100,[14] ion exchange columns represent a very efficient and rapid method of separation due to the like charges, radii, and in general, chemical properties of the ions. The initial work on the rare earths was performed with the Manhattan Project and was published in 1947.[1-6] The application of buffered citric acid solutions to the actinides was an outgrowth of this work and had proved successful at the time the efforts reported here were initiated.[7-10]

Although the citrate elutions were reasonably satisfactory for the actinides, the separations of americium and curium still resulted in considerable overlap of the peaks. Hence it was desirable to find chelating agents with superior capabilities for these two elements. Equilibrium studies with tartaric and lactic acids had indicated they might give improved separations of the rare earths and therefore actinides.[5] Ethylenediamine tetraacetic acid (EDTA) had also been shown to have strong complexing ability and the capacity to produce large separation factors between alkaline earth ions.[15] With these results as a starting point, an investigation of various chelating agents for the ion exchange column separations of americium and curium was undertaken in the summer of 1950. Equilibrium and/or column

experiments were run with tartaric acid, EDTA, lactic acid, hydracrylic acid, α-alanine, and β-alanine.

The two general considerations involved in the chelation of metallic ions for ion exchange separations are the relative competitions of the resin (absorption) and chelating agent (chelation) for the ions. Both aspects have been given considerable attention in the literature and have been adequately reviewed from time to time.[11-13]

The Dowex-50 cation exchange resin[16] used in the present investigation is a cross-linked polymer to which sulphonic acid groups are attached.

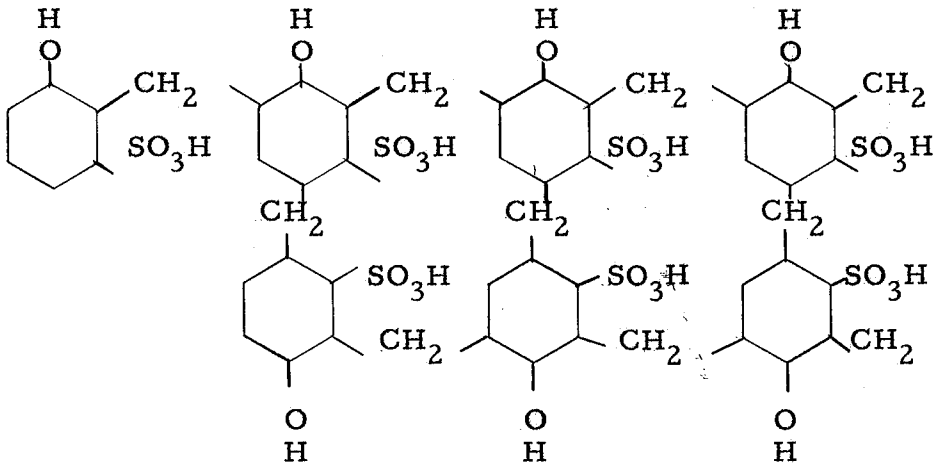

This strong acid resin is available in a number of mesh sizes and crosslinkages. The exchange of charged ions between the resin matrix and external solution can be treated in a number of ways. Mass action, absorption, and Donnan equilibrium formulations have all been used by various investigators. The mass action approach is a logical consequence of the fact that strong acid synthetic cation exchange resins have a definite equivalent weight and stoichiometric exchange properties. Certain investigators, e.g.,

Boyd,[12] are of the opinion that ultimately a quantitative theory of ion exchange will be based on a Gibbs-Donnan equilibrium. The exchange reaction for univalent ions may be written as

$$A^+ + BR = AR + B^+,$$

where R has been taken to represent the structurally bound functional group on the resin. The thermodynamic mass action equilibrium constant is then

$$K = \frac{(a_{B^+})(a_{AR})}{(a_{A^+})(a_{BR})} .$$

The difficulty in using this expression lies in obtaining the activities of the ions in the resin phase. The simplext approximations to these activities are the mole fractions. The expression then becomes

$$K = \frac{(m_{B^+})(\gamma_{B^+})N_{AR}}{(m_{A^+})(\gamma_{A^+})N_{BR}} .$$

It can be seen that important variables introduced by consideration of the resin-solution equilibrium are the concentrations and activity coefficients of both exchanging ions in the solution. It is frequently useful to keep the ion under investigation in low concentration and hold the ionic strength of the solution phase constant with a salt of the ion other than the one whose equilibrium is being studied.

A useful equilibrium parameter for correlating the tendencies of ions to hold onto the resin phase is the distribution coefficient (Kd), which is the ratio of the concentration of an ion in the resin phase to the concentration in the solution phase expressed in any convenient concentration units.

$$Kd \propto \frac{(m)_R}{(m)_S} \propto \frac{N_R}{(m)_S} \propto \frac{(c/m/g)R}{(c/m/cc)S}.$$

The ratio of the Kd's of two ions is called the separation factor between the ions and is symbolized by α. Hence,

$$\alpha_{Am-Cm} = \frac{Kd_{Am}}{Kd_{Cm}}.$$

It is useful to define a new separation factor which emphasizes percentage Kd differences as

$$\alpha'_{Am-Cm} = \frac{Kd_{Am} - Kd_{Cm}}{Kd_{Cm}} \times 100.$$

A large part of the effort in ion exchange separations is applied to the improving of separation factors.

The equilibrium in the direction of the resin phase for a particular ion is greatly influenced by the charge and hydrated radius of the ion. Ions with the greater charge and the smaller hydrated radii are usually preferentially absorbed on the resin. For example, typical lyotropic series are

$$Pm > Sm > Eu > Gd > Tb > Dy > Ho$$

$$Pu > Am > Cm > Bk > Cf > 99 > 100.$$

The second general aspect of the problem concerns the metal chelates. Chelating agents are usually organic molecules or ions capable of forming two or more bonds with a single ion, thus forming a ring structure. The terms bidentate, tridentate, and so on, are applied to chelating agents with two, three, or more functional groups. The bonds may be of the ordinary covalent or the coordinate covalent type. The most common chelating agents used at present for ion exchange work are the α- and β-hydroxy carboxylic acids and the

α- and β-amino acids. The coordination number of the metal is a guide to the formula of the chelate and in general the most stable configurations are reached when the coordination sphere is filled. Further, assuming that the trivalent rare earth ions complex with three citrate ions in a citric acid solution adjusted with ammonium hydroxide to pH 3,[5] one might by analogy write the formula for the Am^{+3} citrate chelate as

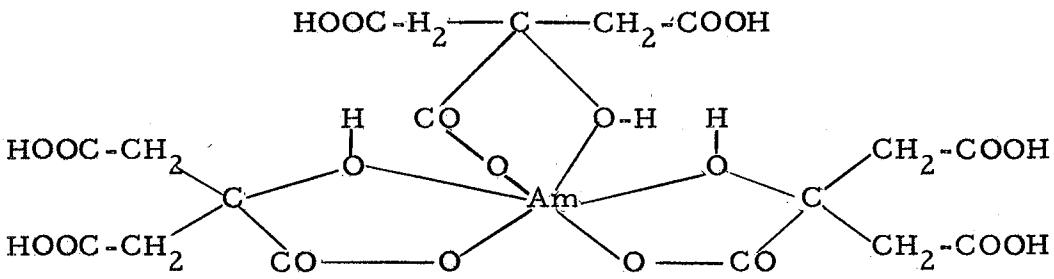

where a coordination number of six has been used for Am^{+3}. Thus each citrate ion would form a bidentate chelate with Am^{+3}. It has been found that metal chelates formed with five- and six-member rings are the most stable.[13] The Am^{+3} chelate represented above contains three five-membered rings.

The stability constant for the metal chelates may be written as

$$K = \frac{(MKe_x)}{(M)\,(Ke)^x}$$

for the reaction

$$M + XKe \rightleftarrows MKe_x.$$

The stability constants for a given lyotropic series vary with the inverse of the non-hydrated radius;[12] the stronger complexes being formed with cations with smaller non-hydrated radii. The tripositive rare earth and actinide lyotropic series are

Ho > Dy > Tb > Gd > Eu > Sm > Pm

100 > 99 > Cf > Bk > Cm > Am > Pu.

Thus, it can be seen that the series are in the reverse order of the resin binding series and consequently differences among the rare earth and actinide elements are enhanced when chelating agents are used to elute them. Since most of the chelating agents are weak acids with acid dissociation constants in range 10^{-3} to 10^{-5} the amount of chelating ion present will be dependent on the hydrogen ion concentration of the solution, so that the pH of the solution becomes another important variable.

The foregoing description has outlined some of the variables and considerations in the equilibria involved. When these factors are applied to chromatrographic elution another factor must be considered; namely, the rate of exchange of the ions. A kinetic analysis of ion exchange reveals that two factors are important in the rate of exchange; the diffusion of the ions in the resin gel and the actual exchange of the ions. It is now recognized that usually the most important rate controlling factor is the diffusion process.[12] Mayer and Tompkins[6] have developed a "plate" theory in ion exchange column separations by analogy to distillation columns in which they treat the elution of an ion as a series of equilibria between the solution and resin phases in a number of theoretical segments or plates in the length of the column. The theory, although based on equilibrium considerations, has been found to describe rare earth column runs and also the actinide runs in the present investigation. On the basis of this theory it might be expected that the efficiency of ion exchange

separations would be improved at elevated temperatures due to the more nearly equilibrium conditions obtained. Such was found to be the case.[6, 9] A large number of the column runs reported here were run at 87° C.

The plate theory also furnishes a simple relation for applying equilibrium data to ion exchange columns,

$$P = kdF(m/v),$$

where P is the elution peak position of an ion in suitable volume units; F is the "free" liquid volume of the column; Kd is the previously described distribution coefficient and (m/v) is the ratio of the resin weight to the solution volume in the column. If the factor (m/v) is on the order of one, the Kd of an ion is seen to represent the number of free column volumes of solution that must pass through a column before the ion is eluted.

B. Tartaric Acid

1. Equilibrium studies. -- The promethium-europium separation factor with citric acid adjusted with ammonium hydroxide to pH 3.05 and Dowex-50 resin has been reported as 1.45.[5] The same separation factor with tartaric acid adjusted with ammonium hydroxide to pH 2.85 was similarly reported as 1.94. By analogy one might expect tartaric acid to enhance large separation factors among the actinides also.

Tartaric acid has two carboxylic acid groups and hence two dissociation constants.[12] Both the singly and doubly ionized tartrate ions are capable of forming metal chelates as can be seen from the structure of tartaric acid.

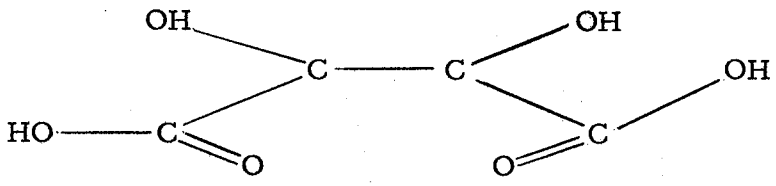

$$K_1 = 1.7 \times 10^{-3},\ K_2 = 9.1 \times 10^{-5}$$

The concentrations of tartaric acid and the two tartrate ions in initially 0.1 molar tartaric acid adjusted with ammonium hydroxide to various pH values are shown in Fig. 1. It can be seen that the singly charged tartrate ion (HT^-) is the most prominent species at pH 3 and the doubly charged ion (T^{--}) is most prominent at pH 5 and 6. A priori one might expect the ion in major abundance to do most of the complexing, however, the stability constants of the chelates formed are undoubtedly quite different, making it hard to arrive at generalizations in this regard.

In order to determine optimum conditions for column runs equilibrium experiments were run with Am^{241} tracer. In each case ten to twenty ml of 0.01 to 0.3 M tartaric acid were adjusted to the desired pH with ammonium hydroxide using a Beckman pH meter and equilibrated at 25° with 0.01 to 0.5 grams of 250-500 mesh Dowex-50 cation exchange resin in the ammonium form. The mixture was shaken for 15 minutes, centrifuged, and the solution phase was assayed for Am^{241} alpha activity. This procedure was repeated until constant assays were obtained. When the assays checked equilibrium was assumed and the distribution coefficient (Kd) calculated. The alpha activity in the resin phase was determined by the difference between the activity at 52 percent geometry added initially and the activity in the solution determined by the solution

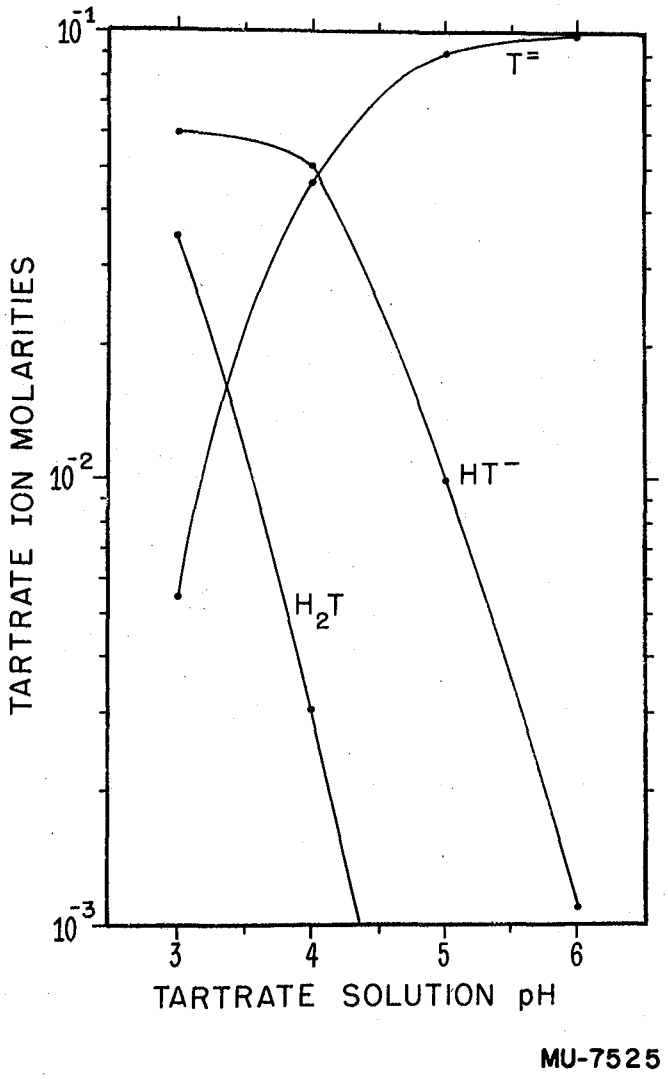

Fig. 1. Calculated tartrate species in 0.1 M tartaric acid adjusted to various pH values.

assays. The Kd values were calculated using the expression

$$Kd = \frac{(c/m)_R}{(c/m)_S} \times \frac{v}{m},$$

where (c/m) terms are alpha counts per minute, R and S refer to the resin and solution phases, and v and m are the volume of solution and mass of the resin.

The static Kd results are presented in Fig. 2. The indeterminant errors from counting statistics and volume measurements resulted in errors on the order of ±20 percent of the Kd values. The theoretical conclusions such as chelate formulas and stability constants that can be drawn from such lines[13] are limited in this case because the ammonium ion concentration resulting from the addition of NH_4OH to adjust the pH plus a small amount to neutralize the tracer added was not carefully determined. Although the Am^{+3}-resin exchange has a third power dependence on ammonium ion concentration the effect is not serious for the purposes of the present investigation since the pH values of the eluting solutions were adjusted with NH_4OH in the same manner as the equilibrium solutions. It may be noted, however, that the slopes of the Kd lines are all about four and one-half. When a correction for the increase of ammonium ion concentration with increase of tartaric acid concentration is applied to the Kd values the lines flatten out to a more reasonable slope of three, indicating that both tartrate species, like the citrate ion,[5] may form MKe_3 chelates. From the relative positions of the lines, the Kd values continuously decreasing with increasing pH, it can be seen that the (T^{--}) ion forms a stronger chelate. With the use of Fig. 2 conditions for suitable elutions of Am^{+3} using tartrate solutions can be determined

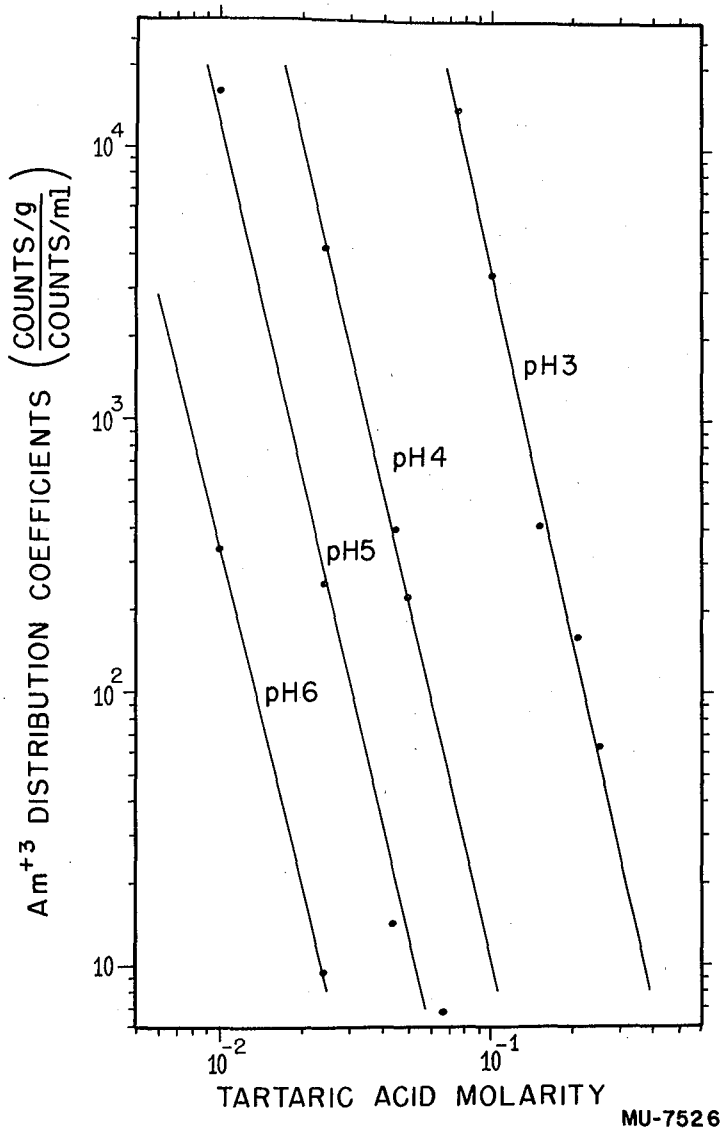

Fig. 2. Equilibrium distribution coefficients of Am^{+3} on Dowex-50 resin in tartaric acid solutions adjusted to various pH values (25° C).

using the simplified relation

Peak volume = Kdx Free Column Volume.

For example, Am^{+3} would be expected to elute after 10 column volumes of 0.1 M, pH 4 tartrate solution passed through the standard 2 mm diameter, 18 cm long Dowex-50 column, since the Kd of Am^{+3} is 10 under these conditions.

Equilibrium measurements were also made at 87° C. Two opposing factors enter in when higher temperatures are used: more tartrate ions are formed at a given tartaric acid concentration and the metal chelates dissociate to a greater extent. The second factor predominates so that Kd values are in general greater at higher temperatures.

The insolubility of ammonium acid tartrate limited the range of concentrations and pH values of tartrate solutions used in the experiments. Attempts to adjust solutions above 0.2 M tartaric acid to pH 3 or 4 resulted in the precipitation of ammonium acid tartrate.

2. Column runs. -- The ion exchange columns used for the separations (similar to columns used for citrate elutions described elsewhere[9,10]) were made by packing 2mm capillary tubing with 17 to 18 cm of 250-500 mesh Dowex-50 resin, from which the fine and coarse particles had been carefully removed. The columns could be operated at 87° or other temperatures by circulating trichloroethylene vapor or other vapors in a surrounding jacket in the standard manner.[9] The flow rates employed varied from 0.15 cm^3/cm^2 min for room temperature runs to 0.6 cm^3/cm^2 min for high temperature runs. In terms of drops this corresponds to one drop per eight minutes and one drop per two minutes, respectively, if the column

volume is assumed to be ca 9 drops. The times for elution of americium and curium ranged from 16 or more hours for the room temperature runs to 3 hours for the fastest high temperature runs. The tracers used were Am^{241}, Cm^{242}, Pm^{147} and $Eu^{152-154}$. The drops from the columns were collected on platinum or stainless steel plates, alpha counted to determine the actinide peaks, and beta counted in a Geiger counter to determine the rare earth peaks. Alpha pulse analyses and beta absorption curves were run where necessary to distinguish the activities.

The first tartrate elutions were run at room temperature using 0.1 M tartaric acid adjusted to pH 4.0 with ammonium hydroxide. A typical column run is shown in Fig. 3. The separation factor (α') between americium and curium, roughly calculated by dividing the distance between the peaks by the distance to the first peak is 30 percent. There is less than 0.2 percent cross contamination in samples corresponding to the total peaks; that is, there is less than 0.2 percent americium alpha activity in the curium peak and less than 0.2 percent curium in the americium peak. These low temperature tartrate elutions apparently represent the best one-step separations of americium and curium yet reported.

A practical difficulty with the low temperature elutions is the slow rate of elution necessary to obtain equilibrium conditions. Column runs that require about 16 hours are obviously impractical for the study of short-lived americium and curium isotopes. For this reason column runs were made at 87^{o} using 0.1 M tartaric acid adjusted to pH 4.3. A typical elution curve is shown in Fig. 4a.

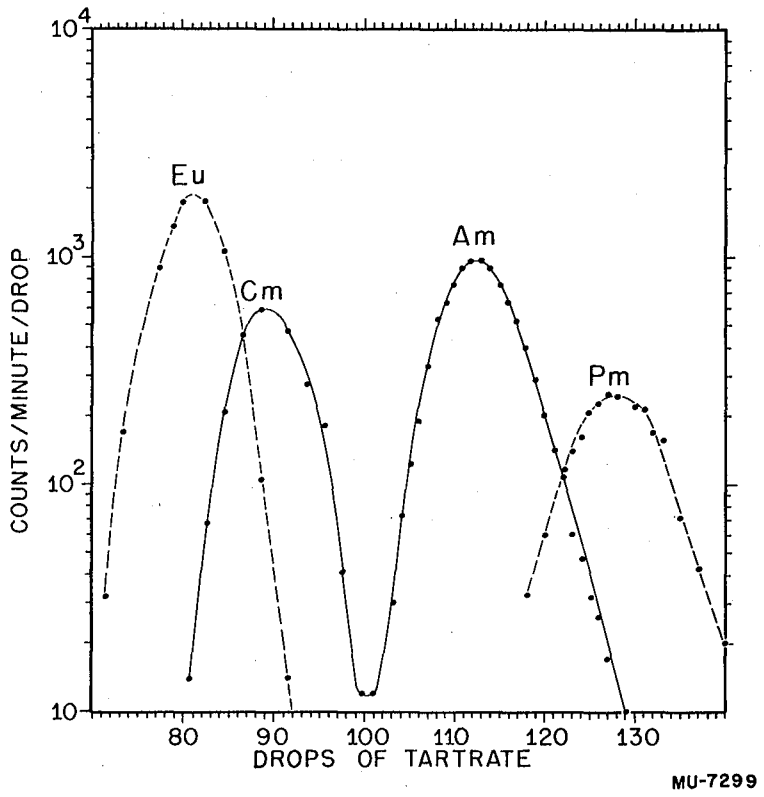

Fig. 3. Tartrate elution of actinide and rare earth elements from a Dowex-50 resin column at room temperature: 0.10 M tartrate, pH 4.0, 1 drop/8 min; separation factors (α' values); Am-Cm = 30 percent; Pm-Eu = 65 percent: ---, beta counting; ——, alpha counting.

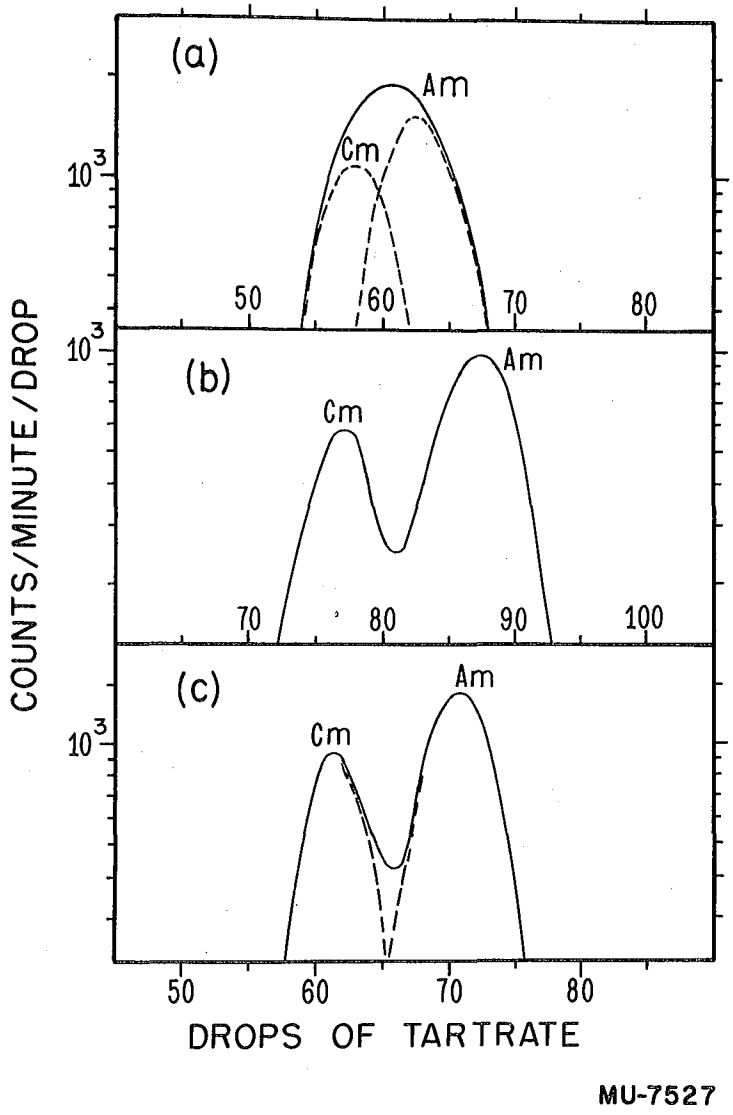

Fig. 4. Tartrate elutions of americium and curium from Dowex-50 resin columns at 87° C: (a) 0.10 M tartrate, pH 4.3, 1 drop/4 min; α'_{Am-Cm} = 8 percent; (b) 0.40 M tartrate, pH 3.2, 1 drop/4 min; α'_{Am-Cm} = 15 percent; (c) 0.79 M tartrate, pH 2.8, 1 drop/3.2 min; α_{Am-Cm} = 19 percent: ---, pulse analysis.

Unfortunately at the higher temperature the large separation factor disappeared, going from 30 percent down to 8 percent. Now, if the separation of americium and curium depends on the singly ionized chelate ion as found to be the case with citrate separations of the rare earths,[5] then steps to insure a large ratio of singly to doubly ionized tartrate ions should improve the separations. For this reason, high temperature elutions were run with higher concentrations of tartaric acid adjusted to lower pH values. The first step was to raise the tartaric acid concentration to 0.4 M and adjust the pH to the lower value of 3.2. Fig. 4b illustrates one of these columns. The average separation factor increased from 8 percent to 14-20 percent. The second step involved increasing the tartaric acid concentration to 0.8 M and adjusting the pH to the still lower value of 2.8. One of the columns run under these conditions is shown in Fig. 4c. The average separation factor again showed an increase, this time up to 19-20 percent; which, however, is still less than the 30 percent separations at low temperature. Further increases in tartaric acid concentration were not practical due to the large amounts of material on the counting plates.

Next an intermediate temperature was tried in the hope that the original large separation factor would be obtained with a faster flow rate. Several columns were run at 60° using 0.4 M tartaric acid adjusted to pH 3.0. A typical column run is shown in Fig. 5a. No appreciable improvement with respect to the higher temperature elutions was observed.

The final attempt at high temperatures was made with a column run at 100° C. It should be noted that for practical purposes a

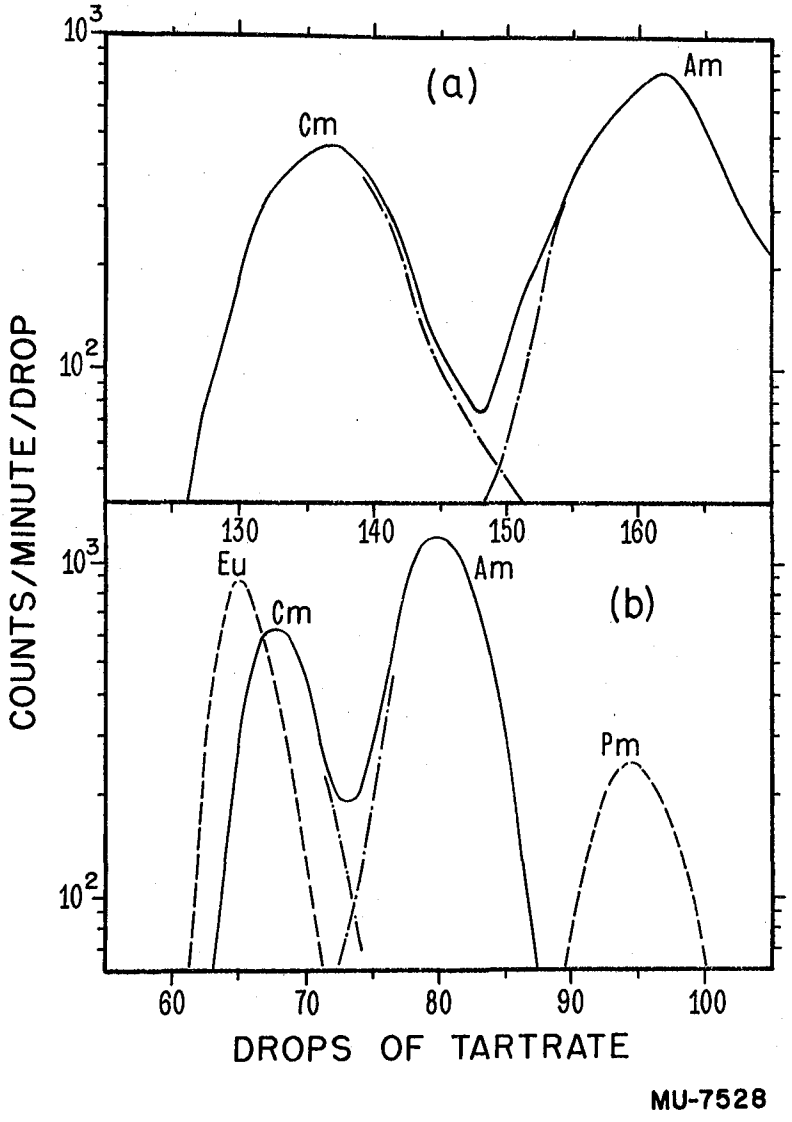

Fig. 5. Tartrate elutions of americium and curium from Dowex-50 resin at 60° C and 100° C: (a) 0.40 M tartrate, pH 3.0, 1 drop/2.5 min, 60° C; $\alpha'_{Am-Cm} = \overline{19}$ percent; (b) 0.41 M tartrate, pH 3.3, 87° C, 1 drop/1.6 min, 100° C; $\alpha'_{Am-Cm} = 20$ percent: -.-.-, pulse analysis.

column run at high temperature resulting in sharp peaks is capable of yielding as good a total separation of americium and curium as one run at a low temperature which results in a larger fractional separation factor and broader peaks. The 100° C column run is shown in Fig. 5b. The americium-curium separation was similar to that obtained in the better runs at 87°.

The conclusions drawn from the tartrate elutions that were run with americium and curium tracer were that excellent slow separations of americium and curium can be obtained using 0.1 M tartaric acid adjusted to pH 4 and separations as good as, if not slightly better than those obtained with citrate can be achieved using 0.4 M tartaric acid adjusted to pH 3.2 and running at 87° C.

Besides the objections of the low solubility of ammonium acid tartrate in what would ordinarily be a good working range and the decrease in separation factors when tartrate elutions are run at high temperature there are two other disadvantages that should be mentioned. The first objection, which is shared with citrate elution, is the sensitivity of the elution positions to pH changes of the solutions used. This is because the relative concentrations of the chelating ions change rapidly with pH in the range studied, so that in general, columns and solutions must be calibrated to predict exact elution positions. The other objection to tartaric acid is noticeable when other than tracer quantities of the actinides and rare earths are eluted. Although citrate elutions are noticeably poorer with other than trace quantities of material, the broadening and overlapping of the peaks with tartrate elutions appears to be even more pronounced.

C. Ethylenediamine Tetraacetic Acid (EDTA)

This very strong chelating agent has found wide usage industrially and in the laboratory in recent years for metal precipitations and columns. The β-amino acid owes its strong chelating ability to the six functional groups in each molecule which are capable of forming three or more five-member chelate rings with each metal ion. The formula and acid dissociation constants for the four hydrogens are as follows:[13] $(HOOCCH_2)_2NCH_2CH_2N(CH_2COOH)_2$, $K_1 = 1.01 \times 10^{-2}$, $K_2 = 2.46 \times 10^{-3}$, $K_3 = 6.90 \times 10^{-7}$, $K_4 = 5.46 \times 10^{-11}$. The chelate formed with Ca^{++} is[13]

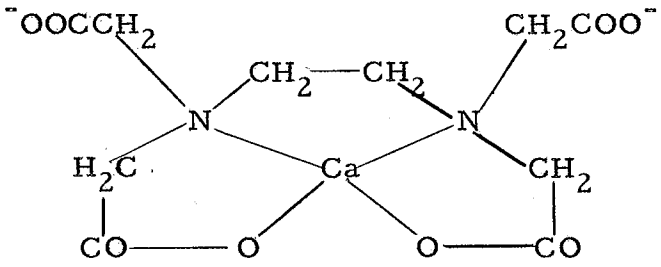

Exploratory equilibrium experiments were run with Dowex-50 at 25° C and 87° C to determine Kd as a function of the concentration and pH of the EDTA solutions. Two experiments were also run at room temperature to determine the rate of approach to equilibrium. In both cases americium tracer was absorbed on the resin and the resin stirred with EDTA solution. Assays of the solution were taken at frequent intervals to observe the increase of americium alpha activity. In both cases the time to reach equilibrium was greater than one-half hour. Thus it appears that the rate of exchange of americium with the chelate is quite slow. The distribution coefficient curves were similar to those for tartaric acid and showed a decrease in Kd with increasing EDTA concentration and pH.

A number of ion exchange column runs were made at 87° using americium and curium tracer. The results were quite striking. Using 0.025 M EDTA, adjusted with ammonium hydroxide to pH 3.2, and a flow rate of 1 drop per four minutes, the americium and curium eluted in one very sharp peak at drop 145 as shown in Fig. 6. The separation of americium and curium activities is essentially zero. Another 87° C elution using 0.0065 M EDTA adjusted to pH 5.6 and a flow rate of 1 drop per 20 minutes showed the same behavior. These two columns were the only ones in which the americium and curium were observed to elute and in these the peaks were considerably further back than predicted on the basis of the Kd data. In contrast, EDTA elutions have recently been reported in the literature indicating separation factors between the light rare earths.[17,18] Thus in the present work it is not obvious that the columns were being run under equilibrium conditions. However, the results are of interest because non-equilibrium conditions usually result in broadened peaks with particularly long tails. No explanation for the observed column behavior is apparent.

D. Investigation of Five- and Six-Membered Chelate Rings

1. Introduction. -- Tartaric acid and EDTA were chosen for study because they were known to have promising chelating properties. After these investigations it was decided that a more fundamental investigation of the chelate structures that promote large separation factors should be undertaken. Thus equilibrium and column experiments were run to determine the chelating characteristics of four simple carboxylic acids; lactic acid, hydracrylic acid,

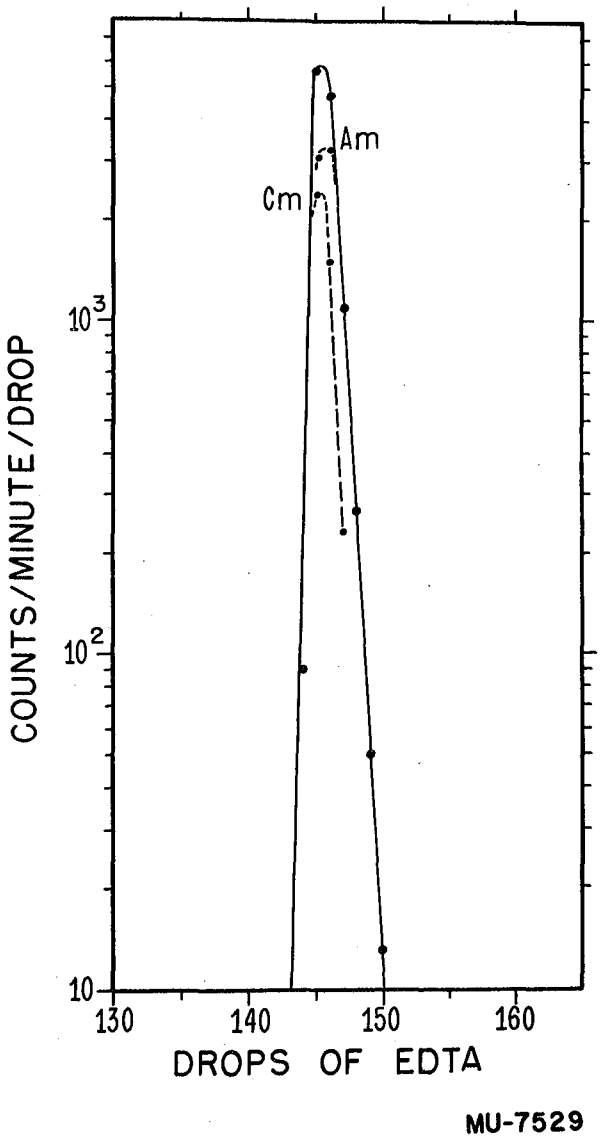

Fig. 6. Ethylenediamine tetraacetate elution of americium and curium from a Dowex-50 resin column: 0.025 M EDTA, pH 3.2, 1 drop/3.5 min, 87° C; ---, pulse analysis.

α-alanine, and β-alanine. The structures and reported acid constants of these chelating agents are

Lactic Acid

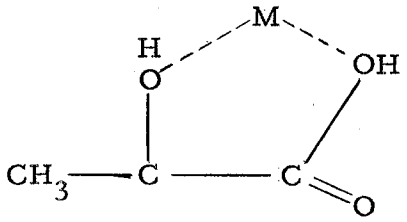

$K = 1.36 \times 10^{-4}$ $(25^{o}$ C$)$[19]

Hydracrylic Acid

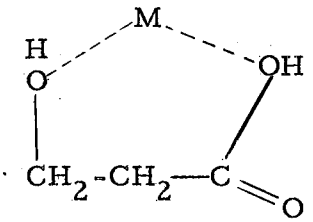

$K = 2.95 \times 10^{-5}$ $(25^{o}$ C$)$[19]

α-alanine

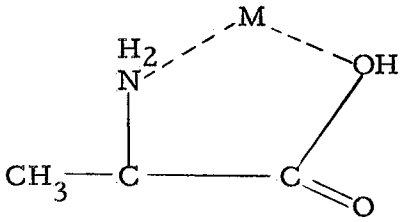

$K_2 = 1.3 \times 10^{-10}$ $(25^{o}$ C$)$[13]

β-alanine

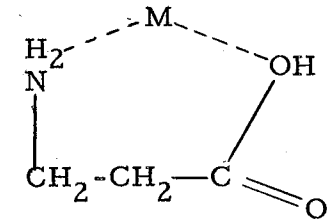

$K = 6 \times 10^{-11}$ $(25^{o}$ C$)$[13]

Unlike citric acid, tartaric acid, and EDTA these simple acids have only one ionizable hydrogen and can form only one five- or six-membered ring. Lactic acid (α-hydroxy propionic acid) and α-alanine (α-amino propionic acid) can only form five-membered chelate rings while hydracrylic acid (β-hydroxy propionic acid) and β-alanine (β-amino propionic acid) can form only six-membered rings.

2. Lactic and hydracrylic acids. -- Distribution coefficients with tracer americium were determined at various acid concentrations and pH values in order to find optimum conditions for column runs, and also to observe which chelating agent formed the strongest complex. The results indicated the lactate ion had considerably

stronger chelating power. For purposes of comparison it will suffice to describe two determinations at pH 4. Simple calculations show that 0.4 M lactate solutions at pH 4 and 0.7 M hydracrylate solutions at pH 4 have about the same dissociated ion concentrations (ca 0.2 M); yet the americium Kd values for these two solutions are quite different.

Chelating Agents	Kd	Ratio
Lactic acid	10	260
Hydracrylic acid	2,600	

Thus, if lactate and hydracrylate ions form the same type of complex, the stability constant for the americium-lactate complex is much larger than the constant for the other chelate.

Although lactate ion was found to form the stronger complexes, it was still not known whether it would yield the greatest americium-curium separation factor. The standard Dowex-50 columns were used to elute americium and curium with lactate solutions at room temperature and 87° C and with hydracrylate solutions at room temperature. The results are shown in Figs. 7 and 8. Although the results aren't definitive, it appears that lactate ion which forms the five-membered ring chelate promotes the larger separation factor.

The americium-curium elution peaks at 87° C using lactate solutions were found to be considerably sharper and also to have slightly larger separation factors than those obtained using citrate solutions. The column elution shown in Fig. 7b resulted in less than 2 percent cross contamination of samples corresponding to the total peaks. Based on these results lactate elutions have recently been used successfully for the separation of the elements americium and

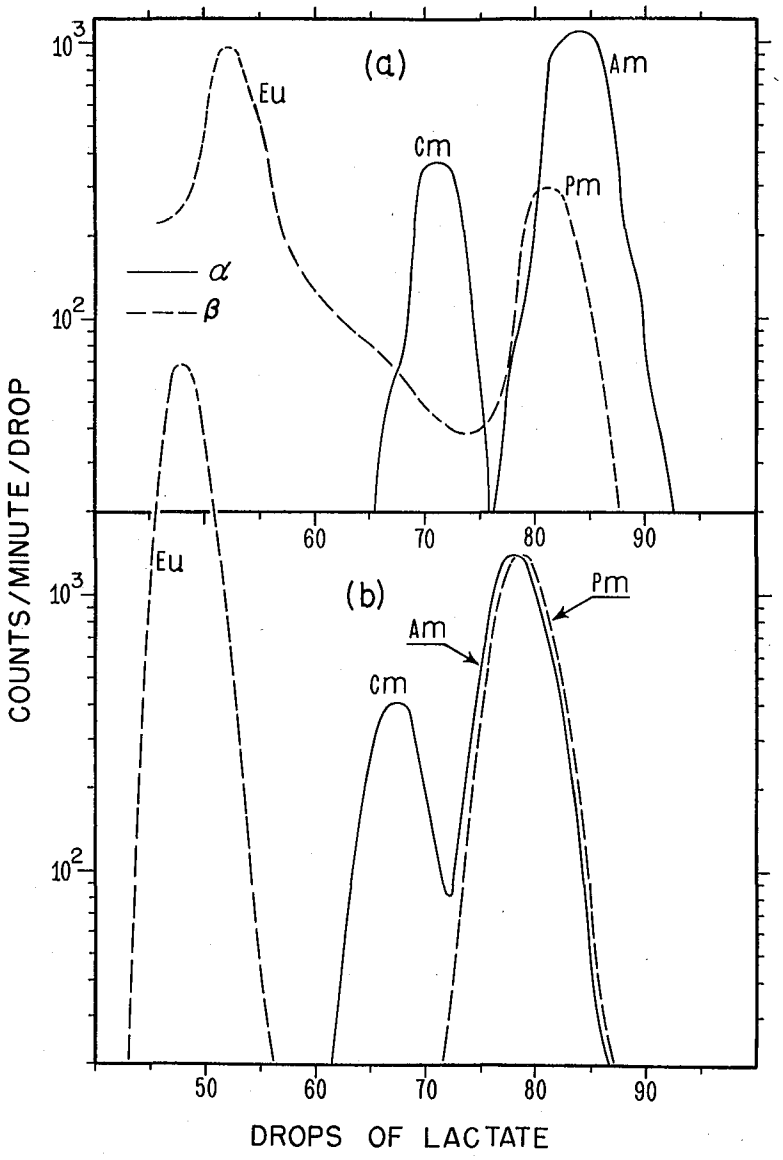

Fig. 7. Lactate elutions of the actinides and rare earth tracers from Dowex-50 resin columns: (a) 0.37 M lactate, pH 4.1, 1 drop/8 min, room temperature; α_{Am-Cm} = 21 percent, α_{Pm-Eu} = 69 percent; (b) 0.40 M lactate, pH 4.6, 1 drop/3 min, 87° C, α_{Am-Cm} = 19 percent; α_{Pm-Eu} = 79 percent: ---, beta counting; ——, alpha counting.

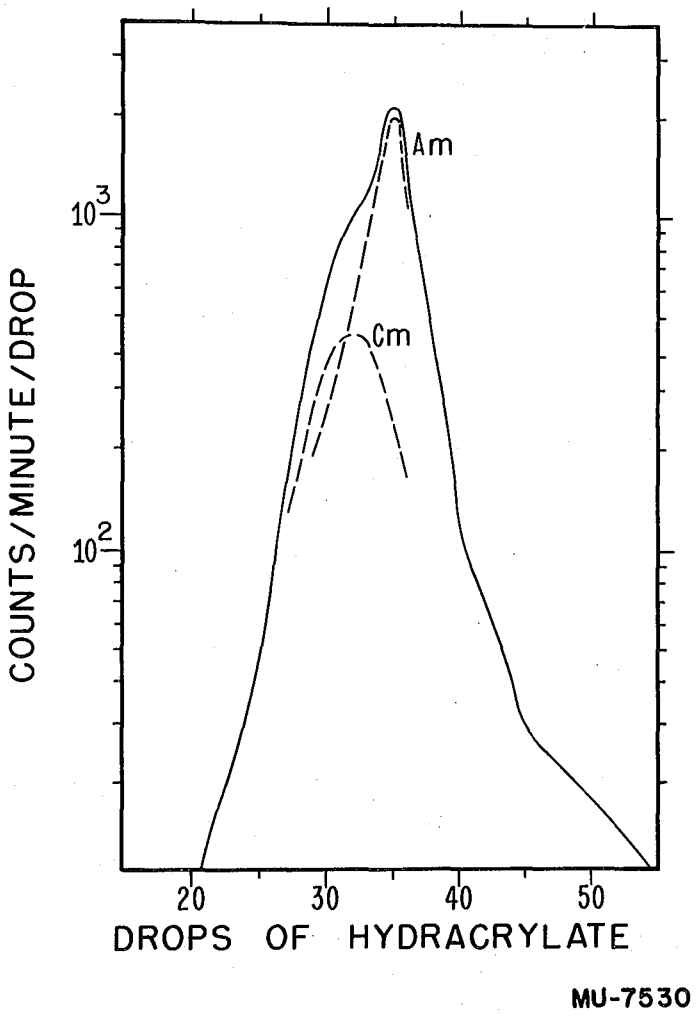

Fig. 8. Hydracrylate elution of americium and curium from a Dowex-50 resin column: 0.7 M hydracrylate, pH 6.0, 1 drop/7 min, room temperature; α_{Am-Cm} = 13 percent: ---, pulse analysis.

above, including the new elements 99 and 100 [14] at the University of California Radiation Laboratory. The advantages of lactate elutions over citrate elutions are the lack of sensitivity to pH changes, the fast rate of elution, and the large separation factors obtained. Recently lactate solutions have been successfully employed for rare earth elutions also.[17, 20]

An interesting result from the chelate elutions run with both actinides and rare earths is the shifting of peaks relative to each other. Using lactate solutions, the rare earths are shifted forward with respect to their relative positions in the tartrate elutions, indicating that lactate ion is complexing them more strongly. A difference in the position of promethium with respect to americium at high and low temperatures is also noted. As might be expected the chelates must have slightly different heats of dissociation.

3. Alpha- and beta-alanine. --Exploratory equilibrium measurements were made with Am^{+3} tracer using the ammonium form of Dowex-50 and one molar solutions of α- and β-alanine in which the pH was varied from about 6 to 10. The results are given in Fig. 9. A decrease in Kd due to chelate formation with β-alanine was not observed. The α-alanine equilibrations, however, indicated a decrease in Kd from pH 6 to pH 10, indicating that chelation was occurring. There is some difficulty in interpreting these data since the first acid dissociation constant of α-alanine is undoubtedly much larger than that of β-alanine; however, it appears to be a reasonable conclusion that α-alanine has a stronger tendency for chelation than β-alanine. Similar results were obtained by Ley[21] using copper. The order of decreasing tendency for chelation which he reported was: glycine,

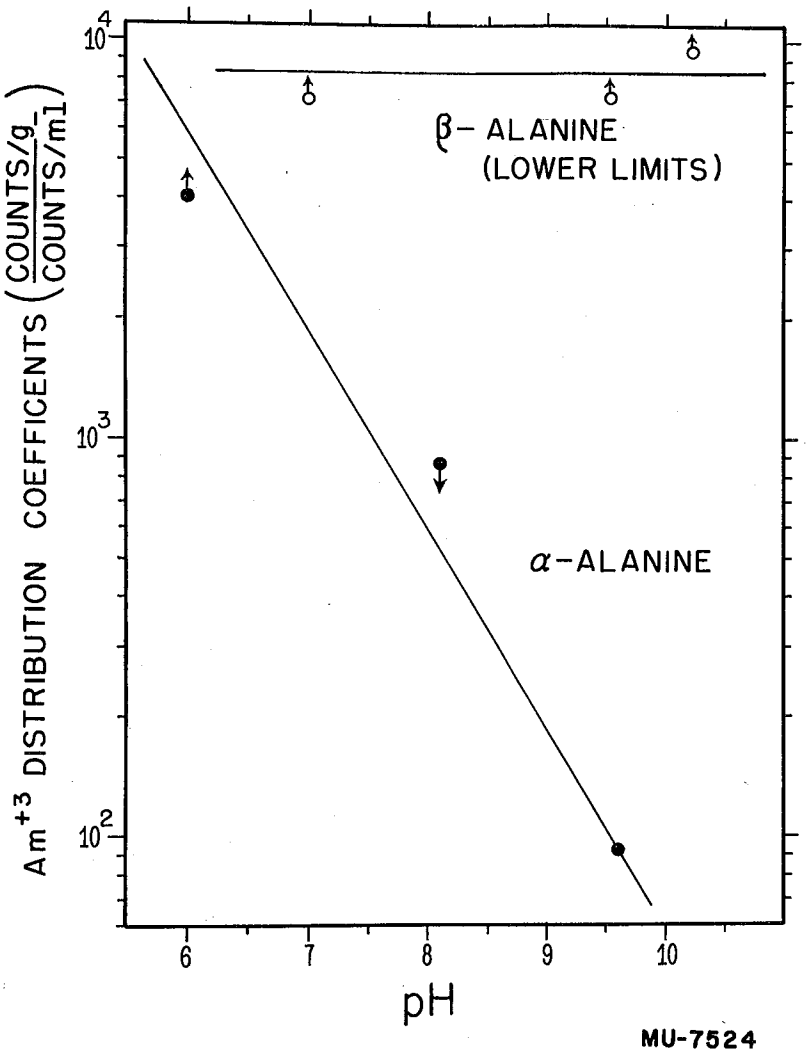

Fig. 9. Distribution coefficients of Am^{+3} on Dowex-50 resin in 1.0 M α- and β-alanine solutions adjusted to various pH values.

α-alanine > β-alanine > γ-aminobutyric acid, = 0.

From this study of five- and six-membered chelate rings it appears that the five-membered ring may form a stronger chelate and also be more effective for the separation of metal ions. On this basis, the favorable chelating properties of tartrate and EDTA are to be expected. It may also be inferred that the chelate ring formed with citrate ions employs the one five-membered ring available, as indicated in the introduction to this section. The conclusions about the stability of the five-membered ring are in accord with the discussion of Martell and Calvin[13] on this subject.

E. Conclusions

Ion exchange separations of americium and curium have shown that lactate elutions are superior to citrate elutions in general performance, and that room temperature tartrate elutions yield the best separations of americium and curium yet reported.

Investigations of five- and six-membered chelate rings indicated that five-membered rings form the stronger chelates and that they also yield better separations in the column adsorption-elution method.

III. FISSION AND SPALLATION COMPETITION IN THE REACTIONS OF Pu^{239} WITH LOW ENERGY ALPHA PARTICLES

A. Introduction

The reaction of nuclei with various bombarding particles can be classified as scattering (elastic and inelastic), capture, spallation, or fission. Spallation refers to reactions in which one or more relatively small particles, e.g., protons, neutrons, and alpha particles, are "boiled off;" and fission, of course, refers to the quite different process in which the nucleus splits into roughly two equal fragments. With particles of greater than thermal energies, since for thermal energy particles de Broglie wave lengths are very important, the sum of the cross sections for the individual reactions is about equal to the geometric cross section of the nucleus, although above 50 Mev the nucleus becomes somewhat "transparent" to the bombarding particles.[1] Consequently, the various reactions can be considered as a competition; that is, a particular type of reaction can only become very prominent at the expense of the other types. Which reaction predominates depends on nuclear properties such as the charge, mass number, and odd-even character of the target nuclei, as well as on the energy of the bombarding particle.

The large number of spallation and fission products including isotopes of many elements that can be produced in a single bombardment makes their study particularly adapted to the techniques of radiochemistry. In the present investigation these techniques were used to isolate spallation and fission products from Pu^{239} which had been bombarded with alpha particles of 20 to 40 Mev energy.

Both the fission and spallation processes have been observed with various bombarding particles (neutrons, heavy charged particles, mesons, and photons) on target nuclei in all parts of the periodic table.[2-4] The reactions can be classified as high or low energy according to the energy of the bombarding particle. Low energy reactions are those caused by particles with less than 50 Mev which can be described in terms of the "liquid drop" model and compound nucleus theory.[5-6] At high energies, above 50 Mev, and especially in the 100 Mev region, the compound nucleus theory breaks down and descriptions such as nucleon-nucleon interactions must be employed.[1] Noticeable changes occur in the character of these reactions with change in bombarding energy and target nucleus. Fission changes from asymmetric to symmetric with increasing energy, accompanied by a broader distribution in fission products and less tendency for redistribution of charge. At the same time, energy requirements for fission to occur increase as the atomic number of the target decreases. Thermal neutron fission occurs in Pu^{239}, U^{235}, and U^{233}, whereas 190 Mev deuterons were used by Goeckermann and Perlman to induce fission in Bi^{209},[7] although in the latter case the threshold is considerably lower. It was proposed that 10-12 neutrons were "evaporated" before fission occurred with the Bi^{209} target. Again, Batzel, Seaborg, and Miller used 340 Mev protons, 190 Mev deuterons, and 190 and 380 Mev alpha particles to produce fission in copper and other medium weight elements.[8, 9] Changes also occur in spallation with change in energy and target material. As the bombarding energy increases products further from the initial nucleus as well as the

intermediate ones are produced, since more particles can be boiled off to dissipate higher excitation energies. In fact, in the bombardments of copper with very high energy particles[9] the spallation and fission products overlap. Changing the atomic number of the target likewise changes the character of spallation. Rudstam, Stevenson, and Folger[10] proposed that protons and neutrons were boiled off with equal probability in the de-excitation of nuclei formed by 340 Mev protons on iron, whereas Goeckermann and Perlman[7] decided that mostly neutrons (at least 10 neutrons to 1 proton) were boiled off with 190 Mev deuterons on bismuth. Hence it appears that coulombic repulsion factors are holding back the emission of protons as the atomic number of the target increases.

The direct study of both fission and spallation in a given target, with the exception of some recent work by Tewes and James on the bombardment of thorium with protons,[11] has been limited to the previously discussed high energy, charged particle reactions. In the region of lower atomic number these high energies are required for fission, and even then the cross sections are small. In addition, the large number of spallation products produced renders the situation quite complicated. On the other hand, in the region around uranium and above, when the particle energies are only 20 Mev above the coulombic barriers fission has become so prominent that its cross section is the same order of magnitude as the geometric. It might be anticipated, therefore, that a favorable place for the study of the competition of fission and spallation would be in the heavy element region with energies in the range between the particle barriers and the point where fission takes over. For example, an

interesting range for the reactions of alpha particles on Pu^{239} is between 20 and 40 Mev. In this range only a few spallation products are possible and the fission cross section is still increasing, so that the picture is still relatively simple, permitting observations to be made on which reactions are being cut out by fission. Since the energy is low the compound nucleus description is still essentially valid.

Some of the previous radiochemical studies of fission have been made by Newton[13] on the products from 37.5 Mev alpha particles on thorium and by Tewes and James[11] on products from 6.7 to 19.5 Mev protons on thorium, who also analyzed for protactinium spallation products. The only previously reported fission yields of Pu^{239} are those for slow and fast neutrons.[2] Few low energy spallation cross sections have been reported for the elements uranium and above; in fact, in order to predict the yields for simple spallation products in this region it is not unusual to refer to similar cross sections on bismuth or thorium. Thus, a valuable outcome of the present study of fission and spallation is the determination of accurate cross sections to aid in the prediction of future bombardment yields.

On the basis of several bombardments of plutonium with deuterons and alpha particles, Street[14] predicted that (α, xn) and (d, xn) cross sections would be low at all energies and tend to be equal in the region from the barrier to 15 Mev above it, because of fission competition. Also, it is to be expected that the odd-even character of the fissioning nucleus as well as the value of the fission ability parameter,[6,15] Z^2/A, will effect the amount burned up in fission. These ideas were the starting point of the present excitation function investigations.

The simple spallation reactions, (α, n), (α, 2n), (α, 3n), (α, p), (α, p2n), and (α, pn), are the only examples outside of the (α, αxn) reactions that are energetically possible below 40 Mev. In the present work yields from the first five of these reactions, as well as the fission yield curves were determined for 37, 33, 28, and 21 Mev alpha particles on Pu^{239}.

B. Bombardment Assembly

1. Monitoring equipment. -- Since careful monitoring of the beam was necessary for the determination of absolute cross sections, the target assembly used for the plutonium bombardments was of the interceptor type[16] commonly used with the Crocker Laboratory 60-inch cyclotron. Inside the assembly the beam encounters three sections: front collimator, duralumin foils, and finally target holder (pistol grip). Essentially all of the entering beam strikes the water cooled target plate. Theoretically three currents (beams) can be measured with integrators, corresponding to the three parts of the assembly. Although the collimator and duralumin foils are generally insulated from each other, in the more recent assemblies the foils and target holder are electrically connected, so that only two currents can be measured.

Two modifications to the previous interceptor were made: the lip of the target holder was lengthened to make the target holder more nearly a Faraday cup, and the target holder was insulated from the foils to allow separate currents to be measured on these two parts. The first modification was an added precaution to prevent secondary electrons from leaving the target and hence causing an

addition to the positive current measured on the target when the target holder and foils were insulated. The lip was lengthened from 1/8 to 1/2 inch. In the 10,000 gauss fringe field of the cyclotron these lengths (radii) will stop particles of 1 and 15 Mev, respectively, from escaping. A simple classical calculation shows that the maximum energy a 40 Mev alpha particle can transfer to an electron by head on collision is 22 kev. Consequently, electrons that get by the lip must come from some other process. Secondary electrons from fission gamma rays can reach several Mev in energy, so they would be stopped only by the longer lip, but no other possibilities were apparent.

Insulation of the target holder from the foils was done because it was feared that there might be some current leakage down the beam path from the foils to the collimator which would add or subtract from the positive target current. However, there was always the additional possibility of leakage from the target to the foils, so for this reason the matter of insulating the target and foils or not depended on which leakage current was more prominent. The objective was to obtain a measurable charge (by current) for each alpha particle striking the target, and hence no migration of charge to or from the target or electrically connected parts could be tolerated. Now, the space between collimator and foils was at the cyclotron tank vacuum of 2×10^{-5} mm Hg, and the space between the foils and target was connected to an external vacuum tank with an air pressure of one to 10 mm Hg. Preliminary investigations by a group from the North American Aviation Company[17] indicated that leakage currents rise rapidly with increasing pressure, as might be expected due to more

ionizable gas being present. Thus, it appeared that the leakage current should be more prominent between the target and foils, so that the foils' current should be combined with the target current, either by adding separate currents or by having the parts electrically connected and measuring one current. At any rate, the target was insulated so that all three currents could be measured: collimator, foils, and target. In the course of the bombardments, negative currents from 10 to 40 percent of the positive target currents were observed on the foils, indicating that negative ions were collecting there. The currents tended to be large when the target-foils vacuum was poor. The conclusion was drawn that the foil currents were due to ionization in the partial vacuum between target and foils as expected, and therefore this current was subtracted from the target current to obtain the true current on the plutonium target.

The bombardments with the modified interceptor indicated that a previously used interceptor with the connected foils and target holder and short lip is probably satisfactory for ordinary cross section work.

Another precaution taken was to insure that all of the beam struck the target and not part on the lip. Such beam would be recorded as target beam without having gone through the target. To insure proper centering, preliminary beam patterns were obtained on Scotch tape placed in the target position. The large and small collimators currently used gave beam patterns of about 1.4 and 0.6 cm diameter, respectively, compared with the 1.5 cm diameter of the target disk. The large collimator usually allowed some beam to strike the lip;

but on the other hand, the small collimator admitted only about one-fifth as much beam through. For this reason the small collimator was reamed out to a diameter just between the diameter of the small and large collimators. The resultant beam patterns of about 1 cm diameter were considered satisfactory. Beam patterns were run before each bombardment to insure that the beam was hitting the target.

The beam integrators recorded the total beam striking the target. This integrated current was then used in the cross section formula for the case where all of the beam hits target:

$$N = \sigma \frac{n}{cm^2} (It),$$

where N is the number of atoms formed, σ is the cross section in cm^2 per atom, n/cm^2 is the number of target atoms per cm^2, and It is the total number of alpha particles that struck the target (number/sec x sec). The integrators of the cyclotron can be calibrated to a precision of greater than 0.1 percent with a reliability (accuracy) of about three percent.[18]

Besides the amount of the beam obtained, its energy is very important. The energy of the alpha beam entering the collimator, applicable to all of the bombardments reported here (before slight cyclotron alterations were made in January 1954) was 40 Mev.[17] The loss of energy in the duralumin foils was 1.64 Mev, making the energy of the beam striking the front target foil 38.4 Mev. The uncertainty in the energy, mainly due to changes in the ion source position, reflecting in the deflection of particles after various numbers

of cycles, is about ±0.5 Mev, but may run as high as ±1 Mev.[17]

The final important consideration with respect to the bombardments themselves was the possible deuteron contamination of the beam. It has been the general feeling at this laboratory that deuteron contamination in the 60-inch cyclotron is large, even of the order of 5 percent of the alpha beam. Attempts to find concrete examples of this type of behavior were unsuccessful. In the present bombardments deuteron contamination was undesirable, mainly because it would cause formation of the (α, p2n) product, Am^{240}, in relatively high yield by a (d, n) reaction, resulting in the deduction of too high a cross section for the formation of this nuclide. There are four different pieces of information which helped in the decision on the magnitude of this effect. In the first place, the deuteron content of the alpha beam has been measured by a range method and found to be on the order of one part per million[17] (0.0001 percent). Further evidence can be obtained from the cyclotron focusing curves. It is estimated from these curves that deuteron contamination of the alpha peak is at most several tenths of a percent.[17] During the present bombardments the magnet current was focused on the leading edge of the alpha peak, away from the position of the deuteron peak.

In addition to this information two yield checks on the amount of deuteron contamination were obtained in the present series of bombardments. In one experiment a small amount of bismuth metal was bombarded to determine the amount of Bi^{210} formed by the (d, p) reaction, and not likely from alpha reactions. The bismuth was precipitated as a sulfide, weighed, and beta counted. From the

known integrated beam and with the use of a previously determined excitation function[19] for the reaction $Bi^{209}(d, n)Bi^{210}$ the amount of deuterons in the alpha beam was calculated to be less than one-tenth of a percent. Again the figure is small, even though in this bombardment contamination was likely, since just before the bombardment the cyclotron tank developed a leak, resulting in the formation of ice with some deuterium on the tank walls. The last check was an internal check from the (α, p2n) excitation function. As would be expected for the (α, p2n) reaction, the cross section was high at 37 Mev and decreased sharply with decreasing energy, dropping off before the threshold of about 25 Mev. If a large part of the Am^{240} was formed by deuteron contamination, the yield would continue high down to 21 Mev, the lowest energy used, since the (d, n) reaction has a positive Q value. Using the lower limit of the cross section for the formation of Am^{240} at 25 Mev of ~0.001 mb and assuming a (d, n) cross section of 10 mb on the basis of bismuth data, the simple ratio of the two indicated that the amount of deuterons in the beam was less than 0.01 percent.

The only conclusion that could be drawn from these data was that deuteron contamination was not a significant factor.

2. Target preparation. -- The isotopically pure Pu^{239} used in the bombardments contained only 0.02 atom percent Pu^{240}.[20] Likewise the plutonium was essentially free of Pu^{241} and its undesirable daughter Am^{241}.

In order to obtain accurate cross sections using the previously described target assembly, which was adapted so that all of the beam

hits the target, it was necessary that uniform targets be prepared. A number of techniques are available for preparing thin, uniform films of radioactive material,[21] e.g., evaporation, electrodeposition, and sublimation. However, the deposits from evaporation are not uniform enough for the purposes here and the losses of valuable target material to obtain uniform films by sublimation are too great. Thus a method of electrodeposition was employed.

The two requirements for the material on which the plutonium was to be plated were that it must not become intensely beta-gamma radioactive for appreciable times after the bombardment, and it must be readily dissolvable to recover fission recoils. Aluminum meets the requirements satisfactorily. As long as at least 1 mil aluminum foil (6.86 mg/cm^2) is used above and below the plutonium all of the fission recoils are stopped.[22] Ten mil, 2S aluminum was used as the base plate ("hat").

Considerable experimentation was required before suitable conditions for electrodeposition were determined. No previous methods for the electroplating of 0.2 to 1 mg of plutonium on only 1.2 cm^2 of aluminum (area of "hat") have been reported. At first a method patterned after the electrodeposition of Pu(VI) from potassium hydroxide solution onto platinum[23] was tried. The plating of quantities of plutonium up to 1 mg/cm^2 were reported. In the plating, of course, potassium hydroxide could not be used directly on aluminum because of its amphoteric nature. Therefore the aluminum plates were pre-plated with about 30 mg of nickel prior to the plutonium plating. Attempts to plate more than 0.1 mg of

plutonium on the nickel in 1 M KOH were unsuccessful.

The final, successful method was patterned after the oxalate method described by Hufford and Scott[21] for plating uranium. A plating cell similar to the one illustrated there was used. About 1 mg of plutonium in acid solution was oxidized to Pu(VI) with 1 M sodium bromate. The solution was evaporated to dryness to destroy excess $NaBrO_3$ and the residue was re-dissolved in 1 to 2 ml of 0.4 M ammonium oxalate. A current of 100 to 200 ma (over the 1.23 cm^2 area of aluminum "hat") was maintained with less than 4 volts between a platinum stirring disk (negative electrode) and the aluminum hat. Under these conditions, if the voltage was kept less than 4 volts and the distance between electrodes less than one cm it was found that ordinarily 0.2 to 0.4 mg of plutonium could be plated in one plating. After the plating the hat was washed, dried, and the Pu(IV) hydroxide carefully flamed to convert to the oxide. Successive platings could also be used to build up the amount of plutonium to even greater thicknesses. Scanning of the plates by a narrow slit low geometry alpha scintillation counter[24] showed their uniformity to be a few percent or even better.

Two checks were available on the amount of plutonium on the plate. The weights were determined for the cross section calculations by careful radiometric assaying of the solutions from the dissolving of the target after bombardment. In addition, before bombardment the target plates were alpha counted in low geometry counters. The specific activity of Pu^{239} was employed for the conversion of alpha counting rates to number of atoms was 7.10×10^7 alpha counts per minute per milligram.[25] A rather surprising outcome of the two results was that the amount calculated from the direct counting of the plate and

without absorption corrections was 5 to 10 percent higher than the figure from assay counting.

Before loading the target holder, various aluminum foils were placed on top of the plutonium to degrade the beam to the desired energy. The table below gives the data on the weighed foils used and corresponding energies.

Foil Thickness (mils)	Weight (mg/cm^2)	Energy on target material (Mev)
0	0	38.4
1	6.56	37.2
5	32.6	33.3
9	63.5	28.0
12	79.7	24.8
15 (10 + 5)	98.7	20.6

The energies were calculated from the range-energy curves of Aron, Hoffman, and Williams.[26]

C. Experimental Procedures

1. Chemical separations. -- The isolation of the fission and spallation products from the bombarded target was performed in a sequence of operations on the entire target, rather than on separate aliquots as is customary. This was done because the total yields of the products in the 2 to 10 microampere-hour bombardments were frequently as low as between one and a thousand counts per minute. After the products were crudely separated from the original solution, specific chemical operations were performed to isolate each of the elements according to procedures found in the Meinke[27] and the

Coryell and Sugarman[28] compilations. An added problem in the chemistry was due to aluminum. The front aluminum foil as well as the target hat, making a total of about 130 mg of aluminum, were dissolved with the plutonium to insure that all fission recoils were recovered. Finally, because of the high specific alpha activity of plutonium, the first chemical separations were performed in a completely enclosed box outfitted with rubber gloves.[29]

The chemical yields of the fission products were determined from the yields of stable isotopes (carriers) of the elements added initially, about 10 mg of an element being added for each target. Standardized bromine, strontium, ruthenium, cadmium, iodine, barium, cerium, and europium carrier solutions were used. The separated fission products and carriers were mounted in their final chemical form on aluminum hats, weighed, zapon coated, and their beta decay followed on shelf two of a standard Geiger-Müller counter. At the same time, the chemical yields of the americium and curium isotopes were determined from the yields of the long-lived Am^{243} and Cm^{244} tracers (not produced in the bombardment) added initially. In this case the drops from the final lactate column were collected on platinum plates, pulse analyzed, and counted in the nucleometer (see the section on counting instruments) to determine amounts of the various activities.

The chemical procedures employed are outlined below. The time for the whole procedure was about 15 hours.

Dissolution of target. -- Since plutonium dioxide tends to be very refractory this step was frequently quite time consuming. Two

methods were used. Ordinarily the target (plus aluminum) was treated with hydrochloric and nitric acids. After the aluminum was dissolved, heating at 80° C for about one hour with 6 M HNO_3 and 0.01 M HF helped effect dissolution. When bromine and iodine were to be taken out, reducing conditions had to be insured. In these cases the target was dissolved in perchloric acid (for later ruthenium distillation) plus a little hydrofluoric acid with prolonged heating. After dissolution, the assays for plutonium were taken. These were given several stages of dilution before alpha counting.

Distillation of fission products. --This procedure was necessary only when iodine, bromine, and ruthenium were to be taken out. The dissolved target was transferred to a glass distilling flask. Nitric acid was then added and the iodine and bromine distilled over into 1-2 M NaOH. Following this the ruthenium (as RuO_4) was distilled with perchloric acid into NaOH solution.

Iodine. -- The basic distillate was neutralized with HNO_3 and the bromine and iodine were reduced with $NaHSO_3$. Iodide ion was oxidized to iodine with $NaNO_2$ and extracted into carbon tetrachloride. After adding bromide ion carrier, the CCl_4 extract was washed with water containing $NH_2OH \cdot HCl$, which reduces any bromine present. Next the iodine was reduced and back extracted by stirring with water containing $NaHSO_3$, and the whole extraction cycle was repeated. The iodine was finally precipitated as silver iodide, weighed, covered with black zapon, and counted. The isotopes I^{131} (8.14 days) and I^{133} (20.5 hrs) were resolved from the complex decay curves obtained. All half-lives referred to in this part of the paper from the Table of Isotopes.[30]

Bromine. -- The bromide ion in the water layer left from the CCl_4 extraction of iodine was oxidized to bromine with permanganate and extracted with CCl_4. Then the bromine was reduced and back extracted with a water solution of NH_2OH-HCl. Iodide carrier was added followed by $NaNO_2$. The iodine formed was extracted with CCl_4. Next the bromide ion was re-oxidized and extracted. Following final reduction and back extraction, the bromine was precipitated as silver bromide and mounted. The short-lived Br^{83} (2.33 hrs) as well as the shielded isotope Br^{82} (35.9 hrs), were observed in the decay curves.

Ruthenium. -- Ethyl alcohol was added to the basic ruthenium distillate to reduce the RuO_4 to RuO_2. The precipitate was dissolved in boiling 6 M HCl and ruthenium metal precipitated by adding magnesium metal. The metal was mounted for counting. The activity of Ru^{105} (4.5 hrs) was resolved from the decay curves.

Aluminum removal. -- The aluminum was removed from the target solution by successive precipitations of the other metallic elements present with 10-15 M NaOH. The aluminum stayed in solution as AlO_2^-. Unfortunately, it took three to five successive washings or dissolutions and reprecipitations to get the aluminum into solution. In addition, even though Na_2CO_3 was added to insure that the alkaline earths precipitated as carbonates or hydroxides, barium, strontium and also cadmium, which tend to coagulate very slowly, were frequently not carried with the hydroxide precipitate and had to be recovered from the supernatant later. This step usually took longer than an hour and was considered poor procedure.

Barium and strontium removal. --The hydroxide precipitate from the aluminum removal step was dissolved in concentrated HCl, which was then saturated with HCl gas. The barium and most of the strontium came down as the chloride in the 13 M HCl solution. These were redissolved in water and precipitated again with HCl gas. A third cycle was performed if necessary to reduce the alpha activity to a bench-top level.

Barium. -- The barium and strontium solution was buffered to about pH 5 with acetic acid and acetate ion and barium chromate precipitated from it with Na_2CrO_4. Following this the chromate was methathesized to the carbonate with hot saturated Na_2CO_3 and this dissolved in acid. Strontium holdback carrier was added and $BaCrO_4$ reprecipitated. This was then mounted for counting. The isotopes Ba^{139} (85 min), Ba^{140} (12.8 days) - La^{140} (40 hrs) were resolved from the decay curves.

Strontium. -- Strontium remained in the supernatant from the $BaCrO_4$ precipitation. After another $BaCrO_4$ scavenge the strontium was precipitated as the carbonate and prepared for counting. In the various bombardments Sr^{92} (2.7 hrs) - Y^{92} (3.60 hrs), Sr^{91} (9.7 hrs), and Sr^{89} (53 days) were observed in the decay curves.

Cadmium removal. -- The cadmium was removed with a Dowex-A1[31] anion exchange column. The rare earths pass through such a column in 10-12 M HCl.[32] After washing the column with 1 M HCl and a little water, the cadmium was stripped off with 0.75 M sulfuric acid.

Cadmium. -- The cadmium from the column was precipitated as the sulfide by bubbling in H_2S gas. Then the sulfide was dissolved in

HCl, and an antimony sulfide scavenge made from 1 M HCl, in which the cadmium will not precipitate. A final sulfide precipitation from about 0.1 M HCl completed the chemistry. The isotopes Cd^{117} (3.0 hrs), Cd^{115} (53 hrs), and Cd^{115m} (43 days) were present in the decay curves. The yield of Cd^{115m} was in all cases only a small fraction of the Cd^{115} yield.

Rare earth - actinide separation. -- The actinide and rare earth elements were separated from other elements by co-precipitation with lanthanum carrier as the fluoride. After dissolution of the fluoride with saturated boric acid and precipitation of the hydroxides with ammonium hydroxide, the fraction was dissolved with HCl gas and transferred to an alcoholic-HCl elution column. Dowex-50 cation exchange resin columns employing 13 M HCl for elution have previously been used[34] for actinide-rare earth separations. Recently alcoholic-HCl elutions from columns have been developed in this laboratory[35] which give fast and complete separations of these groups of elements. The elution solution was 80 percent concentrated HCl, 20 percent absolute alcohol which had been saturated with HCl gas. This was used with Dowex-50 resin,[31] either 4 percent crosslinked spheres or 12 percent colloidal fines, packed in a 3 mm capillary tube to a length of 4 cm. A flow rate of 1-2 minutes per drop was used and the americium and curium eluted between drops 16 and 24. Rare earth break-through did not occur until after 30 drops had passed through the column.

Americium and curium. -- The 87° C lactate elutions used to separate these two elements were described in Section II of this thesis. The drops from the column were collected on platinum plates, flamed,

and counted. The isotopes determined by alpha pulse analysis were Cm^{240} (26.8 days), Cm^{241} (35 days), Cm^{242} (162.5 days), and Am^{242m} (16.0 hrs). The last isotope was determined from the growth of its Cm^{242} daughter. The isotope Am^{240} (47 hrs) was determined by nucleometer counting.

Cerium and europium separation. --Cerium and europium fractions were isolated in bombardments when the actinides were not. Their fluorides were precipitated following the Dowex-Al column. These in turn were dissolved with HNO_3 - H_3BO_3 and the rare earth hydroxides precipitated. The hydroxides were dissolved in 1 M HCl and passed through a Jones reductor to reduce the europium to the divalent state. Cerium hydroxide was precipitated from the resulting solution with O_2 and CO_2 free ammonia, while all reduced europium remained in solution. Due to the easily oxidized nature of europium, the final chemical yield was always low because of this step.

Europium. -- The supernatant was oxidized with NaOCl causing $Eu(OH)_3$ to precipitate. The precipitate was then dissolved in 1 M HCl and the reduction step repeated. The europium was finally precipitated as the oxalate and mounted for counting. The decay of Eu^{157} (15.4 hrs) and Eu^{156} (15.4 days) was observed.

Cerium. --The cerous hydroxide from the europium separation was dissolved in nitric acid and the cerium oxidized to Ce^{+4} with $NaBrO_3$. Iodic acid was then added to precipitate ceric iodate, the other rare earths remaining in solution. This was dissolved with HCl and H_2O_2. For a scavenge step, zirconium carrier was added

which caused $Zr(IO_3)_4$ to precipitate, after which $NaBrO_3$ was added to the supernatant to precipitate the $Ce(IO_3)_4$ again. After dissolution of the iodate the cerium was precipitated as the oxalate and prepared for counting. The cerium isotopes Ce^{145} (1.8 hrs) and Ce^{143} (33 hrs) were resolved from complex decay curves.

2. Counting instruments and treatment of data. -- Three types of instruments were used to determine the counting rates and hence numbers of atoms for the individual isotopes separated. Two of these were used for the actinide spallation products (alpha pulse analyzer and nucleometer) and the third was used for the fission products (Geiger-Müller counter). Energy and half-life data were used to distinguish the various activities with the instruments.

Alpha pulse analyzer. -- The alpha active samples were analyzed in a 48-channel differential alpha particle pulse analyzer.[36] The instrument electronically sorts the alpha pulses from the ionization chamber according to energy and records them on 48 separate registers covering any desired range in energies. For a well resolved analysis; a well defined peak extending over 3-5 channels is obtained, and the area under the peak is proportional to the absolute number of disintegrations/minute of that particular energy and hence isotope. The curium and americium fractions (peak drops) from the lactate columns were both pulse analyzed. The curium fraction was frequently volatilized onto platinum to obtain better resolution on the analyzer. Four curium peaks were observed: Cm^{240} (6.25 Mev), Cm^{242} (6.11 Mev), Cm^{241} (5.95 Mev), together with Cm^{244} tracer (5.80 Mev). The Cm^{241} peak was occasionally small and difficult to

resolve as was the Cm^{242} peak when the bombardment energy was high, due to the large tail from Cm^{240}. The absolute disintegration rates of the individual curium isotopes produced in bombardment were calculated by multiplying the ratio of the integrated area of each peak, correcting for decay back to the end of bombardment, to that of the Cm^{244} tracer by the disintegration rate of the total Cm^{244} added, correcting for decay back to the end of bombardment. For example,

$$\frac{d}{m}(Cm^{242}) = \frac{A\ Cm^{242}}{A\ Cm^{244}} \times \frac{d}{m}(Cm^{244}),$$

where the A's stand for the integrated areas under the pulse analysis peaks. In the case of Cm^{241} a correction had to be made for the electron capture branching ratio.

The americium fraction was pulse analyzed to determine the amount of Cm^{242} grown in from Am^{242m} as well as the yield of Am^{243} tracer. On the basis that each beta decaying atom of Am^{242m} produced an alpha decaying atom of Cm^{242}, and after decay, branching ratio, and chemical yield corrections were made, the atoms of Am^{242} at the end of bombardment were calculated. The Am^{243} from pulse analysis determined the chemical yield for the electron capture isotope, Am^{240}, as well as for Am^{242m}.

Nucleometer. --The nucleometer[37] is a windowless proportional counter with a continuous methane flow. The instrument is particularly favorable for counting electron capture events since Auger electrons can be counted. For reproducible determinations of counting rates, operation on the plateau is necessary. There are two plateaus separated by the proportional region on the instrument. Between 2600

and 3000 volts the alpha particle plateau occurs. At a second plateau, in the region of 3900 volts, the instrument is used to count beta particles, electrons, and alpha particles. In this second region, at 3900 volts, the counting rates for the pure alpha emitters, Am^{241}, Pu^{239}, and Cm^{242}, evaporated onto platinum from solution, were determined to be 1.70 times the alpha counting rate at 52 percent geometry. The plateaus for a number of beta decaying nuclides were determined and are given below.

Nuclide	Decay energy (Mev)	Plateau
Electron capture		
Np^{235}	0.2	3800 - 4100
Cm^{241}	0.9	3400 - 4100
Am^{240}	1.5	3400 - 4300
$Beta^-$		
$Eu^{152,154}$	1.9	3800 - 4200

The decay energies were listed for comparison purposes because exact decay schemes are not known. On the basis of these data, 3900 volts was chosen as the operating voltage.

One of the biggest problems with the instrument is the electron capture counting efficiency. There are two different values in common use for electron capture isotopes. On the basis of his own work and that of others, Higgins[38] preferred to use the value of 60 percent. On a similar basis, Hulet[39] preferred to use a value between 30 and 45 percent. The factor of two between the limits of these two values reflects the present status of electron

capture counting efficiencies. There is no a priori reason why the counting efficiencies for all nuclides should be the same number, but it was nevertheless difficult to understand why there should be such a large difference. In the present work the yields of two electron capture isotopes, Cm^{241} and Am^{240}, were determined. The counting efficiency of the first of these isotopes was determined to be 58 percent by a method of counting the electron capture daughter, Am^{241}. For this reason, plus the fact that the beta$^-$ counting efficiency of RaE has been recently determined by Ghiorso[40] to be 90 percent, the higher value of 58 percent, which was applied to the unmeasured Am^{240} case, was adopted.

Geiger-Müller counter. -- The beta$^-$ particle emitting fission products were counted and followed for radioactive decay on a standard Geiger-Müller counter. The Geiger-Müller tube itself was an end window tube (Amperex type 100c obtained from the Amperex Electronics Company, New York) filled with a chlorine-argon mixture. These tubes have a smaller efficiency for counting beta particles than the previously used argon-alcohol tubes, but are considerably more stable.[41] The tube is mounted in a lead case above the sample holder and connected to a standard scaler. In this holder the shelf to window distance is 2.1 cm.

The conversion of counting rates on shelf two of this type counter to total disintegration rates is complicated and frequently results in errors of greater than 20 percent. The factors entering into this conversion are given in the formula below:

$$\frac{d}{m} = \frac{c}{m} \frac{AW}{[(BS)(SSA)]} \frac{100}{g} ,$$

where d/m is the disintegration rate, c/m the counting rate, AW the air plus window absorption and scattering correction, BS the back-scattering correction and SSA the correction for self scattering and self absorption in the sample itself, and g the geometrical factor of the counter. Each isotope has a slightly different set of these factors depending upon the energy of the particles and the nature of the sample and backing materials. A number of investigators[33, 42-44] have tried to correlate these variables with experimental data to be able to predict the factors with fair success.

The geometrical factor for the counter is a product of two factors; the physical geometry of the counting sample with respect to the tube window (solid angle intercepted) and the counting efficiency of the tube gas for the particles that actually get into the tube. The geometrical factor is experimentally determined by counting samples in the counter whose disintegration rate is known from 4π counting in a windowless proportional counter (nucleometer). The geometry of the counter used was determined to be 3.16 percent, which is slightly lower than the average counter (by about 10 percent). The air window correction can be experimentally determined by the back extrapolation of absorption curves through the 2.1 cm of air and 2-4 mg/cm^2 mica of the tube window. The factor is about 1.1 for high energy beta particles and higher for lower energy particles, and can be calculated with fair accuracy. The back scattering factors vary with atomic number of the backing plate as well as particle energies. The saturation back scattering factor on

aluminum varies from 1.23 to 1.30 for the fission products studied. The last factor, self scattering and self absorption, must also be empirically determined by counting samples of varying thicknesses. Corrections of from about 1.05 to 1.15 were necessary for the samples in the present work which ranged from 4 to 8 mg/cm^2. These last two factors have recently been determined for a number of the fission products obtained here.[33] Where factors were not available they were estimated from various curves.[42]

D. Results - Excitation Functions

The disintegration rates of the spallation and fission products were converted into numbers of atoms produced with the usual formula

$$N = \left(\frac{dn}{dt}\right) \frac{t_{1/2}}{0.693} ,$$

where $t_{1/2}$ is the half-life of the nuclide. Cross sections in cm^2 were then calculated with the formula

$$\sigma = \frac{N}{n/cm^2 (It)} ,$$

where N is the number of atoms produced; n/cm^2 is target density in atoms of Pu^{239} per cm^2; and (It) is the integrated beam in terms of total alpha particles. In the cases where the half-life of the nuclide was comparable with the bombardment time, e.g., Ba^{139} (85 min), the formula used was

$$\sigma = \frac{0.693\ N}{t_{1/2} n/cm^2\ I(1 - e^{-\lambda t})} ,$$

where N is the number of atoms at the end of bombardment, I is the beam intensity in particles per unit time; and $(1 - e^{-\lambda t})$ is the

correction term due to decay during bombardment. This equation was applicable because the beam intensity, I, for a given bombardment was reasonably constant. The factors for the cross section calculations for some of the bombardments are recorded in the following table (Table 1).

Table 1

Target and Beam Factors for the Cross Section Formula

	Alpha Energy (Mev)				
	37.2	33.3	28.0	24.8	20.6
(m/cm^2)[a]					
mg Pu	0.86	0.52	0.45	0.73	0.80
(n/cm^2)	1.8×10^{18}	1.1×10^{18}	9.1×10^{17}	1.5×10^{18}	1.6×10^{18}
(It)					
μamp hrs	4.17	4.49	6.90	2.25	8.19
particles	4.67×10^{16}	5.03×10^{16}	7.73×10^{16}	2.52×10^{16}	9.17×10^{16}
(m/cm^2)(It)					
(for calc. in mb)	5.5×10^{7}	5.3×10^{7}	7.1×10^{7}	3.8×10^{7}	1.5×10^{8}

[a] The target area was 1.23 cm^2.

No Am-Cm tracer was added to the products of a bombardment at 27.5 Mev, which was the bombardment used to produce considerable amounts of Cm^{241} in order to measure its branching ratio. The actinide cross sections for this run were determined relative to Cm^{242} which was then fixed on the flowly varying excitation function for the (α, n) reaction. The energy of 27.5 Mev was the mean energy of initially 28.0 Mev alpha particles in passage through 9.5 mg plutonium. This calculation was made on the basis of range-energy data.[26]

The cross sections for the actinide spallation products are given in Table 2. Energy thresholds for the various reactions are listed below the products. These were calculated from the formula

$$\text{Threshold } (E_a) = Q\frac{M_{Cm}^{243}}{M_{Pu}^{239}} = Q\frac{243}{239}.$$

The spallation cross sections given in Table 2 are also shown in Figs. 1 and 3. The corresponding fission product cross sections have been tabulated in Table 3, and presented in Fig. 2. The integrated values of these latter cross sections, to give total fission cross sections, are also given in Table 3, and summarized along with the spallation cross sections in Fig. 3.

Table 2
Spallation Cross Sections in Millibarns

Product (reaction)	Alpha Energy (Mev) 20.6	24.8	27.5	28.0	33.3	37.2
$Cm^{242}(\alpha, n)$ (12.1 Mev)	0.99 ± 0.15[a]	0.79 ± 0.12	0.95 ± 0.14[b]	1.0 ± 0.15	0.54 ± 0.08	0.82 ± 0.12
$Cm^{241}(\alpha, 2n)$ (19.2)	---	8.6 ± 1.3	12 ± 1.8	17 ± 2.5	8.3 ± 1.2	4.0 ± 0.60
$Cm^{240}(\alpha, 3n)$ (25.4)	---	---	0.093 ± 0.014	0.086 ± 0.013	0.22 ± 0.03	1.6 ± 0.24
$Am^{242m}(\alpha, p)$ (12.0)	0.031 ± 0.005	0.059 ± 0.009	0.074 ± 0.011	0.31 ± 0.05	1.4 ± 0.21	0.30 ± 0.05
$Am^{240}(\alpha, p2n)$ (24.5)	---	<0.0013	0.47 ± 0.07	---	8.2 ± 1.2	---

[a] Cross section in millibarns.

[b] Set at this value and other isotopes from this run adjusted to it.

Table 3
Fission-Product Cross Sections in Millibarns

Mass no.	Alpha Energy (Mev)				
	20.6	24.0, (25.0)[c]	28.0	33.3	37.2
82[a] (Br)		0.049 ± 0.01			
83 "		0.22 ± 0.05			
89 (Sr)	0.06 ± 0.02	0.93 ± 0.05 (2.01 ± 0.10)[c]	3.55 ± 0.20	4.45 ± 0.20	8.70 ± 0.70
91 "	0.115 ± 0.005	2.03 ± 0.10 (3.60 ± 0.20)		5.58 ± 0.30	8.50 ± 0.70
92 "	0.135 ± 0.005	1.35 ± 0.30 (3.22 ± 0.15)		6.0 ± 1.0	
105 (Ru)				9.0 ± 2.0	
115 (Cd)	0.055 ± 0.005	0.80[d] (1.00 ± 0.05)	3.0 ± 0.10	6.16 ± 0.40	9.2 ± 0.50
117 "	0.04 ± 0.005[b]			6.52 ± 0.45[b]	
131 (I)		1.59 ± 0.05			
133 "		2.04 ± 0.10			
139 (Ba)	0.16 ± 0.02	2.45 ± 0.20 (5.5 ± 0.35)	6.0 ± 0.30	11.4 ± 1.0	
140 "	0.20 ± 0.01	3.00 ± 0.30 (4.54 ± 0.20)	6.64 ± 0.50	12.3 ± 1.0	17.2 ± 1.0

Table 3 (Cont'd)

Mass no.	Alpha Energy (Mev)				
	20.6	24.0, (25.0)[c]	28.0	33.3	37.2
143 (Ce)		2.86 ± 0.10		11.8 ± 0.80	
145 "				15.0 ± 3.0	
156 (Eu)		0.31 ± 0.04		0.7 ± 0.20	
157 "		0.29 ± 0.04			
Total fission cross section	4.4 ± 0.66	6.3 ± 0.50 (9.8 ± 1.0)	160 ± 24	330 ± 50	510 ± 10

[a]Shielded mass Br^{82}; [b]Values so indicated have been multiplied by a factor of 1.61 over observed yields to correct for independent and isomeric yields; [c]There is reason to believe that the two bombardments were at about these energies although the aluminum target foil used was the same; [d]interpolated from yield-energy curve.

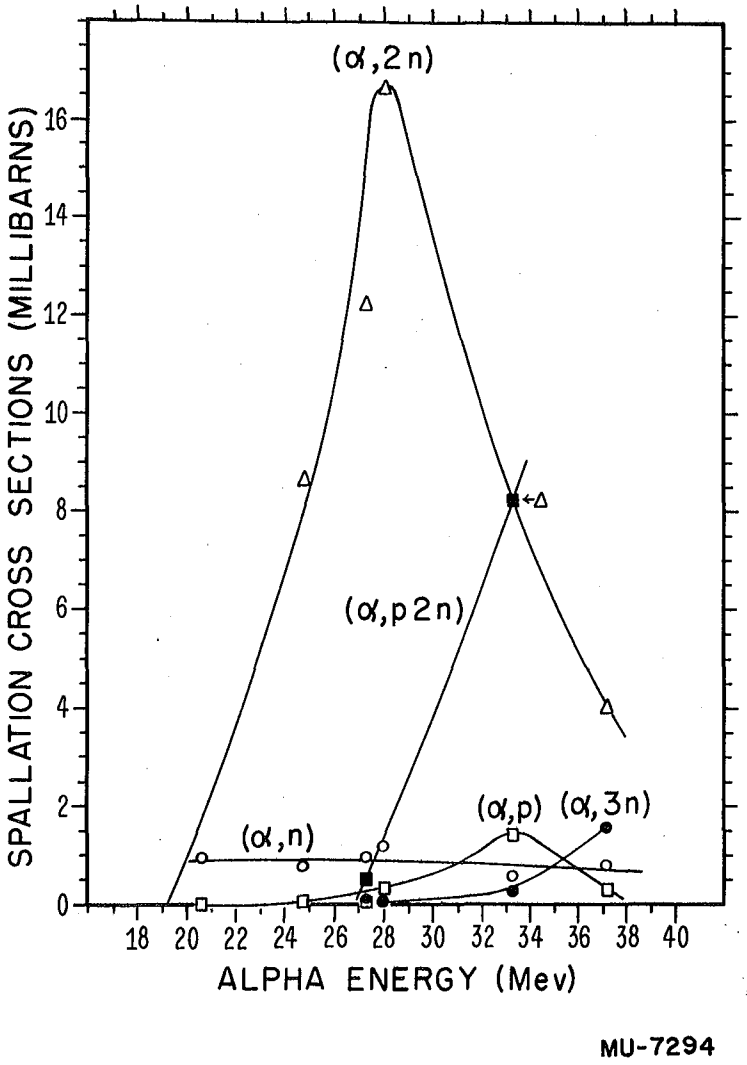

Fig. 1. Spallation excitation functions for alpha particle-induced reactions of Pu^{239}.

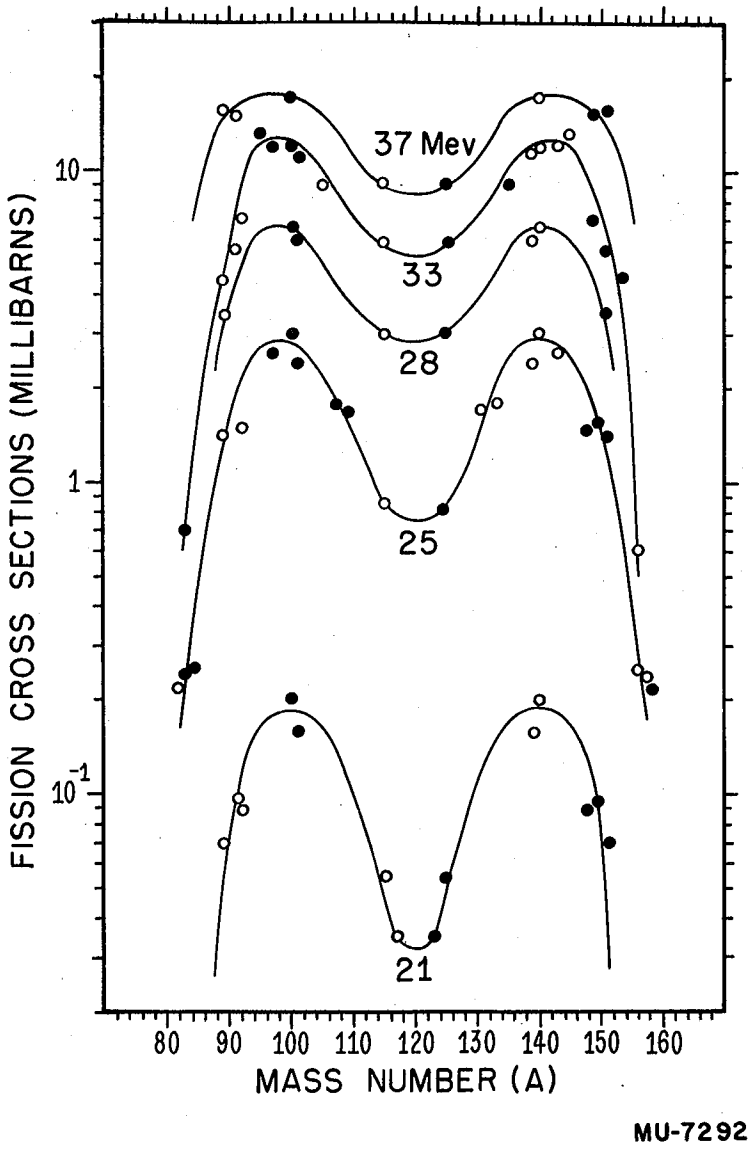

Fig. 2. Absolute fission yield curves for alpha particle-induced fission of Pu^{239}.

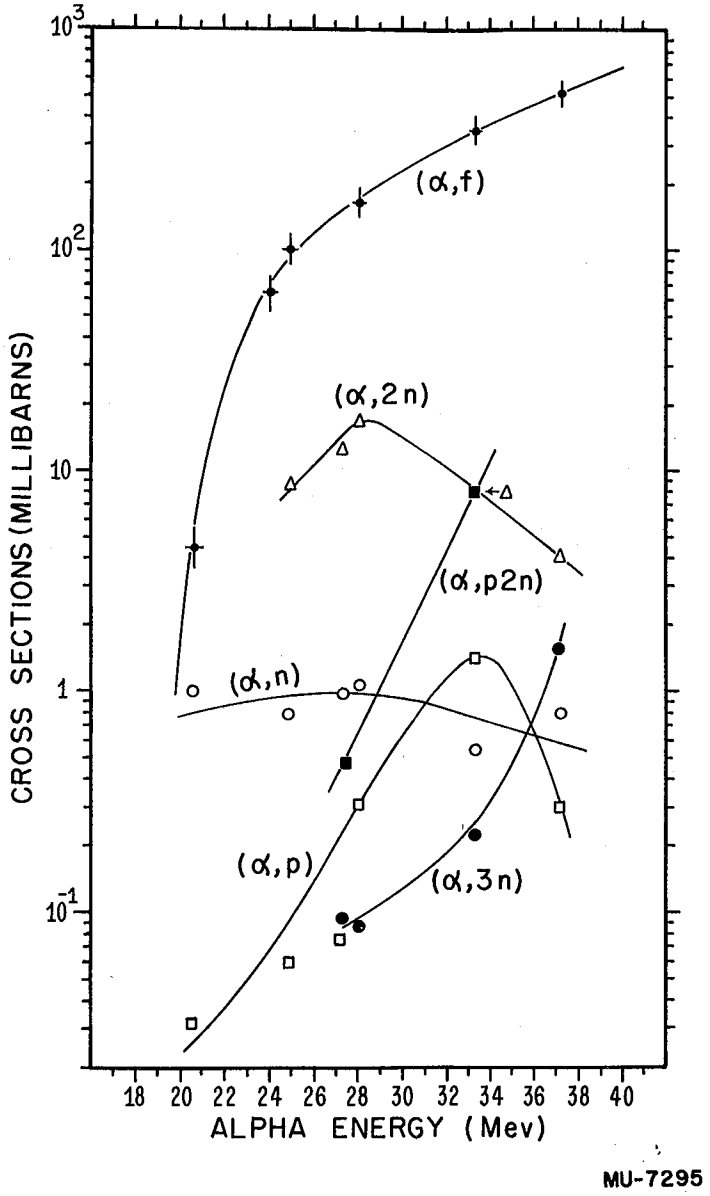

Fig. 3. Spallation and fission excitation functions for alpha particle-induced reactions of Pu^{239}.

E. Discussion

It shall be assumed that the first step of the reaction of Pu^{239} with a low energy alpha particle is the formation of the compound nucleus, Cm^{243*}. The various reaction possibilities from this compound nucleus along with the minimum energy requirement in Mev for each step (neglecting coulomb and recoil requirements) can be pictured as follows:

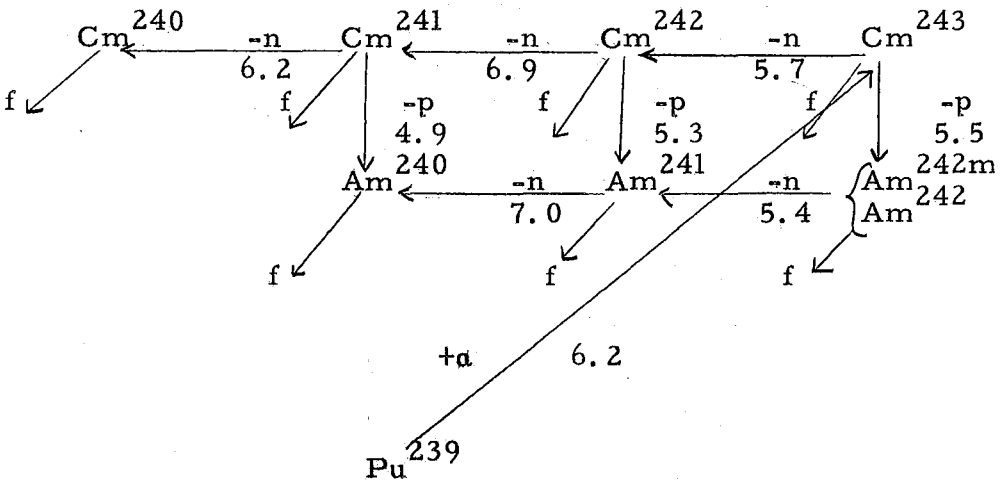

The only other energetically possible reactions below 40 Mev are the (α, αxn) reactions, which may be appreciable.[45] Coulomb energy barriers for the charged particle steps can be calculated from the simple formula

$$V_o = \frac{Z_a Z_A}{r_a + r_A},$$

where a is the small charged particle and A the large particle, assuming the radius function

$$r = 1.48 \times 10^{-13} A^{1/3}.$$

The barrier for alpha particles on Pu^{239} is calculated to be 23 Mev while that of the proton on Cm^{243} is about 12 Mev. It should be noted that energy threshold requirements are much more strict than

coulomb energy requirements, since appreciable barrier penetration is possible.

The excitation energy of the compound nucleus is given by

$$E_{ex.} = E_{\alpha} \frac{243}{239} - 6.2.$$

This can be used to boil off a neutron or proton or it can cause fission if the energy requirement for fission, about 5.3 Mev,[3] is available. If a neutron or proton is boiled off the product nucleus again can de-excite by fission or further evaporation of particles, as long as the energy requirements are met, otherwise de-excitation by gamma emission occurs which results in the ground state of the same nucleus being formed. Thus it can be seen that the final products are a result of a rather complex pattern of competitions.

Many of the general features of the spallation functions are about what would be expected. All cross sections drop to low values below the alpha particle barrier, which, in fact, cuts off the (α, n) peak from its normal position, leaving the tail to peak gradually under that for the (α, 2n) product. More precisely, it might be stated that the (α, n) reaction maximum is reduced on the low energy side by the barrier and on the high energy side by unfavorable competition with the (α, 2n) reaction. The (α, 2n) and (α, 3n) products become relatively more prominent in succession with increasing energy. At the same time, the proton emission reactions are at first hindered by the proton barrier, causing the (α, p) cross sections to peak late at 33 Mev. Both the (α, p2n) and (α, 3n) excitation functions are still rising at 37 Mev. As anticipated, the spallation cross sections are considerably lower than those for corresponding reactions with a

lower Z target. With bismuth, the (α, 2n) and (α, 3n) cross sections reach on the order of one barn at their peaks,[19] whereas the same cross sections for plutonium are in a region only one-hundredth as great.

At the same time, the total fission cross sections rise rapidly to 0.5 barn at 37 Mev. Although fission is the most prominent reaction, its cross section is still only a fraction of the 2.7 barns calculated geometric cross section (assuming the radius function previously used). As expected,[3] the minimum in the fission yield curve tends to flatten out with increasing energy. Newton[13] found a peak to valley ratio of two in his bombardments of thorium with 37.5 Mev alpha particles which is about the same as the ratio from the fission yield curve at 37 Mev in the present investigation. The general trend from asymmetric to symmetric fission with increasing energy was also observed by Tewes and James[11] in their bombardments of thorium with protons.

Although the general features of the excitation functions such as high fission and very low spallation cross sections are in agreement with the speculations of Street,[14] the individual features of the spallation cross sections are not as expected. The first unexpected feature is the high (α, 2n) peak. It appears that this reaction can compete more favorably with fission than the other (α, xn) reactions, in fact, the slight leveling off of the fission excitation function at 28 Mev may be a result from the high (α, 2n) cross sections. At first inspection it appears that the effect may be due to the fact that the Cm^{241} product is the only one which has an odd neutron and therefore is not destroyed to such a large extent by fission.

Seaborg[15] has discussed the idea that the spontaneous fission of odd nucleon nuclei may be slowed by their larger radii as well as the fact that gamma de-excitation is favorable due to a greater number of low-lying energy levels. Preliminary investigations of relative yields of other products indicate similar results. Hulet[46] has determined the (α, 2n) yields of a number of products relative to the (α, n) neighbors with about 33 Mev alpha particles. His reactions were as follows:

Reaction	$\sigma(\alpha, 2n)/\sigma(\alpha, n)$
$Am^{241} \xrightarrow{\alpha, n} Bk^{244}$	~4/1
$\xrightarrow{\alpha, 2n} Bk^{243}$	
$Am^{243} \xrightarrow{\alpha, n} Bk^{246}$	~4/1
$\xrightarrow{\alpha, 2n} Bk^{245}$	
$Cm^{244} \xrightarrow{\alpha, n} Cf^{247}$	~3/1
$\xrightarrow{\alpha, 2n} Cf^{246}$	

In all three examples the (α, 2n) reaction was much more prominent than the (α, n) reaction, even in the case of Cm^{244} in which the (α, 2n) product is the even-even isotope Cm^{242}. In connection with the Cm^{244} case, an exploratory alpha bombardment of an isotopic mixture of Pu^{238} and Pu^{242}, containing small amounts of Pu^{239} and Pu^{240}, at about 28 Mev,[46] indicated that the (α, 2n) products, which in this case were the even-even nuclides Cm^{240} and Cm^{244}, were again in high yield relative to the (α, n) product from Pu^{238}. Although in this bombardment cross sections were not determined and the data are preliminary, on the basis of these results it would

appear that high (α, 2n) cross section relative to those for the (α, n) reaction may be the usual result regardless of nuclear type. There may be, however, definite odd-even effects superimposed. With higher excitation energies one might have anticipated that the (α, 3n) reaction would have peaked to a value at least as high as the (α, 2n) reaction for energies as high as 37 Mev in the Pu^{239} excitation function, by analogy with the bismuth cross sections.[19] In this case, however, perhaps the higher Z^2/A can be used to explain the low cross sections rather than the even-even character of Cm^{240}. Thus, the effect of odd-even type is not clear. A low (α, n) yield due to barrier cut-off, plus a normally high (α, 2n) yield, followed by a low (α, 3n) yield due to large fission competition as a result of the high Z^2/A of the product can be used to explain the present results.

The values of Z^2/A for the spallation products in the present study are as follows:

	Z^2/A
Cm^{240}	38.4
Cm^{241}	38.2
Cm^{242}	38.1
Cm^{243}	37.9
Cm^{244}	37.8
Am^{240}	37.6
Am^{242}	37.3

It can be seen immediately that the lack of a high Cm^{240} peak may be due to its relatively high value of Z^2/A with the attendant high competition by the fission reaction. At the same time, the

high yield of Am^{240} may be due to its relatively low value of Z^2/A. Other investigators have observed yield effects that can also be attributed to this effect of Z^2/A. The results from the fore-mentioned bombardment of Pu^{238} and Pu^{242} offer the first clear cut comparison of cross sections from identical reactions on nuclei with the same Z and nuclear type. From pulse analysis of the curium from the bombardment the yield of the (α, 2n) product (Cm^{244}) from Pu^{242} was 4.4 times as great as the yield of the (α, 2n) product (Cm^{240}) from Pu^{238}. The difference in yields apparently is caused by a difference of only 0.6 in Z^2/A. Hulet,[46] however, working with electron capture isotopes, failed to find a very large difference between the products from alpha particles on Am^{241} and Am^{243}.

A striking feature of the spallation excitation functions is the high (α, p2n) cross sections at the highest energies. If the proton barrier (12 Mev) is added to the Q of the reaction (24 Mev) and the two neutrons are assumed to be given out with zero energy the requirement of 36 Mev for the reaction is obtained. Although a high cross section at 37 Mev is then possible (but not probable considering the zero energy neutrons) the cross section value at 33 Mev is not. It is necessary then that either the protons are escaping with energy considerably below the barrier or they are being given out in some other form such as tritium, which is more economical energy-wise by the binding energy of the triton particle. Whichever process is responsible for the high cross sections, and indeed both are possible, the fact remains that a reaction in which

a charged particle is emitted is surprisingly prominent. It is interesting to note that the relative prominence of proton emission goes through a minimum in going from low to very high Z. Rudstam, Stevenson, and Folger[10] found that proton and neutron emission were equally probable around iron while Goeckermann and Perlman[7] found the neutrons were favored by about 10 to 1. Now it appears that proton emission is again competing favorably in the plutonium region. Because different energies were used in these investigations it is impossible to make quantitative comparisons.

That the (α, p) reaction is not correspondingly high may be due to a number of things. First it must be remembered that the yield of only one Am^{242} isomer has been determined, and angular momentum considerations may favor the production of the unobserved long-lived Am^{242} isomer. Secondly, if the Am^{240} product is largely produced by an (α, t) reaction the (α, p) product is bypassed. Perhaps the (α, p2n) cross sections are higher because the reactions use the excitation energy available more efficiently; that is, with less kinetic energy being given to outgoing particles. In other words, above the energy where the proton barrier hindrance is important the (α, p2n) reaction may predominate over the (α, p) for the same reason that the (α, 2n) reaction predominates over the (α, n) beyond the alpha particle barrier. Again this explanation is questionable unless triton emission is assumed because of the forementioned energy difficulties of the (α, p2n) reaction. Although the odd-odd character of Am^{240} may help explain why its yield is not reduced by fission to the same extent as the even N, (α, xn) products, the effect of Z^2/A is probably the most important factor.

Another example of a high (α, p2n) cross section resulted from the work of Lessler,[47] who found that the yield of the (α, p2n) reaction on U^{238} was greater than three times as large as that of the (α, p) reaction with alpha particle energies in the region of 30 Mev. In his investigation not only was the (α, p2n) reaction more prominent than the (α, p) but the difficulty of finding energy to satisfy Q and barrier requirements is even more pronounced than in the Pu^{239} bombardments.

The same kind of conclusions about the prominence of charged particle emission can be drawn from the bombardments of U^{238} with nitrogen ions.[48] In this case the yields of (N, αxn) reaction products (Bk^{243} and Bk^{245}) were found to be on the order of ten times as great as the (N, xn) yields.(99^{246} and 99^{247}). However, the excitation energies in this case are considerably larger than those for the Pu^{239} bombardments. In this case the berkelium isotopes have a lower Z^2/A than the 99 isotopes.

The low total fission cross sections from this work at the higher energies studied were rather surprising. Newton[13] determined a fission cross section of 0.6 barn for Th^{232} bombarded with 37.5 Mev alpha particles by integrating the area under the radiochemically determined fission yield curve. At the same time Jungerman[12] obtained a cross section of about 0.8 barn for U^{235} bombarded with 35 Mev alpha particles by counting pulses in a fission chamber. One would have expected that the cross section for Pu^{239} at similar energies would have been even higher due to its greater Z^2/A, but at 37.2 Mev the cross section was determined

to be only 0.51 barn. The fission excitation function, however, is still rising at this energy and probably will level off at a considerably higher value.

The outcome of the bombardment below the alpha barrier (23 Mev) at 20.6 Mev is very interesting. Processes such as barrier penetration of the alpha particle to form the compound nucleus or coulomb excitation must be employed to explain the products. Both spallation and fission have been observed below potential barriers, for example, in the investigations of Kelley and Segre[19] and of Jungerman.[12] In the present investigation the (α, n) and (α, f) reactions are still observed below the barrier. The (α, f) reaction, however, appears to be dropping off more sharply. This effect may become very important in the bombardments of heavier target nuclei where high yields of spallation products relative to fission are desired; for example, when the target nucleus is very scarce and extensive loss due to fission is undesirable.

The present investigation has merely touched on the possibilities in this area of research. Data on a much larger range of atomic number and mass number from target nuclei of all nuclear types and with protons and deuterons are needed to fill out the general picture. Investigations are in progress at this laboratory[49] to determine absolute fission and spallation cross sections for a number of heavy element target nuclei, e.g., U^{235}, U^{238}, Pu^{238}, and Pu^{242}.

F. Decay Scheme Studies

In the course of determining the cross sections for the americium and curium isotopes, investigations were made on the decay schemes of Cm^{241} and Am^{240}. In addition to the previously

described instruments, a sodium iodide (thallium activated) crystal detector connected to a 50-channel differential pulse analyzer, was used to determine the gamma spectra of these nuclides.

Curium 241. -- This isotope is reported[30] to decay with a 35 day half-life predominantly by electron capture and to the extent of 0.2 percent by emission of 5.90 Mev alpha particles. No gamma rays are reported. The most important piece of information desired about Cm^{241} was an accurate value for the alpha-electron capture branching ratio which was necessary to determine its absolute yield from the alpha pulse analysis curves. Higgins[38] determined the value of 0.2 percent by assuming a nucleometer counting efficiency of 60 percent, but his determination was subject to considerable uncertainty due to activities other than Cm^{241} in the sample. In order to determine the electron capture branching, 9.5 mg of high isotopic purity Pu^{239}, which has been carefully purified from Am^{241}, were bombarded for a total of 12 μamp hours on the 60-inch cyclotron at 27 Mev to produce a large amount of Cm^{241}. This was then purified by the usual adsorption-elution column chemistry and vaporized onto a platinum plate for pulse analysis. A number of pulse analyses were run to determine the growth of Am^{241} from the electron capture decay of Cm^{241}. The resulting growth curve of Am^{241}, along with the decay curves of Cm^{241}, Cm^{240}, and Cm^{242} obtained from the pulse analyses are given in Fig. 4. The alpha branching ratio was calculated from the formula

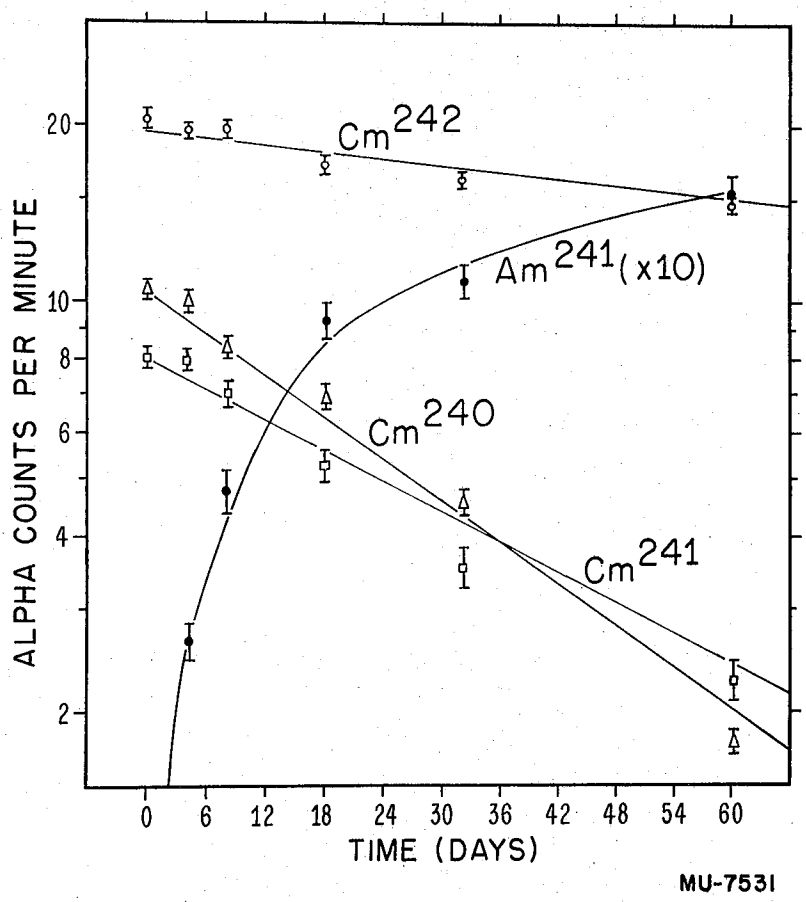

Fig. 4. Growth of Am^{241} daughter activity from Cm^{241} electron capture decay.

$$\alpha \text{ B.R.} = \frac{\Delta N \, Cm^{241}{}_{\alpha}}{\Delta N \, Cm^{241}{}_{\alpha} + \Delta N \, Am^{241}},$$

where the numerator is the number of atoms of Cm^{241} that have decayed by alpha emission in a given time and the denominator is the sum of this term (negligible here) and the number of atoms of Am^{241} that have grown in, which represents the number of atoms of Cm^{241} that have decayed by electron capture. The branching ratio obtained was 0.72 ± 0.10 percent which is over a factor of three greater than the figure obtained by Higgins. From the electron capture disintegration rate obtained, the nucleometer counting efficiency was calculated to be 58 ± 9 percent by the formula

$$\text{counting efficiency} = \frac{\text{(c/m) nucleometer}}{\text{(d/m) electron capture}} .$$

The new alpha branching ratio permits a recalculation of the partial alpha half-life of Cm^{241}. The value obtained, 13 ± 2 years, is more in line with the current theory[50] of alpha decay of odd-nucleon nuclei than the old figure.

The gamma spectra of the curium plate indicated two prominent gamma rays which were assigned to the electron capture of Cm^{241}. They were too high in intensity and energy to be associated with the alpha decay of the even-even isotopes Cm^{240} and Cm^{242} and further were in too high intensity to be in the alpha decay of Cm^{241}. The gamma rays and their intensities, using a shelf one geometrical efficiency of 16 percent[51] and the gamma counting efficiencies of O'Kelley and McLaughlin[52] were as follows:

470 ± 10 kev (28%)

592 ± 10 kev (7%)

These gamma rays plus K and L x-rays were the only lines of appreciable intensity, although there was some indication of weak gamma rays of 65 and 163 kev. The proposed decay scheme for Cm^{241} along with levels of Am^{241} observed in the alpha decay of Bk^{245} [30] are given in Fig. 5a. The electron capture energy of Cm^{241} was calculated from closed cycles. The 0.47 Mev level from electron capture and 0.43 Mev level from alpha decay may in fact be different levels, although they are the same within the limits of both errors. The alpha particle energies of Cm^{241} and Cm^{240} were also redetermined. Four alpha pulse analyses from different bombardments were employed. The standards used were Am^{241}, Cm^{242}, and Cm^{244}, which have all been measured with the alpha spectrograph.[30] The values were as follows:

	New values	Previous values[30]
Cm^{241}	5.95 ± 0.02 Mev	5.90 ± 0.02 Mev
Cm^{240}	6.27 ± 0.02 Mev	6.26 ± 0.02 Mev

Americium 240. -- This isotope is reported[30] to decay by electron capture with a 50 to 53 hour half-life. It is also reported that no gamma ray greater than 0.7 Mev occurs in the decay.

In the present work a half-life of 47 ± 2 hours was obtained from the nucleometer decay curves from the cross section bombardments. The decay curve of a 1 Mev gamma ray that was found also yielded a half-life of 47 ± 2 hours.

The gamma spectra of the americium fractions were run on the sodium iodide crystal counter. The gamma rays and their intensities, again using a shelf one geometrical efficiency of 16 per-

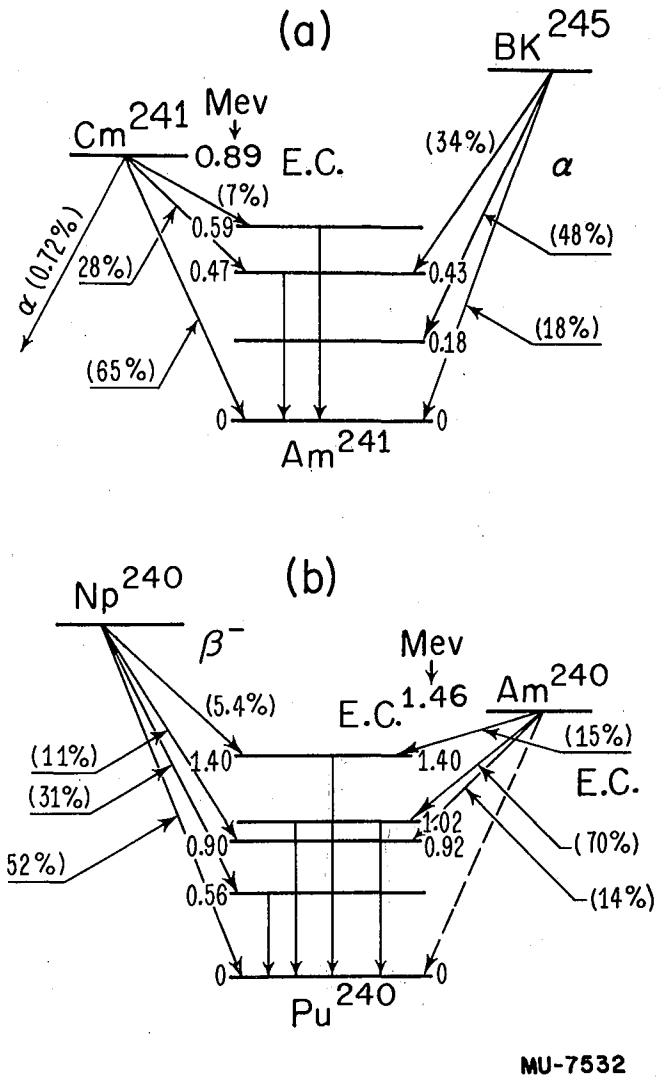

Fig. 5. Proposed decay schemes for Cm^{241} and Am^{240}.

cent and the counting efficiencies of O'Kelley and McLaughlin are tabulated below. In this case a 50 percent nucleometer counting efficiency for electron capture was assumed.

0.92 ± 0.03 Mev (14%)

1.02 ± 0.02 Mev (70%)

1.40 ± 0.03 Mev (15%)

These can be combined with the previously reported decay scheme of Np^{240} to give a more complete picture of the level scheme of Pu^{240}, as shown in Fig. 5b. It is quite interesting that the 1 Mev level is preferred with respect to the 0.9 Mev level in the decay of Am^{240} whereas in the decay of Np^{240} only the 0.9 Mev level is populated. These levels around 1 Mev may correspond to the first vibrational level as proposed in the case of Np^{238}.[52] If the abundances of the gamma rays in Am^{240} are correct it means that essentially all of the decay is to high-lying levels. However, if the nucleometer counting efficiency for this isotope is in the region of 30-40 percent all of the abundances will drop almost a factor of two allowing considerable decay to go to the ground state. On the other hand, leaving the nucleometer counting efficiency at 58 percent and using a lower gamma counting efficiency curve would result in abundances that totaled considerably over 100 percent. Although the decay scheme is pictured with electron capture going to each of the observed gamma rays, the 0.9 and 1 Mev levels could be fed by cross-over transitions from the 1.4 level; however, this is not likely in the case of the 1 Mev gamma. Cross-over gamma rays would not have been seen in the gamma ray spectra, due to the fact that the region below the high energy peaks was

masked by their broad Compton peaks.

It is interesting to note that Cm^{241} and Am^{240} represent the furthest points from the first forbidden line in Hoff's[53] graph of electron capture half-lives vs. energy. With the present decay schemes, indicating less electron capture to the ground state, these points fall more in line with his empirical curves.

IV. MASSES AND SYSTEMATICS OF THE HEAVIEST ELEMENTS

A. Approach to the Systematics

The correlation of known radioactive decay energies (and other energies derived from them) and half-lives as well as the prediction of these properties where unknown, which, of course, is dependent on the former, is vital to the study of heavy nuclides. Hence, it is important that when new data are reported, methods of listing and graphing data have been developed which will clearly show the relationship of the new information to that already collected. At the same time, in the search for new elements and isotopes some idea of the half-lives and energies expected must be estimated from trends in known properties so that experiments can be designed efficiently. The field that embraces methods of listing and graphing (correlating) as well as resultant predicting and interpreting of data is that of nuclear systematics. Known alpha, beta$^-$, and electron capture energy and half-life values can be correlated with any of the nuclide numbers such as atomic number (Z), mass number (A), or neutron excess (A - 2Z or I) as well as with other nuclear properties, and corresponding systems of alpha, beta$^-$, and electron capture systematics can be developed. Systematics of calculated data such as nucleon binding energies also can and have been developed. This section presents the major part of the present systematics of the transmercury nuclides as employed at the Radiation Laboratory.

The most concise tabulation of all energy data would be a table containing the masses and half-lives of the nuclides, since, due

to the interconversion of mass and energy, the masses contain all possible energy relations between nuclides. Although the masses are the most concise form of presentation, plots of alpha energy, beta energy, or neutron binding energy versus mass number, as well as other similar graphs, show trends in these properties not immediately apparent from inspection of the masses. The systematics can not only be used as a basis for predicting properties of undiscovered isotopes and elements by interpolation and extrapolation using relations such as those just described, but also as a basis for predicting those measured energies and half-lives which may be in error due to the failure of the reported properties to follow the systematic trends observed with other known nuclides. In addition to the use of systematics for the correlation and prediction of energies and half-lives, a third general application is important, namely, the relating of systematic trends to theory. The theories associated with the half-life relations are the present alpha,[1] beta,[2] and electron capture[3] theories. At the same time, the decay energies and derived masses can be considered in relation to the statistical model (liquid drop) of the nucleus in terms of the semi-empirical mass equation and its parameters.[4-6] Details of spins and parities effect both half-lives and energies: in the former case by determining the hindrance of decay and in the latter by determining relative stabilities of nuclides, e.g., odd-even effects. It is not the purpose of this section to give extensive consideration to the theoretical aspects of the systematics.

A useful model to refer the purely energy aspects of the systematics to is the "energy surface".[7-9] When the masses or mass defects of the isotopes of the elements are represented on a three-dimensional diagram with atomic number (Z) and mass number (A) as the horizontal axes a surface is obtained which outlines the total energy of the nuclides. From such a diagram the energy difference between two nuclides by processes such as radioactive decay or nuclear reaction can readily be calculated. A large part of this surface in the lower element regions has already been determined from measurements with mass spectrographs. This method is presently limited, however, to the study of stable or relatively long-lived nuclides. In the heavy region few masses have been determined[10] and these with uncertainties in the Mev range. In practice, the large body of energy data from alpha, beta, and electron capture disintegration processes which establishes energy differences between decaying parents and product daughters is used to calculate masses in the heavy region. By conversion of the decay energy to mass units the relative masses of parent and daughter are obtained, and if the absolute mass of one nuclide is known either by direct measurement or from further decay chains connecting it to a known mass the other is then determined. Another source of relative masses is the data from energy balances (Q values) of induced nuclear reactions. For example, determinations of the thresholds for (γ, n)[11] reactions yield the neutron binding energies of the target nuclides.

The region of elements above mercury offers a particularly favorable place for the determination of relative masses due to the

phenomenon of alpha decay peculiar to the region. Decay by alpha particle emission is the only simple disintegration process in which energy differences between nuclides with different mass numbers can be established. All of the nuclides in the four radioactive decay series, both naturally occurring and artificially produced, are connected to the lead and bismuth isotopes by chains of alpha, beta, and electron capture decay. The nuclides in the 4n series all eventually decay to Pb^{208}. In the 4n + 1 series, no members of which are naturally occurring, the terminal nuclide is Bi^{209}. Likewise, Pb^{206} and Pb^{207} are the ends of the chains for the 4n +2 and 4n + 3 series, respectively. Thus in each particular series, all of the nuclides are related energetically, insofar as the decay energies have been determined, and hence the relative masses also. Connections are established between the four radioactive series by the neutron binding energies obtained from (n, γ), (γ, n), (d, p), and (d, t) reactions on the lead isotopes. The neutron binding energies of Pb^{207}, Pb^{208}, and Pb^{209} are sufficient for this purpose. Finally, the relative masses are put on an absolute basis by relating them to the mass of Pb^{208}, which has been determined mass spectrographically. The resultant energy surface for the heavy region is shown in Fig. 1. General features of the surface are the continuous increase in slope with increase in A and Z, indicating that added neutrons and protons are bound in this region, and the Heisenberg valley,[7, 8] which indicates that for each value of A there is a minimum representing the most stable value of Z. Odd-even effects have been smoothed out in Fig. 1, and in reality there are four energy surfaces corresponding to the four nuclear types.

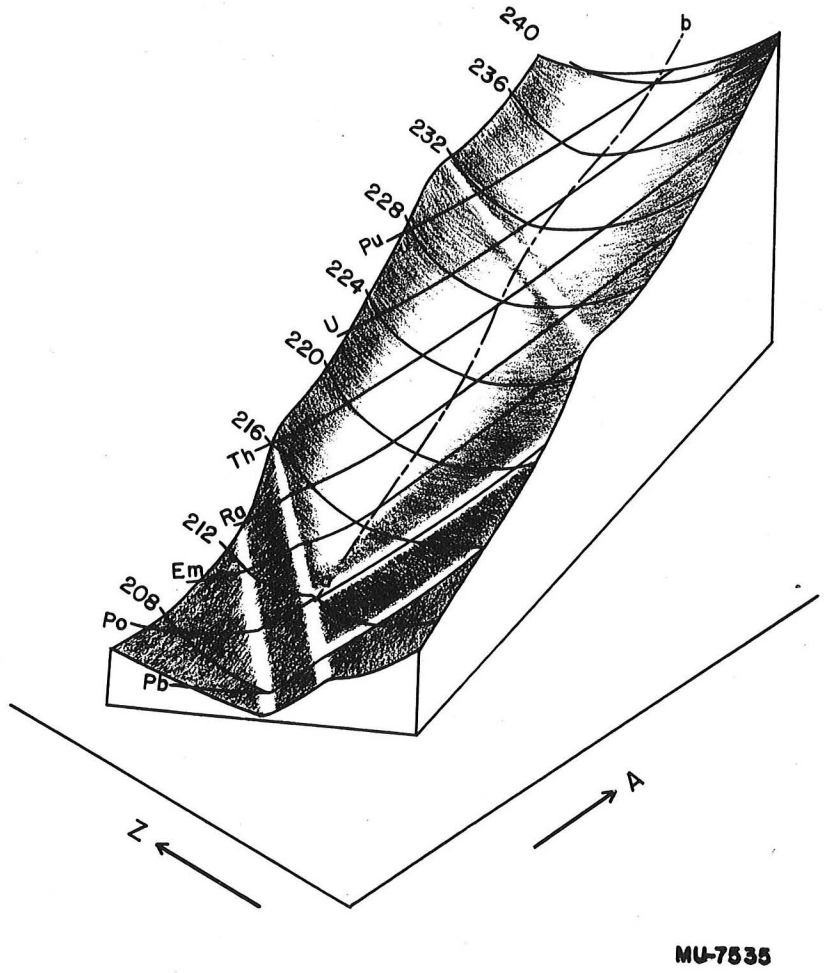

Fig. 1. Energy surface in the region of the heaviest elements.

By crossing the energy surface in different ways, e.g., at constant Z, A, or N-Z, with the object of observing different nuclear processes, the various systematics are formed. First consider the phenomenon of alpha decay. Alpha decay energies are calculated from the energy difference between the nuclides Z^A and $(Z - 2)^{A-2}$ by the formula

$$E\alpha_{(Z^A)} = M_Z A - M_{(Z - 2)}A - 2 - M_\alpha,$$

where E refers to energy and M to mass. Individual alpha decay energies represent differences on the energy surface along lines at a small angle with the line of beta stability (bottom of the Heisenberg valley) and thus give an idea of the pitch or slope along the length of the valley, particularly when considered in relation to nuclei at about the same distance from the line of stability (analogous nuclei). The alpha decay energies can be plotted versus mass number and lines of constant Z[9] or constant neutron excess $(A - 2Z)$[12] connected. Due to the fact that alpha decay occurs in a direction forming a small angle with the line of stability, for a given Z the alpha decay energies decrease with increasing A, as discussed by Perlman, Ghiorso, and Seaborg.[9]

At the same time, beta decay energies, both beta$^-$ and electron capture, which are indicated by mass differences along lines of constant A, and thus given an outline of the curvature of the Heisenberg valley, can be calculated from the following formulas

$$E_{\beta^-(ZA)} = M_Z{}^A - M_{(Z+1)}{}^A$$

$$E_{EC(ZA)} = M_Z{}^A - M_{(Z-1)}{}^A.$$

One method of plotting these energies, similar to that used for alpha energies, is on a graph of decay energies versus mass number, on which lines of constant Z or neutron excess may again be connected. Graphs of this type have been presented by Way and Wood[13] for all beta energies available for all of the elements. A graph of the beta separation energy between two elements, where beta$^-$ energies are considered positive and electron capture energies negative, shows that the separation energy becomes more positive with increasing A (or N) as would be expected, since beta$^-$ decay is favored as the number of neutrons in a given element is increased. Suess and Jensen in a similar manner have plotted beta decay energies versus neutron number (N) and connected points of constant neutron excess.[14]

Another method of graphing beta decay energies, this time as a function of atomic number at constant mass number describes the well-known Bohr-Wheeler parabolas[4, 8] which outline the energy differences passing across the Heisenberg valley. These curves, in connection with Bohr-Wheeler form[4] of the mass equation, can be used to calculate the curvature of the parabolas of the energy surface as well as the most stable Z for a given A (bottom of the parabola). Moreover, Bohr-Wheeler considerations give a convenient form for the calculation of the energy separations between the four surfaces formed by the nuclides of the four nuclear types.

Analyses of beta decay energetics have been made by Brightsen;[15] Coryell, Brightsen, and Pappas;[16] Kohman;[17] and Coryell[18] (review), among others. Also, beta as well as alpha energetics are useful for determining closed shell influences. Such analyses have been made by Way and Wood,[13] Suess and Jensen,[14] and Feather[19] in addition to the previously mentioned authors, the latter two considering effects along lines of constant isotopic number.

A third correlation of variations in the energy surface is obtained by consideration of neutron and proton binding energies. These energies can be calculated from the masses by the formulas

$$E_{n(Z^A)} = M_Z{}^A - M_Z{}^{A-1} - M_n$$

$$E_{p(Z^A)} = M_Z{}^A - M_{(Z-1)}{}^{A-1} - M_p.$$

Individual neutron binding energies represent differences on the energy surface along lines of constant Z whereas proton binding energies represent differences along lines of constant neutron number (N), thus describing energy differences from two more ways of crossing the Heisenberg valley. The nucleon binding energy systematics differ from the alpha and beta systematics among the heavy elements by the fact that the vast majority of these energies are obtained from calculations involving the decay energies and thus must be classified along with the masses as derived properties. A study of the available experimental neutron binding energies has been made by Harvey,[20] who considered shell discontinuities as well as the parameters of the semi-empirical mass equation. In the heavy element region Way and Wood[13] and Feather[19] employed different forms of nucleon binding energy closed cycles to aid in the

interpretation of beta decay systematics. The neutron binding energies have also been extensively studied in this region by Huizenga and Magnusson[21] and by Wapstra.[22, 23] The former used decay energies from the Table of Isotopes plus recent beta energies determined at their laboratory for the 4n + 1 series to calculate all possible neutron and proton binding energies above thallium, which they plotted versus mass number. Wapstra plotted the neutron binding energies, from which a function of A had been subtracted, versus A and obtained smooth curves for the elements above thallium. Other studies of nucleon binding energies have been made by Kravtsov,[24] Sengupta,[25] and Edmonds,[26], and Karlick[27] with the particular object of looking for regions of special stability. All of the foregoing authors have noted the special stability associated with the 126 neutron, 82 proton region.

Finally, the masses themselves, in addition to decay energies and nucleon binding energies, can be investigated for trends on the energy surface. For example, Hogg and Duckworth[28] have made a study of the region between 82 and 126 neutrons in an attempt to find evidence for closed subshells. It is obvious that all possible methods of plotting energy surface data have not been exhausted. New energy functions and new parameters will undoubtedly be used in future correlations. One thing is certain, however, and that is that all considerations will be based on measured decay energies, masses, and Q values, and the validity of the conclusions derived will depend on the accuracy of the measurements. Which of the systematics is preferred is essentially a matter of choice, since whichever method

of crossing the energy surface is employed the same features can be deduced. The method chosen depends on which properties are to be emphasized.

The studies of half-life energy relations are of equal importance with the energy surface investigations. For purposes of this introduction it will suffice to say that in general, for the alpha, beta, and electron capture processes, the half-lives are shorter the greater the energy of disintegration. In the ensuing parts of this section, half-life versus energy plots are presented for all three types of decay. Except in the case of even-even alpha emitters, half-life versus energy curves are not clearly defined due to the fact that different quantum states of parent and daughter are usually involved and selection rules hinder decay to varying degrees.

The emphasis in the approach to systematics at this laboratory has been largely on alpha systematics. This is both because the alpha decay properties are the most accurate and extensive body of decay data available in the heavy element region and because a large number of known alpha energies have been determined at this laboratory. Besides the naturally occurring nuclides, alpha active isotopes have been produced both by cyclotron bombardments, as illustrated by the discovery of neutron deficient collateral chains by Meinke, Ghiorso, and Seaborg,[29, 30] and Meinke and Seaborg,[31] and by neutron irradiation in atomic piles, as illustrated by the recent results from prolonged neutron irradiation of plutonium.[32] The basic systematics of alpha radioactivity herein developed was presented in a series of three papers by Perlman, Ghiorso, and Seaborg in the period

1948-1950.[33, 34, 9] Closed cycle calculations were discussed in these papers. At the same time, in an attempt to develop an electron capture systematics, Thompson[35] used closed cycle calculations to obtain electron capture energies to make his graph of electron capture half-life versus disintegration energy. His treatment has since been extended by Hoff[36] to include consideration of ft products and selection rules as well as a much larger range of nuclides. The energy aspects of heavy region systematics, i.e., closed cycles, masses, and neutron and proton binding energies were most recently put forth by Seaborg.[37]

It is worthwhile to mention the philosophy adopted in the present approach to systematics. The main emphasis is on the energies and half-lives themselves rather than their theoretical interpretations. The systematic trends are looked upon as means for evaluating previous data and pointing to possibly inaccurate data as well as predicting properties for undiscovered isotopes. Characteristics observed in energy and half-life data are presented and the discussion limited to qualitative statements, leaving the more theoretical analysis, which is not the purpose of the present treatment, for studies directed to this purpose. It is realized that since data is continually being added and changed the present systematics is merely a further step along a never ending road.

The procedure in the present investigation can be outlined briefly. Measured alpha and beta energies are presented in the form of closed cycles. Further energies are calculated from conservation of energy (so-called nuclear thermodynamics) on these cycles. All of the alpha and beta energies are then plotted on separate

graphs of decay energy versus mass number. The trends of the curves are in turn used for the estimation of other desired energies. These estimates are placed on the closed cycles and all possible further energy calculations made. This completes the collection of decay energy data. Then, using three measured neutron binding energies among the lead isotopes and the measured mass of Pb^{208}, the cycles energies are employed to calculate the masses of all the nuclides considered, both known and unknown. Next the neutron and proton binding energies are calculated and presented on plots of binding energy versus A. In the following part, the closed cycle beta energies are employed to calculate the Bohr-Wheeler parameters, B_A, Z_A, δ_{AE}, and δ_{AO}. Finally the half-life versus energy plots are presented for alpha, beta$^-$, and electron capture decay. Other possible correlations are excluded from the present investigation. For example, the relations of slow neutron capture cross sections[38] and the ratios of slow neutron fission to capture cross sections[39, 40] both to neutron binding energies are not considered. Likewise, no mention is made of the application of the masses to the calculation of Q values of spallation reactions.

It should be re-emphasized that, due to the fact that decay energies and half-lives are continually being added or revised, development of the systematics is a never ending process. In certain areas significant alterations in predicted properties have been necessary in the past. Although the general features of the energy surface are believed to be correct, future revisions in some places are certain to occur. The present collection of data was terminated as of April 1954.

B. Accumulative Decay Energy

1. Closed energy cycles. -- The first important aspect of any systematics, of course, is the collection of experimental data employed. In the present work the measured alpha and beta decay energies are presented in the form of "closed decay energy cycles". All data not given specific reference in this section of the thesis were taken from the recent Table of Isotopes.[41] The use of the cycles can be illustrated simply. For example, Bi^{212} decays by beta emission to Po^{212} which in turn decays by alpha particle emission to Pb^{208}. The sum of the beta decay energy of Bi^{212} (2.25 Mev) and the alpha decay energy of Po^{212} (8.94 Mev) is 11.19 Mev. At the same time some of the Bi^{212} nuclei (33.7 percent) decay by alpha emission to Tl^{208} which then decays to Pb^{208} to complete the cycle. In this case, the alpha decay energy of Bi^{212} (6.20 Mev) and the beta decay energy of Tl^{208} (4.99 Mev) again make a total of 11.19 Mev. The fact that the total energies are the same is a consequence imposed by the law of conservation of energy, since the initial and final nuclei, as well as the two types of particles emitted, are the same by both paths. Thus it is seen that the cycles bear a similarity to the Born-Haber and Carnot type cycles of thermodynamics; in fact, the decay energy cycles have been referred to as "Nuclear Thermodynamics".[40] The cycle just described is represented diagramatically as follows:

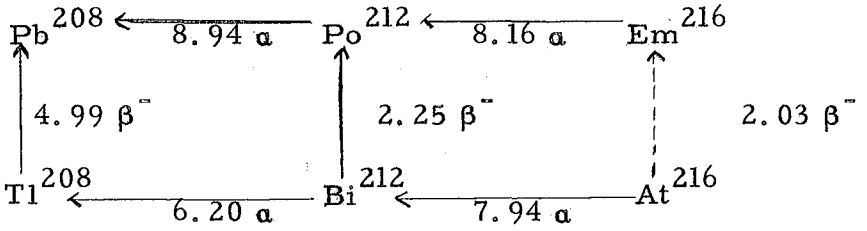

Alpha decay is represented as proceeding from right to left and beta$^-$ decay as proceeding upwards. Also pictured in the diagram are two isotopes, Em^{216} and At^{216}, which decay by alpha emission into Po^{212} and Bi^{212}, respectively, in the completely closed cycle just discussed. By closing the third side of the new cycle formed, by subtacting 8.16 Mev from the sum of the 7.94 Mev and 2.25 Mev sides a beta$^-$ energy of 2.03 Mev is calculated for At^{216}. Hence, beta instability is predicted for this isotope for which it is not observed, due to its very short half-life. By extending the alpha chains even further, additional beta decay energies can be calculated. All known alpha and beta decay energies of nuclides above mercury are collected in the complete closed cycles which are presented in Figs. 2-5. Since alpha and beta decay chains connect only nuclides in a given series, four sets of cycles are necessary. Additional decay energies connected with the aid of lead and thallium neutron binding energies are presented in Fig. 6. Energies included in the cycles which are not catalogued in the Table of Isotopes or are not listed as the preferred values are listed in Table 1. The neutron binding energies for Fig. 6 are tabulated later in Table 5.

Because it is the energy surface made up of the ground states of the nuclei that is of interest here, it is important that ground state transitions be observed in the decay of the isotopes. In the sample cycle just described, the alpha particle representing the 6.20 Mev alpha decay energy of Bi^{212} is in only 27.2 percent abundance, the main alpha group going to a 0.04 Mev excited

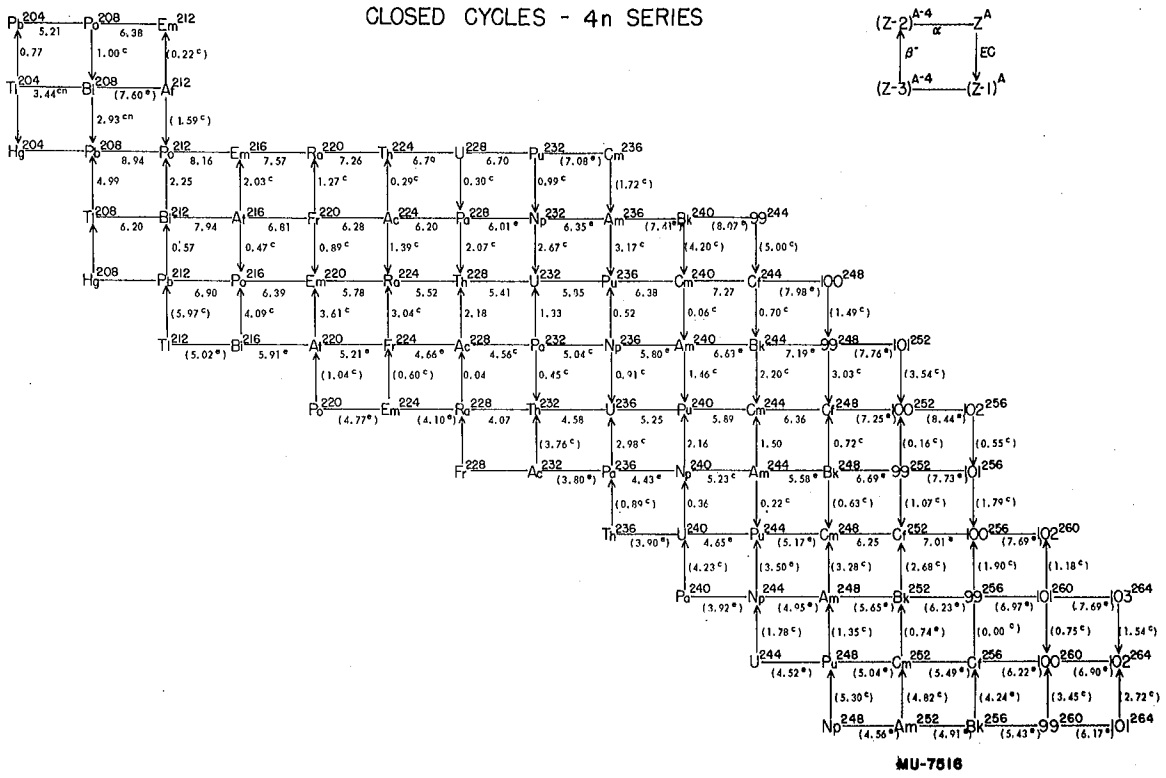

Fig. 2. Closed decay energy cycles for the 4n series: c, calculated energies; e, estimated energies; ( ), uncertain energies.

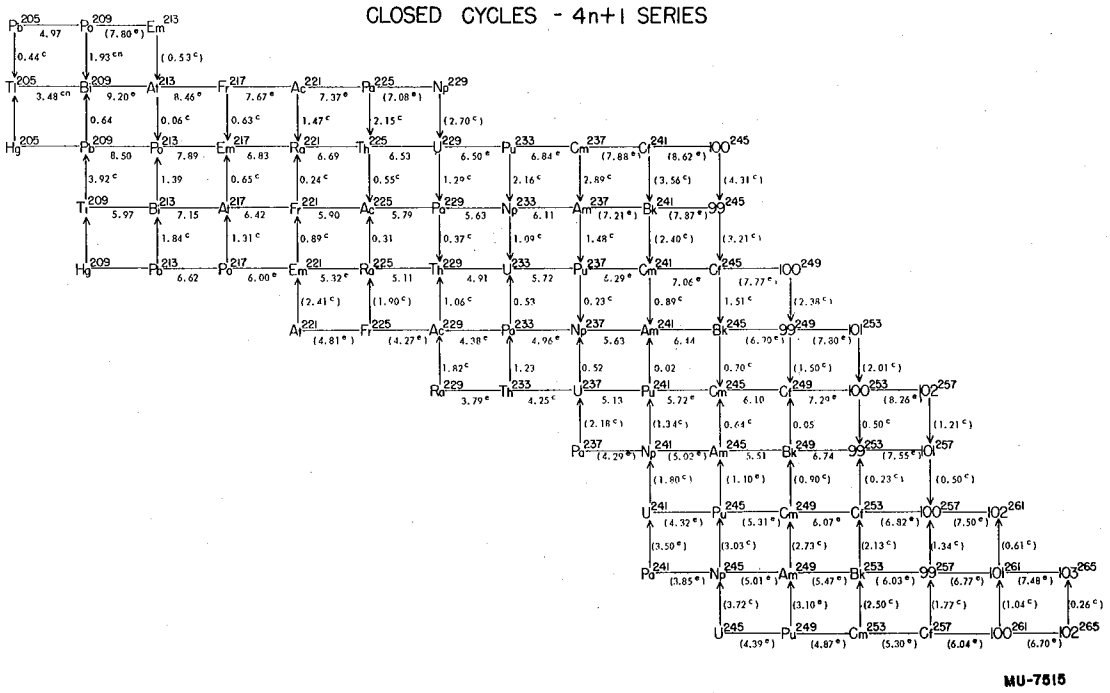

Fig. 3. Closed decay energy cycles for the 4n + 1 series: c, calculated energies; e, estimated energies; ( ), uncertain energies.

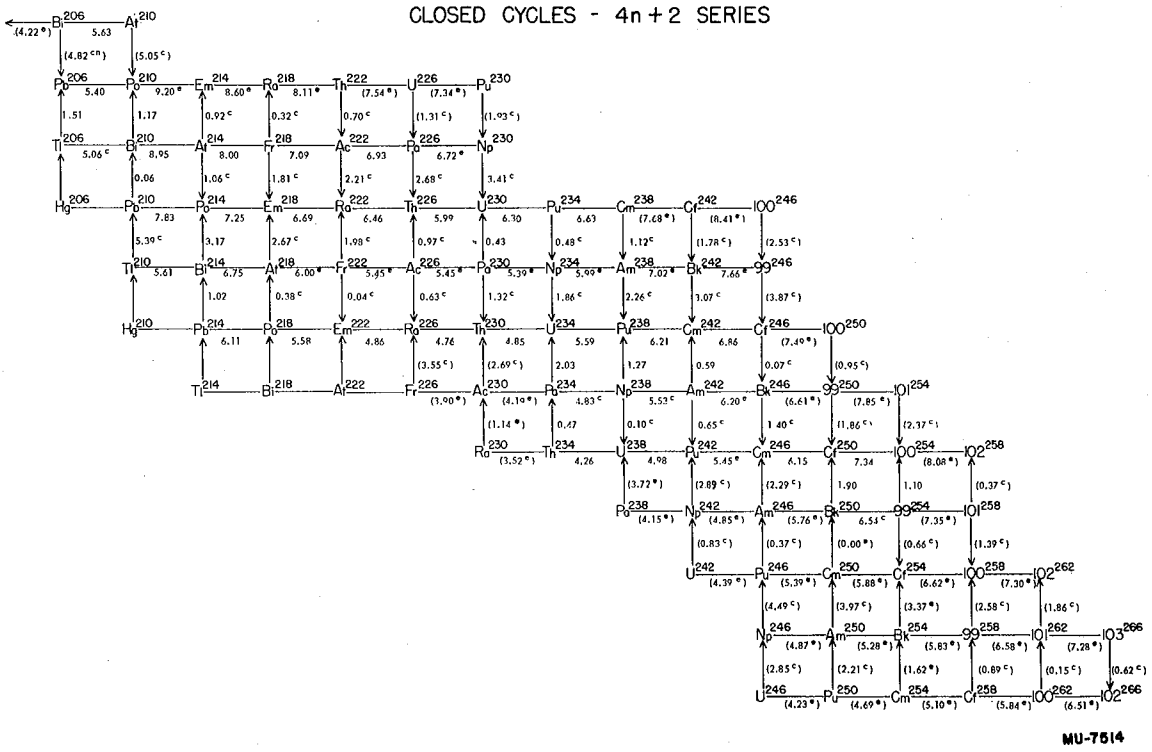

Fig. 4. Closed decay energy cycles for the 4n + 2 series: c, calculated energies; e, estimated energies; ( ), uncertain energies.

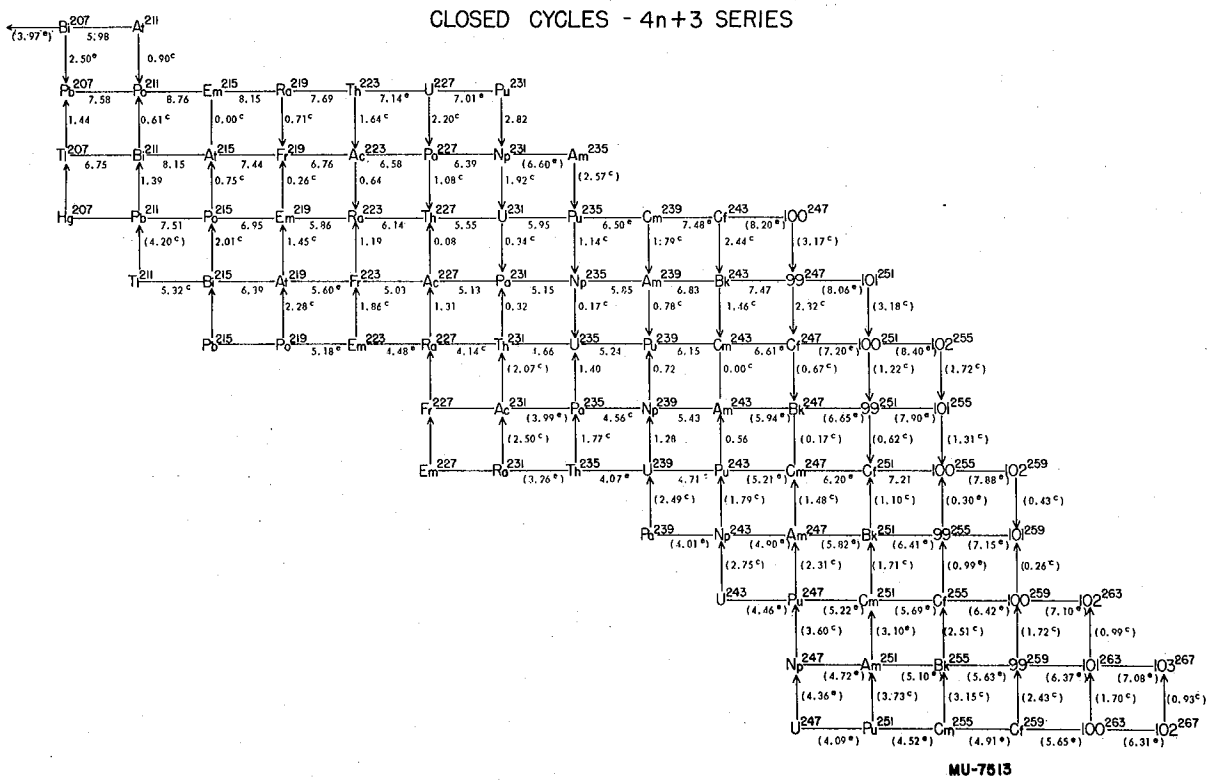

Fig. 5. Closed decay energy cycles for the 4n + 3 series; c, calculated energies; e, estimated energies; ( ), uncertain energies.

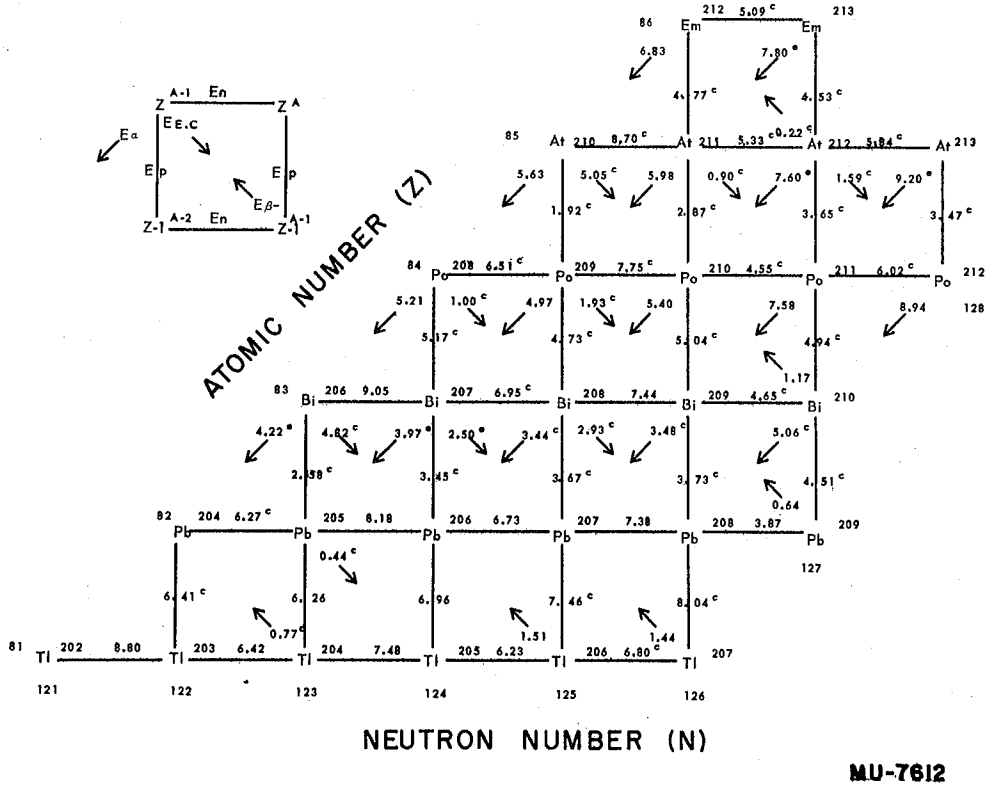

Fig. 6. Neutron binding energy cycles in the region of bismuth.

Table 1
Decay Energies Included in the Cycles and Not in the Table of Isotopes

Nuclide	Decay Energy (Mev)		
	Type	Energies accepted	Decay energy accepted
4n series			
Po^{212}	α	8.945 α [42]	8.94
Pb^{212}	β^-	0.569 β^-	0.57
Em^{220}	α	6.394 α [43]	6.39
U^{232}	α	5.411 α [44]	5.41
Th^{232}	α	4.068 α [45]	4.07
Pa^{232}	β^-	0.28 β^- + 1.05γ	1.33
Np^{236}	β^-	0.52 β^- [46]	0.52
Cm^{240}	α	6.38 α [47]	6.38
Np^{240}	β^-	2.156 β^- [48]	2.16
U^{240}	β^-	0.356 β^- [48]	0.36
Am^{244}	β^-	1.50 β^- [49]	1.50
Cf^{248}	α	6.36 α [50]	6.36
Cf^{252}	α	6.25 α [51]	6.25
4n + 1 series			
U^{237}	β^-	0.25 β^- + 0.27γ [52]	0.52
Am^{241}	α	5.63 α	5.63
Pu^{241}	α	4.98 α [53] + 0.15γ	5.13
Cf^{249}	α	6.10 α [49]	6.10
Bk^{249}	β^-	0.05 β^- [54]	0.05
	α	5.51 α [54]	5.51
99^{253}	α	6.74 α [55]	6.74
4n + 2 series			
Pb^{214}	β^-	0.73 β^- [56] + 0.29 α [56]	1.02
Ra^{222}	α	6.687 α [44]	6.69
Em^{222}	α	5.583 α [43]	5.58
Th^{226}	α	6.456 α [44]	6.46
U^{230}	α	5.993 α [44]	5.99
Pa^{230}	β^-	0.43 β^-	0.43

Table 1 (Cont'd)

Nuclide	Decay Energy (Mev)		
	Type	Energies accepted	Decay energy accepted
4n + 2 series (Cont'd)			
Pa^{234}	β^-	1.15 β^{-} [57] + 0.88γ [57]	2.03
Th^{234}	β^-	0.19 β^{-} [58] + 0.28 I.T. [59]	0.47
U^{238}	α	4.259 α [45]	4.26
Np^{238}	β^-	1.272 β^-	1.27
Am^{242}	β^-	0.59 β^-	0.59
Pu^{242}	α	4.980 α [53]	4.98
Cf^{250}	α	6.15 α [49]	6.15
Bk^{250}	β^-	1.9 β^{-} [49]	1.90
100^{254}	α	7.34 α [55]	7.34
99^{254}	β^-	1.1 β^{-} [55]	1.10
4n + 3 series			
Ra^{223}	α	5.855	5.86 [60]
Fr^{223}	β^-	1.14 β^{-} (1.15 ± 0.05 [61]) + 0.05γ [61]	1.19
Ra^{227}	β^-	1.31 β^{-} [62]	1.31
Pu^{243}	β^-	0.56 β^{-} [63]	0.56
100^{255}	α	7.21 α [55]	7.21

state of Tl^{208}. In the case of Am^{241} only 0.34 percent of the alpha decay goes to the ground state of U^{235} while in Cm^{243} alpha decay the ground state transition has not been observed. For nuclei with an odd number of neutrons and/or protons in the regions of bismuth and uranium, the ground state transitions are in general not the most abundant. On the other hand, for even-even nuclei the ground state transition is always in major abundance; in fact for Po^{212} the 8.94 Mev alpha particle is the only one observed. The beta decay energies present a similar problem in determining ground state transitions. For example, the main path of decay for Tl^{208} is by the emission of a 1.79 Mev beta particle followed by two gamma rays of 0.58 Mev and 2.62 Mev, respectively, making a total of 4.99 Mev decay energy. At the same time, a 2.25 Mev beta particle carries off all of the transition energy for Bi^{212}. It should be noted that all alpha energies in this section of the thesis are alpha disintegration energies; that is, the alpha recoil energy is added to the alpha particle energy. The disintegration energy can be simply calculated from the alpha particle energy by the formula

$$Ed_{\alpha} = E_{\alpha} \frac{Ap}{Ad},$$

where Ap is the mass number of the alpha emitting nuclide and Ad is the mass number of the product nuclide.

The energies tabulated in the cycles have been determined in three ways. The energies without superscripts are measured values, while those with superscript "c" have been calculated by "closing cycles", and those with superscript "e" have been estimated. Calculated values are based on both measured and

estimated energies. The numbers of energies determined by the various methods in the four sets of cycles are given in Table 2.

Table 2

Energies Used in the Cycles

Type	Measured	Calculated	Estimated
α	105	13	179
β^-	41	108	13
EC	0	116	1

Total nuclides known: 181

Total nuclides unknown: 163.

The alpha and beta energy estimates have been made by interpolation and extrapolation from measured values on the energy versus mass number graphs (Figs. 7 and 8, respectively). In addition to the energies listed in the table, a number of measured alpha energies for nuclides with less than 126 neutrons, which are not as yet placed in the cycles due to the fact that they are only connected by electron capture decay, are employed in the energy-mass number and half-life-energy correlations.

It can immediately be seen from Table 1 that the bulk of the measured energies are alpha disintegration energies. These form the framework for the cycles. Actually, between two neighboring chains of successive alpha emitters, only one measured beta energy is needed to calculate the rest of the beta energies along the chain. For example, U^{229} and Pa^{229} decay by the emission of four alpha particles to Po^{213} and Bi^{213}, respectively. Then with the measured beta energy of Bi^{213}, the beta separation energies of At^{217} - Em^{217},

Fr^{221} - Ra^{221}, Ac^{225} - Th^{225}, and Pa^{229} - U^{229} can be calculated. In this 4n + 1 series, a total of only ten beta energies are necessary to establish the connections between alpha chains. Where more than one beta energy has been measured in a long chain, the problem is overdetermined. In this case, if the second measured energy is the same as the value calculated on the basis of the first, a good check on the accuracy of the energies in the chain is obtained. In the event that the energy is different, the measured value as well as other measured and estimated energies in the chain must be critically evaluated to determine which may be in error and corresponding changes in the cycles made. For example, the measured beta$^-$ energies of Bi^{214}, Ac^{226}, and Pa^{230} all occur along the same chain in the 4n + 2 cycles. In this case the measured energies of Bi^{214} (3.17 Mev) and Pa^{230} (0.43 Mev) are accepted and that of Ac^{226} (1.17 Mev), which was determined by an absorption method, assumed to be high by 0.2 Mev. Although there are alpha estimates in the chain and the Pa^{230} beta$^-$ energy was also determined by absorption, the best over-all fit is believed to be that shown in the cycles. This is partly because the alpha estimates of Fr^{222}, Ac^{226}, and Pa^{230} are interpolations from smooth lines on the alpha energy - mass number graph (Fig. 6) and are considered to be fairly accurate. In addition, if the estimated alpha energy of Fr^{222} were increased by over 0.04 Mev to fit the Ac^{226} energy, Em^{222} would be indicated to be beta$^-$ unstable, which is not thought to be the case at present. Thus, the beta$^-$ energies chosen between each chain of alpha emitters are a result of a consideration of their effects on all cycles involved. Once a suitable set of calculated beta

energies is obtained, they can be used to aid in the working out of decay schemes for the nuclides in the cycles.

If is of interest to note how the cycles have been filled out. Consider, for example, the 4n + 2 series just referred to. The long-lived parent of the series, U^{238}, maintains the rest of the naturally occurring series in equilibrium. The main decay chain occurs through the following series: U^{238} (α), Th^{234} (β^-), Pa^{234} (β^-), U^{234} (α), Th^{230} (α), Ra^{226} (α), Em^{222} (α), Po^{218} (α), Pb^{214} (β^-), Bi^{214} (β^-), Po^{214} (α), Pb^{210} (β^-), Bi^{210} (β^-), Po^{210} (α), and Pb^{206} (stable). From a study of these nuclides a large number of alpha and beta$^-$ energies are obtained for the cycles. In addition to this basic chain the collateral alpha chains starting with $U^{230\ 64}$ and $Pa^{226\ 30}$ have been produced by high energy alpha particle and deuteron bombardments of Th^{232}. These help fill out the neutron deficient side of the 4n + 2 series. It can be seen that another collateral series starting with Pu^{230} or U^{226} still remains to be discovered, although in this case the half-lives are expected to be very short. Other isotopes in the series have been produced by bombardments of known nuclides in the cyclotron or chain-reacting piles. In the latter case, since neutrons are added to the starting nucleus, the neutron excess or beta$^-$ unstable side of the series is reached. This side of the series is rather difficult to obtain by cyclotron bombardments because reactions such as the (d, 3p, n) are required. For example, Ra^{230} was produced from Th^{232} by this reaction.[65] In this connection, it might be anticipated that a search for alpha branching products of Ra^{228} in the 4n series would yield data on the neutron excess side of beta stability. The

transuranium nuclides in the cycles were produced by both cyclotron bombardments and pile irradiations.[66]

The uncertainties in the energies listed in the four cycles vary greatly with the individual decay considered. In general, alpha spectrograph and beta spectrometer values are accurate to at least ±0.01 Mev. Alpha pulse analyzer (ionization chamber) energies are probably accurate to ± 0.02 Mev. On the other hand, beta energies determined by absorption methods may be uncertain by ±0.1 Mev or greater. Gamma energies likewise have a rather wide range of uncertainties, depending on whether they have been determined from conversion electron energies in a beta spectrometer (ca. ±0.01 Mev), in a scintillation counter (ca. ±0.02 Mev), or by absorption (ca. ±0.1 Mev). An additional uncertainty arises when it is not certain that the ground-state transition (or transitions) have been observed. For example, it is likely that the alpha particle from Np^{235} leading to the ground state of Pa^{231} has not been observed. In lieu of further information in this case, however, the measured alpha energy is accepted. In view of this type of situation, no extensive error treatment leading to the assignment of an uncertainty to each energy has been performed. On the other hand, it is felt that the overall picture is not a poor one; that is, it is considered unlikely that errors have accumulated in one direction along a decay chain to the extent of 0.5 Mev. This is both because there are few noticeable exceptions to the regularities observed in alpha energy, beta energy, binding energy, and Bohr-Wheeler systematics, and because certain checks on accumulative decay energy are available

when the measured masses and neutron binding energies in the region of lead and the region of thorium and uranium are considered in relation to the decay energies between the regions. The latter arguments are presented further on in the thesis. One of the great advantages of developing an overall systematics is just this matter of cross-checks on the data.

An indication is given of anticipated uncertainties in individual energies in the cycles by the use of parentheses. Energies without parentheses are believed to be accurate to at least a tenth of a Mev or so. Those with parentheses may be inaccurate by greater than 0.1 Mev. Of course, energies for the undiscovered elements 101, 102 and 103 are likely to be in error by 0.5 Mev or greater. In general, alpha energies estimated from Fig. 8 which require an extrapolation of over one mass number for a given element from isotopes whose energies have been measured are placed in parentheses. Likewise, all beta$^-$ estimates are placed in parentheses. In addition, all energies calculated from energies in parentheses are themselves placed in parentheses. This type of assignment is also applied to other properties derived from the decay energies such as nuclear binding energies, masses, and Bohr-Wheeler parameters.

It might be questioned whether it is worthwhile quoting all energies listed to the hundredth of a Mev and extending the cycles far beyond the measured values. In regard to the first question, the energies are presented to the second decimal place because a large share of the determined energies are accurate to this extent and

many of the estimated energies may be that accurate, so for uniformity of presentation, all energies are tabulated to three significant figures. As more data are collected, it is anticipated that future cycle energies will approach more and more closely this level of accuracy, so that refinements in the present cycles will continually lead to a truer representation of energy relations. In regard to the second question, it is obviously of value to have predictions of energies for unknown isotopes and elements. Before elements 99 and 100 were discovered predictions of their properties were available. At the present time predictions for isotopes of 101, 102, and 103 are included in the cycles. Even in cases where the predicted decay will probably never be observed, the prediction of an energy is of value. For example, the alpha energy of Cm^{249} is estimated in the 4n + 1 cycles. Although this is of limited value in itself the energy is a link in the chain between the estimated Pu^{245} beta$^-$ energy and the calculated 101^{257} electron capture energy, thus, a preferred beta$^-$ energy estimate (Pu^{245}) can be used to calculate an energy more difficult to estimate by itself. The present illustration is particularly of value in that it indicates that 100^{257} is not the first beta$^-$ unstable isotope of element 100 and hence element 101 cannot be reached by neutron irradiation of element 100 at this point. Thus, the cycles are presented which include a large number of undiscovered nuclides. It is hoped that they will include all the isotopes that will be found within the next several years at least.

Another valuable result from the cycles is the prediction of beta stable nuclides. These nuclides are analogous to the stable isotopes in the lighter element region and, indeed, they would be

stable themselves were it not for alpha instability, which is a property of all nuclides above the lead region. Beta stability is predicted for a nuclide if both neighboring isobars are beta unstable with respect to it. Thus, Np^{237} is beta stable due to the fact that U^{237} decays to it by beta$^-$ emission (0.52 Mev decay energy) and Pu^{237} decays to it by electron capture (0.23 Mev) as indicated in Fig. 3. The beta stable isotopes included in the cycles are shown in a chart of the nuclides, Fig. 7. Beta stable isotopes are indicated by black squares. The nuclides to the right of these squares, of course, are beta$^-$ unstable while those to the left are electron capture unstable. In general there are between five and seven beta stable isotopes for each element with an even atomic number. There is usually only one beta stable isotope for each odd Z element, although there are occasionally two. For a number of mass numbers the beta stable nuclide or nuclides are not certain. These are indicated by shaded squares representing possible beta stable nuclides. It is possible that there are no beta stable isotopes of astatine and probable that there are none of berkelium. These elements, then, would be analogous to technetium and promethium which are missing in nature. The fact that astatine may have no beta stable isotopes might be a consequence of its position just beyond the 126 neutron closed shell.[9] It is also interesting to note that Em^{212} may be beta stable due to the fact that it has 126 neutrons. If Cm^{240}, Cm^{243}, and Cm^{250} are beta stable, curium has nine such isotopes, a number greater than that for any element with the exception of tin. Again this may be a consequence of a closed

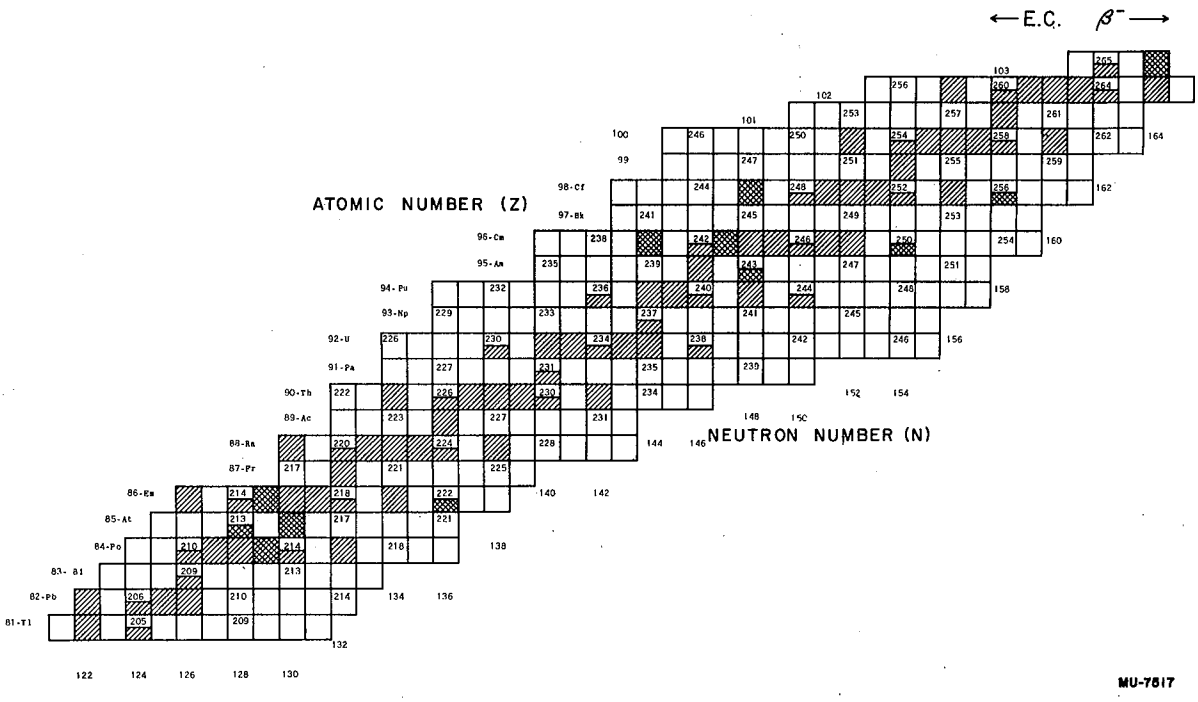

Fig. 7. Chart of the nuclides showing the occurrence of beta stable isotopes in the region of the heaviest elements.

subshell at 96 protons as suggested by Seaborg.[67] The case of Am^{243} and Cm^{243} is of particular interest inasmuch as Am^{243} has been observed for beta$^-$ decay[68] and Cm^{243} has been observed for electron capture decay.[69] These isobars may, indeed, have identical masses as predicted by the closed cycles.

The discussion of individual energies in this section will be limited to a few examples, mainly because in general the problems in the cycles can be resolved only by further experimental data, and although there is some value in pointing out places where these data are more urgently needed, it can easily be seen from the Table of Isotopes where conflicting information has been reported and also from the cycles where the experimental energies are sparse. In all of the cycles there are only three cases where the small cycles are completely closed by measured energies. These are the fore-mentioned example of the Bi^{212} - Pb^{208} cycle, the Ac^{227} - Ra^{223} cycle, and the Pu^{241} - Np^{237} cycle. The first cycle balances quite naturally; that is, without adjustment of the energies involved, although a rather elaborate decay scheme for Tl^{208} is required. In the second cycle the beta$^-$ decay energies of Ac^{227} and Fr^{223} are open to question although it is doubtful that either energy is wrong by more than 0.05 Mev. The 0.04 Mev measured beta energy of Ac^{227} is of doubtful accuracy as are all the low beta energies in the cycles, such as those for Pb^{210}, Ra^{228}, and Bk^{249}, but again the beta$^-$ energy itself can hardly be wrong by more than several hundredths of a Mev. In addition, the ground state alpha particles from Ac^{227} or Th^{227} may not have been observed, in which case either or both alpha energies may be too low. For Th^{227} there is some evidence that

this is so,[60] although it is difficult to see whether the compensating energy should be added to the Ac^{227} or Fr^{223} decay. The Pu^{241} - Np^{237} cycle balances if the 0.15 measured gamma ray of Pu^{241} is assumed to be in coincidence with the measured alpha.

A fourth cycle, which is nearly balanced by measured energies is the Bi^{210} - Pb^{206} cycle, which can be used to illustrate the problem of isomers. The cycle as shown in Fig. 4, which employs the beta$^-$ energy of RaE along with the alpha energy of Po^{210} and the beta$^-$ energy of Tl^{206}, is used to calculate an alpha disintegration energy of 5.06 Mev for RaE. This energy is greater than the energy of 5.03 Mev measured for the alpha particles of the long-lived Bi^{210} isomer and therefore it appears at first observation that RaE is an excited state of Bi^{210}, lying about 0.03 Mev above the long-lived isomer. Indeed, this may be the case, but on the other hand it is not certain that the 5.03 Mev alpha from the long-lived isomer leads to the ground state of Tl^{206}. If the decay leads to an excited state of greater than 0.03 Mev, RaE is the ground state of Bi^{210}. The problem of isomers in this case is not serious because the energy involved is not large. It is more serious in the UX1 - UX2 - UZ - UII chain. This chain is directly initiated by the decay of U^{238} and has been known and studied for a long time. Despite the efforts to determine the decay schemes involved, the cycle beta$^-$ decay energies of Th^{234} and Pa^{234} must be considered as relatively poor. The sum of the decay energies is known to be 2.50 Mev, derived from the sum of the 0.19 Mev β^- of Th^{234} and the 2.31 Mev β^- of Pa^{234m}. Due to the complexity of the beta and gamma structure

in UX_2 (Pa^{234m}) and UZ (Pa^{234}), however, efforts to firmly establish the isomeric transition energy have been unsuccessful.[57, 58] Either the determination of the exact UZ decay scheme or the direct observation of the isomeric transition gamma ray in UX_2 are needed to establish this transition energy. The value of 0.28 Mev accepted in the present work represents one possible decay scheme of UZ[57] and is intermediate between the extreme values reported: 0.39 Mev[41] and 0.23 Mev.[70] The total decay energy of Th^{234} and Pa^{234} (2.50 Mev) can be combined with the alpha decay energy of U^{238} (4.26 Mev) and the beta$^-$ energy Np^{238} (1.27 Mev) to give the electron capture energy of Np^{238} (0.10 Mev). This energy represents the degree of stability of U^{238} to beta$^-$ decay and it is seen that U^{238}, and therefore its decay chain, might have been missing in nature if the energy surface in this region were slightly different.

Finally, a few of the important decay energies that need further investigation should be mentioned. In the case of the beta$^-$ decay of Pb^{212} it is not known whether 0.57 Mev or 0.59 Mev is a better value for the beta particle leading to the ground state of Bi^{212}. In addition, the complete beta$^-$ decay schemes of Pa^{232}, Ra^{225}, Pa^{233}, Ac^{226}, and Pa^{230} have not been determined up to the present time.

2. Alpha energy systematics. -- All of the alpha energies employed in the cycles are shown on the graph of alpha disintegration energy versus mass number, Fig. 8. This graph represents a considerable extension of previous graphs[9] of this type, in that the latest measured values as well as a large range of estimates are included. For the elements from francium through berkelium the alpha energies in general decrease regularly with increasing mass

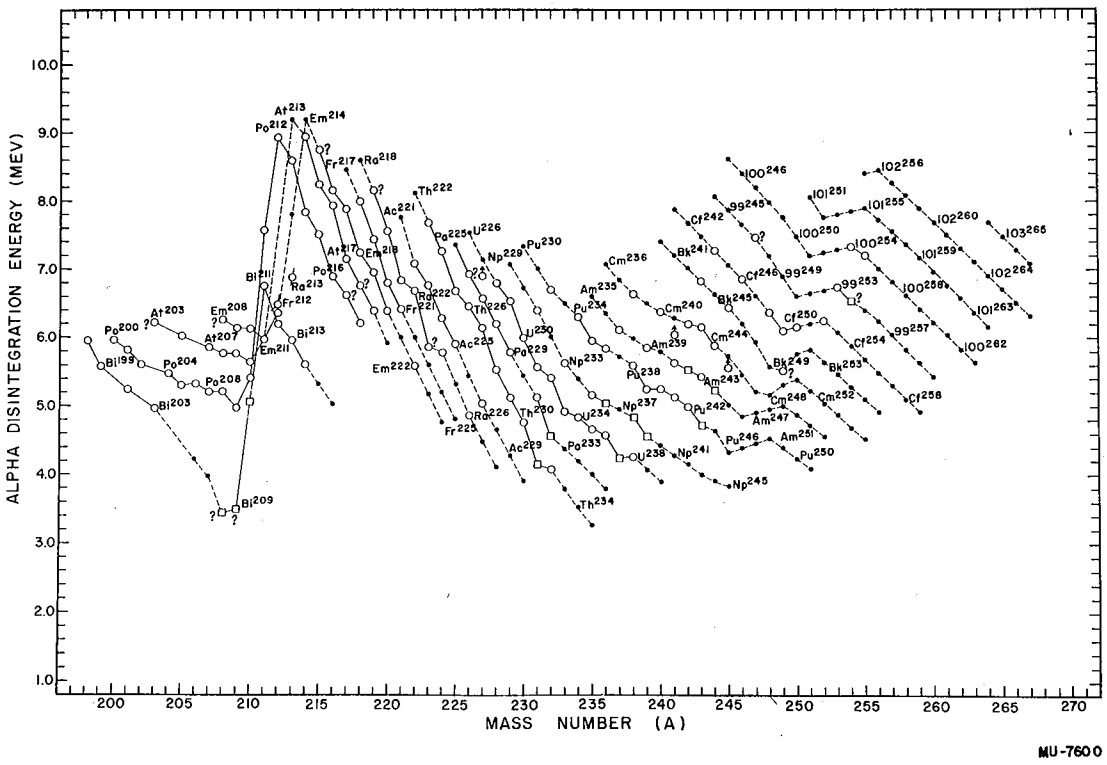

Fig. 8. Alpha decay energies for the isotopes of the elements above lead as a function of mass number: O, experimental energies; □ calculated energies; ●, estimated energies.

number, which is a consequence of the manner in which the alpha decay process crosses the energy surface.[9] In addition, the lines connecting each element above the region of uranium are successively at higher energies, indicating that the slope along the length of the Heisenberg valley is increasing rather sharply.

The estimations of alpha energies have been made by interpolations between measured and calculated values and extrapolations from them. Although there appear to be many small discontinuities in most of the lines for the elements, because of the lack of regularity in the deviations in some cases, the estimates have in general been taken from smooth lines extended between and beyond the measured energies. In the extrapolations account is taken of the slight concavity upwards of the lines; a particularly noticeable effect in the cases of uranium and plutonium. The lines for elements 101, 102, and 103 were placed on the graph by assuming that the spacing between these lines and that between elements 100 and 101 would be about the same as the average spacing between the californium and element 99 lines, and the element 99 and element 100 lines. It is possible, of course, that the spacing will again become smaller and more nearly the same as that observed among the lighter elements, indicating that the Heisenberg valley is leveling off, in which case the estimates will be in error.

The two most striking irregularities in the lines are the sharp discontinuities in the region of mass number 213 and in the region of mass number 250. The first series of irregularities is undoubtedly associated with the special stability of nuclei with

126 neutrons (closed shell) as discussed by Perlman, Ghiorso, and Seaborg.[9] The nuclide Po^{212} for example, decays to Pb^{208}, which has both 126 neutrons and 82 protons and therefore is stabilized by two closed shells. As a result of this its alpha energy lies at the peak of the polonium line. The nuclide Po^{210} on the other hand contains 126 neutrons and is itself stabilized, leading to a low value for its alpha energy. Similar behavior is observed in the lines for other elements which are associated with the closed shell. At present there is no satisfactory explanation why the isotopes with one neutron less than 126 have lower alpha energies than those with 126 neutrons. This behavior is exhibited in the cases of Bi^{208}, Po^{209}, At^{210}, and Em^{211}. The effect of the 126 neutron closed shell is reflected in a discontinuity of about 3-4 Mev in the alpha lines of the elements involved.

The second series of discontinuities may be associated with a subshell at 152 neutrons.[71] In this case the most compelling experimental evidence lies in the alpha energy line for the californium isotopes. The alpha energies for Cf^{250} and Cf^{252} represent a rather sharp break from a linear extrapolation of the Cf^{244}, Cf^{246}, and Cf^{248} points. In addition, the low alpha energy of Bk^{249}, which contains 152 neutrons, may indicate special stability for this nuclide, although in this case the ground state alpha transition may not have been observed. In this connection it is worthy of note that the highest energy alpha particles of Bk^{243} and Bk^{245} have 0.17 Mev and 0.19 Mev greater energy, respectively, than the groups in largest abundance. If about this energy is added to the Bk^{249} measured alpha energy the

point on the graph is not quite as low. At the same time, however, such an increase would cause the calculated beta$^-$ energies for Am^{245} and Np^{241} to be rather low, as can be seen from Fig. 9. The high alpha energies for 99^{253}, 99^{254} (calculated), 100^{254}, and 100^{255} also tend to indicate that the same type of discontinuity may occur in the 99 and 100 lines even though it has not as yet been observed. If linear extrapolations to lower mass numbers are made on the basis of 99^{253} and 99^{254} energies and on the basis of 100^{254} and 100^{255} energies, unduly high alpha energies are obtained for the neutron deficient isotopes of these elements with respect to the californium isotopes. If the assignment of 99^{247} is correct it appears that there may indeed be a discontinuity in the element 99 line similar to that observed in the californium line. That the discontinuity may carry on through the lighter elements is indicated by the fact that the calculated alpha energies of Am^{244} and Pu^{243} are low with respect to the other americium and plutonium isotopes in the same way that Cf^{248} is low with respect to Cf^{244} and Cf^{246}. All three energies are examples of a drop in alpha energy occurring several isotopes before the 152 neutron subshell. At the present time it seemed desirable to draw discontinuities similar to the break in the californium line for all elements extending to the 152 neutron region, as would be expected to be the case if the 152 neutron configuration is, in reality, particularly stable. The interpretation of the behavior of the californium line[71] is that Cf^{252}, with 154 neutrons, decays into a subshell at 152 neutrons and therefore has a high alpha energy, whereas Cf^{250} and Cf^{249}, with 152 and 151 neutrons, are stabilized and hence have low alpha energies. The situation is similar to that for the 126 neutron

closed shell where the isotope with one less neutron than the closed shell number has the lowest alpha energy, although again the highest energy measured alpha particle of Cf^{249} (with one odd neutron) may not be the ground state transition. The magnitude of the discontinuity in the californium alpha energy line is about 0.6 Mev; that is, the alpha energy of Cf^{252} is 0.6 Mev higher than would have been predicted on the basis of the Cf^{244}, Cf^{246}, and Cf^{248} energies. There is no corresponding effect noticeable in the beta energy and binding energy correlations presented further on; however, these properties, which have for the most part been calculated from other energies, are subject to cumulative errors that would tend to mask the effect. In any event, a great deal more data is necessary before the subshell is proved or disproved.

Besides the large discontinuities in the alpha energy lines, there are many smaller irregularities that do not appear to be associated with closed shell effects. Since the terms referring to nuclear type will be frequently used in the remaining portions of the thesis, they have been tabulated and defined in Table 3. The types are listed in order of decreasing stability; that is, even-even nuclei are the most stable and odd-odd nuclei the most unstable.

Table 3
Nuclear Types

Type	Example	Atomic number (Z)	Neutron number (N)
Even-even	Cm^{242}	Even	Even
Even-odd	Cm^{241}	Even	Odd
Odd-even	Am^{241}	Odd	Even
Odd-odd	Am^{242}	Odd	Odd

In general the smoothest lines that can be drawn on the graph are those connecting the alpha energies of even-even isotopes. Many even-odd nuclides have alpha energies which lie below these lines. For example, the points for U^{231} and U^{233} are low. Again the points for Pu^{235} and Pu^{239} are below a line connecting the alpha energies for the neighboring even-even isotopes. In the cases of Ra^{223} and Pu^{239} the alpha spectra have been determined with an alpha spectrograph and it is likely that the ground state transitions have been observed. At the same time, the alpha energies of Th^{227}, U^{229}, and Cm^{243} are high with respect to the energies of the neighboring even-even isotopes, so there appears to be no unique correlation of alpha energies with the odd-even character (nuclear type) of the alpha emitter. For three even-odd nuclides included in Fig. 8 it is assumed that the measured alpha energy does not correspond to the ground state transition. These nuclides are U^{227}, Cm^{241}, and Cm^{245}. In the case of U^{227} the measured alpha energy is uncertain. Energy is added to the curium alpha energies both because the measured energies are considerably below the line formed by the points for the other isotopes and because in the case of another odd neutron isotope, Cm^{243}, the alpha particle in highest abundance leads to an excited state of Pu^{239} which is several tenths of a Mev above the ground state.

Another characteristic of the alpha energy versus mass number graph is the nearly straight line obtained when the points for alpha emitters with the same number of neutrons are connected. For example, the alpha energies for U^{238}, Np^{239}, Pu^{240}, Am^{241}, Cm^{242}, Bk^{243}, and Cf^{244}, all containing 146 neutrons, all lie on a

nearly straight line.

The calculated values for the alpha energies of Bi^{208} and Bi^{209} are also of interest because they fill out the dip in the line connecting the bismuth alpha energies. These energies have been calculated from the binding energy cycles presented in Fig. 6. In the case of Bi^{209} the calculated energy has been accepted in preference to recently reported measured values[72, 73] because these were determined from a small number of alpha tracks in nuclear emulsions and there is a discrepancy among the calculated alpha half-lives.[74]

There are additional regularities and further individual energies of interest with regard to the alpha energy graph, but the previously discussed examples sufficiently illustrate the energy aspects of the alpha systematics. The alpha energy versus mass number graph is the most important energy correlation employed here, mainly because it is felt that in general the alpha decay energies are known with a reasonable degree of certainty, and therefore regularities in the lines for the elements can be used with confidence as a basis for estimating a large number of decay energies. In this connection, estimations of alpha energies followed by calculations of beta$^-$ energies are the usual procedure, rather than the direct estimations of beta$^-$ energies themselves.

3. Beta energy systematics. -- A correlation of beta decay energies from the cycles is presented in Fig. 9, which is a graph of beta decay energy versus mass number. As in the alpha energy graph, the energies for each element have been connected by solid lines; that is, the points representing the beta separation energy between

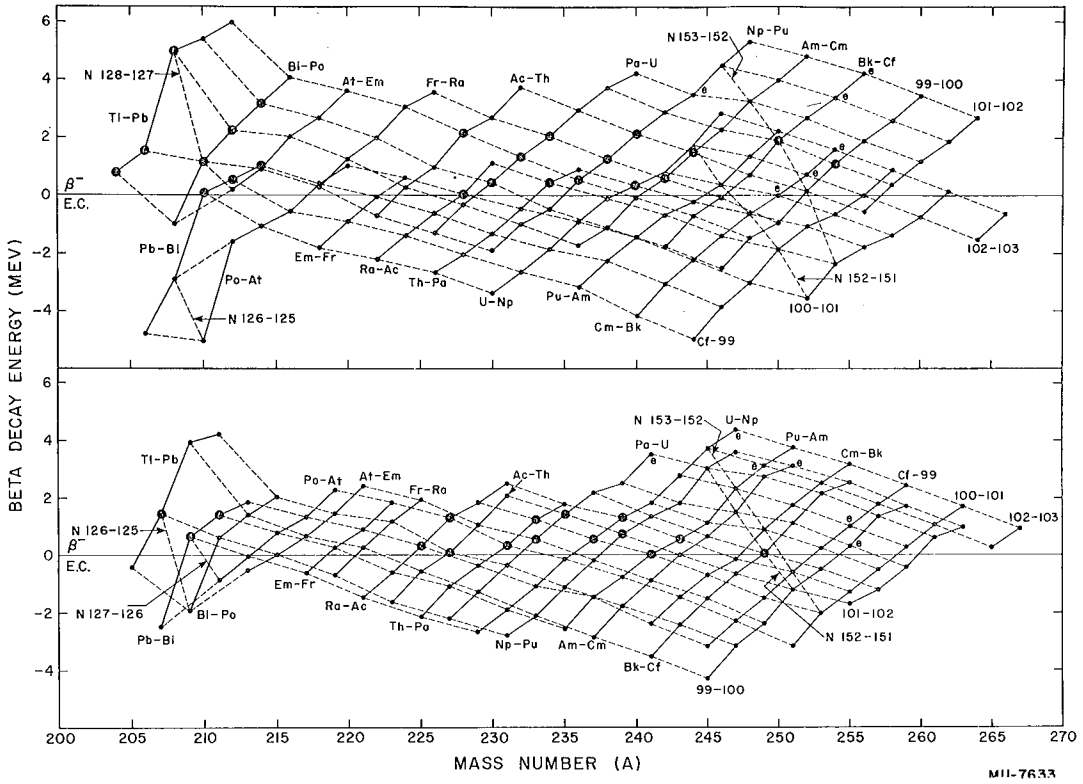

Fig. 9. Beta decay energies for the isotopes of the elements above mercury as a function of mass number: O, experimental energies; ❶, calculated energies; e, estimated energies.

neighboring elements are connected. Two graphs are necessary because for any given element the isotopes are of two nuclear types, one with an even mass number and the other with an odd mass number, with different magnitudes of decay energies. In the graph for nuclei with even A, beta decay occurs between even-even and odd-odd isobars. The decay energy has a small absolute value when the decay is from an even-even nuclide to an odd-odd one and has a large absolute value in general when the decay is in the reverse direction. Thus the line representing the Ac-Th separation energy is above that for the Th-Pa separation energy in Fig. 9a because in the former case the beta$^-$ decay of the actinium isotopes is from odd-odd to even-even nuclides and in the latter case the decay is from even-even to odd-odd nuclides. In Fig. 9b, on the other hand, since only odd mass number nuclides are represented, the lines for the various elements are in the order of atomic number, because the even-odd and odd-even types of nuclei lie almost on the same energy surface.

Dashed lines are also used in the graph to connect points for nuclides with the same isotopic numbers (I values). Observing the graph along lines of constant isotopic number is advantageous because it stresses beta energies along the same chain of alpha decay energies, which are related by the fact that the calculated beta energies are all based on the measured beta$^-$ energy in the series. For example, the beta separation energies for At^{221}-Em^{221}, Fr^{225}-Ra^{225}, and Ac^{229}-Th^{229}, as well as a number of others lie on the line for I = 51 and have been calculated from the measured beta$^-$ energy of Pa^{233}, which

is also on this line. The form of presentation in this type of graph where points of constant Z are connected is discussed in detail in a paper by Way and Wood,[13] whereas the form where points of constant I are connected has been presented by Suess and Jensen.[14]

The general trends of the lines are reasonable since as more neutrons are added to a given element, successively higher beta$^-$ decay energies are observed. At first inspection it appears that the lines are more regular than the alpha-energy lines, but it must be remembered that most of the beta energies shown have been calculated from cycles involving these alpha energies and hence cannot be more accurate. Although the beta energies have a sharp discontinuity at the 126 neutron closed shell, there is no obvious effect in the region of 152 neutrons; but as previously stated, this could be due to cumulative errors. The discontinuities in the beta energy lines at the closed shell at 126 neutrons indicates, as expected, that nuclides which decay into the closed shell have high beta decay energies and those which lie on the closed shell have low energies. For example, notice the high beta$^-$ energy of Tl^{208} which decays into the 82 proton closed shell as well as the 126 neutron shell.

The same type of conclusions about beta stability that can be reached from the cycles and are presented in Fig. 7 can also be drawn from Fig. 9. In this graph beta$^-$ unstable nuclides lie above the zero line and electron capture unstable nuclides below the line. Again, beta stability is indicated when a nuclide itself does not have energy available for either type of decay. It can be seen that only a small alteration in the lines for curium and californium would effect the predicted beta stability for Cm^{250} and Cf^{256}, respectively.

The beta$^-$ estimations made on the bases of the lines for measured and calculated energies are confined to the region above thorium. None of the estimated energies are for nuclei either at or decaying into the proposed 152 neutron subshell, because it was anticipated at the time the estimations were made that there might be discontinuities in the lines. Consider for example the estimated beta$^-$ energies for Bk^{254} and Bk^{256}. First, referring to the berkelium line in Fig. 9a, it is seen that the beta$^-$ energy of Bk^{250} is measured. This is followed by the calculated beta$^-$ energy of Bk^{252}, which is based on the estimated energy of Np^{244} because Bk^{252} itself is just beyond Bk^{250} which decays into the 152 neutron subshell and because the Np^{244} value can be extrapolated from a rather straight Np - Pu separation line. Then the line connecting the Bk^{250} and Bk^{252} points has been extrapolated to indicate what energy should be estimated for Bk^{254} and Bk^{256}.

As is apparent in the alpha energy lines in Fig. 8 there are a number of irregularities in the energy lines which may be due to the nature of the energy surface or the inaccuracy of measured or estimated alpha and beta$^-$ energies. For example, even though the estimated beta$^-$ energy for Pa^{241} lies on the Pa - U line the dependent, calculated beta$^-$ energies for Np^{245}, Am^{249}, Bk^{253}, 99^{257}, and 101^{261} lie above the lines for their respective elements. Now, it is doubtful that these points along a line of constant isotopic number should really all be high, since the isotopic number has no fundamental significance in this regard. On the other hand it is highly suggestive that there is an error in one or more energies

along the same series of closed cycles. At the present time the changes to be made are not apparent. The rest of the irregularities can also be considered in relation to their positions along lines of constant Z and I.

C. Masses and Nucleon Binding Energies of the Heaviest Elements

1. Isotopic masses and neutron and proton binding energies. -- The atomic masses of all of the nuclides in the closed cycles (Figs. 2-5) have been calculated from energy data and are presented in Table 4 along with all possible calculated neutron and proton binding energies. The calculation procedure can be described briefly. All masses are made relative to the atomic mass of Pb^{208} which has been set at 208.04100, which corresponds to the value of 208.0410 ± 0.0015 determined with a time-of-flight mass spectrograph by Richards, Hays, and Goudsmit.[75] The masses of Pb^{206}, Pb^{207}, and Pb^{209}, the terminal nuclides of the 4n + 2, 4n + 3, and 4n + 1 series, respectively, were calculated relative to Pb^{208} with the use of three measured neutron binding energies:

$$Pb^{206-207} = 6.73 \text{ Mev}^{76}$$
$$Pb^{207-208} = 7.38 \text{ Mev}^{76}$$
$$Pb^{208-209} = 3.87 \text{ Mev}^{77}$$

The mass of the neutron used to calculate masses from neutron binding energies is 1.00898, which corresponds to the value of 1.008982 ± 0.000003 reported by Ajzenberg and Lauritsen.[78] In addition, the conversion of energy to mass was made on the basis that one atomic mass unit equals 931.2 Mev, in accordance with the recent value of 931.162 ± 0.024 Mev reported by DuMond and Cohen[79]

Table 4

Masses and Neutron and Proton Binding Energies
of the Transmercury Nuclides

The bases for the following calculations are:

1. Mass of Pb^{208} = 208.04100

   He^{4} = 4.00387

   $_{0}n^{1}$ = 1.00898

   $_{1}H^{1}$ = $_{0}n^{1}$ - 0.78/931.2

2. Neutron Binding energies

   $Pb^{206-207}$ = 6.73 Mev

   $Pb^{207-208}$ = 7.38 Mev

   $Pb^{208-209}$ = 3.87 Mev

3. One atomic mass unit = 931.2 Mev

Element and Mass	Binding Energies (Mev)	
	En	Ep
81-Thallium		
(202.03497)		
203.03450	(8.80)(meas)	
204.03658	6.42 (meas)	
205.03753	7.48 (meas)	
206.03982	6.23 (meas)	
207.04149	6.80	
208.04636	3.83	
209.05003	4.94	
210.05497	3.76	
(211.05861)	(4.97)	
(212.06391)	(3.43)	

Table 4 (Cont'd)

Element and Mass	Binding Energies (Mev)	
	En	Ep
82-Lead		
204.03576		6.41
205.03800	6.27	6.26
206.03820	8.18 (meas)	6.96
207.03995	6.73 (meas)	7.46
208.04100	7.38 (meas)	8.04
209.04582	3.87 (meas)	8.08
210.04919	5.23	8.37
211.05410	3.78	8.39
212.05750	5.20	(8.62)
213.06229	3.90	(9.09)
214.06596	4.94	
83-Bismuth		
(206.04337)		(2.58)
207.04263	(9.05)	3.45
208.04415	6.95	3.67
209.04514	7.44 (meas)	3.73
210.04912	4.65	4.51
211.05261	5.11	4.39
212.05689	4.38	4.99
213.06031	5.17	4.96
214.06487	4.12	5.18
215.06820	5.26	5.50
216.07317	3.73	

Table 4 (Cont'd)

Element and Mass	Binding Energies (Mev)	
	En	Ep
84-Polonium		
208.04522		5.17
209.04721	6.51	4.73
210.04786	7.75	5.04
211.05196	4.55	4.94
212.05447	6.02	5.85
213.05882	4.31	5.78
214.06146	5.90	6.51
215.06604	4.10	6.49
216.06878	5.81	7.04
217.07327	4.18	7.49
218.07639	5.45	
219.08138	3.72	
(220.08450)	(5.45)	
85-Astatine		
(210.05329)		(1.92)
211.05292	(8.70)	2.87
(212.05618)	(5.33)	(3.65)
213.05889	(5.84)	3.47
214.06260	4.90	4.06
215.06523	5.91	4.07
216.06928	4.59	4.56
217.07186	5.96	4.71
218.07599	4.52	5.05

Table 4 (Cont'd)

Elements and Masses	Binding Energies (Mev)	
	En	Ep
85-Astatine (Cont'd)		
219.07893	5.62	5.22
220.08339	4.21	5.71
(221.08617)	(5.77)	(6.03)
86-Emanation		
212.05594		4.77
(213.05945)	(5.09)	(4.53)
214.06161	(6.35)	5.04
215.06523	4.99	5.13
216.06710	6.62	5.84
217.07116	4.58	5.83
218.07312	6.54	6.41
219.07737	4.40	6.29
220.07951	6.37	7.04
221.08358	4.57	7.40
222.08626	5.87	(7.50)
223.09081	4.12	
(224.09350)	(5.86)	
87-Francium		
217.07184		3.17
218.07506	5.36	3.95
219.07709	6.47	3.88
220.08047	5.22	4.70

Table 4 (Cont'd)

Elements and Masses	Binding Energies (Mev)	
	En	Ep
87-Francium (Cont'd)		
221.08263	6.35	4.68
222.08630	4.94	5.05
223.08881	6.02	5.20
224.09285	4.60	5.68
(225.09521)	(6.17)	(5.99)
(226.09916)	(4.68)	
88-Radium		
218.07472		4.90
219.07786	5.44	4.98
220.07910	7.20	5.71
221.08237	5.32	5.81
222.08417	6.68	6.14
223.08754	5.23	6.43
224.08959	6.45	6.86
225.09317	5.03	7.29
226.09535	6.33	(7.45)
227.09949	4.50	(7.27)
228.10177	6.24	
229.10562	4.78	
(230.10844)	(5.73)	
(231.11272)	(4.38)	

Table 4 (Cont'd)

Elements and Masses	Binding Energies (Mev)	
	En	Ep
89-Actinium		
221.08395		3.07
222.08655	5.94	3.69
223.08822	6.80	3.81
224.09108	5.70	4.28
225.09283	6.73	4.56
226.09602	5.39	4.92
227.09809	6.44	5.03
228.10173	4.97	5.50
229.10366	6.56	5.82
(230.10722)	(5.05)	(6.09)
(231.11003)	(5.74)	(6.10)
(232.11405)	(4.62)	(6.34)
90-Thorium		
222.08730		4.46
223.08998	5.86	4.38
224.09077	7.63	5.21
225.09342	5.89	5.40
226.09498	6.91	5.58
227.09800	5.55	5.74
228.09939	7.07	6.37
229.10252	5.44	6.84
230.10433	6.68	6.96

Table 4 (Cont'd)

Elements and Masses	Binding Energies (Mev)	
	En	Ep
90-Thorium (Cont'd)		
231.10781	5.12	7.03
232.11001	6.31	7.60
233.11356	5.06	8.04
234.11609	6.00	
235.12009	4.64	
(236.12296)	(5.69)	
91-Protactinium		
225.09573		2.96
226.09786	6.38	3.45
227.09916	7.15	3.69
228.10161	6.08	4.22
229.10292	7.14	4.29
230.10575	5.73	4.58
231.10746	6.76	4.66
232.11049	5.54	5.08
233.11223	6.74	5.51
234.11559	5.24	5.69
235.11819	5.94	5.63
236.12200	4.81	5.80
(237.12433)	(6.19)	(6.49)
(238.12853)	(4.45)	
(239.13100)	(6.06)	

Table 4 (Cont'd)

Elements and Masses	Binding Energies (Mev)	
	En	Ep
91-Protactinium		
(240.13556)	(4.12)	
(241.13850)	(5.62)	
92-Uranium		
(226.09927)		(4.29)
227.10152	(6.26)	4.17
228.10193	7.98	5.00
229.10431	6.15	5.07
230.10528	7.45	5.38
231.10783	5.99	5.64
232.10907	7.21	6.09
233.11167	5.94	6.49
234.11341	6.74	6.49
235.11668	5.31	6.56
236.11880	6.39	7.01
237.12199	5.39	7.59
238.12454	5.99	(7.39)
239.12833	4.83	(7.77)
240.13101	5.86	(7.57)
(241.13474)	(4.89)	(8.34)
(242.13775)	(5.56)	(8.28)
(243.14213)	(4.28)	
(244.14555)	(5.18)	

Table 4 (Cont'd)

Elements and Masses	Binding Energies (Mev)	
	En	Ep
92-Uranium		
(245.15050)	(3.75)	
(246.15422)	(4.90)	
(247.15934)	(3.59)	
93-Neptunium		
(229.10720)		(2.67)
230.10895	6.74	3.26
231.10989	7.48	3.29
232.11193	6.46	3.76
233.11284	7.52	4.07
234.11540	5.97	4.10
235.11687	7.00	4.36
236.11978	5.65	4.70
237.12143	6.82	5.13
238.12464	5.37	5.11
239.12695	6.21	5.33
240.13063	4.94	5.44
(241.13281)	(6.33)	(5.91)
(242.13686)	(4.59)	(5.61)
(243.13918)	(6.20)	(6.25)
(244.14364)	(4.21)	(6.18)
(245.14650)	(5.69)	(6.69)
(246.15116)	(4.03)	(6.97)

Table 4 (Cont'd)

Elements and Masses	Binding Energies (Mev)	
	En	Ep
93-Neptunium		
(247.15466)	(5.10)	(7.17)
(248.15996)	(3.42)	(7.00)
94-Plutonium		
(230.11102)		(4.03)
231.11292	6.59	3.88
232.11300	8.29	4.69
233.11516	6.35	4.58
234.11592	7.65	4.71
235.11809	6.34	5.08
236.11922	7.31	5.39
237.12168	6.07	5.81
238.12328	6.87	5.86
239.12618	5.66	6.15
240.12831	6.38	6.32
241.13137	5.51	6.89
242.13375	6.14	(6.70)
243.13726	5.10	(7.21)
244.13988	5.92	(6.93)
(245.14325)	(5.22)	(7.94)
(246.14633)	(5.49)	(7.74)
(247.15079)	(4.21)	(7.92)
(248.15427)	(5.12)	(7.94)

Table 4 (Cont'd)

Elements and Masses	Binding Energies (Mev)	
	En	Ep
94-Plutonium		
(249.15908)	(3.88)	(8.40)
(250.16263)	(5.06)	
(251.16760)	(3.73)	
95-Americium		
(235.12085)		(2.99)
236.12262	6.71	3.36
237.12327	7.76	3.81
238.12571	6.09	3.83
239.12702	7.14	4.10
240.12988	5.70	4.14
241.13135	6.99	4.75
242.13445	5.47	4.71
243.13665	6.31	4.88
244.14011	5.14	4.92
245.14207	6.54	5.54
(246.14594)	(4.76)	(5.08)
(247.14831)	(6.15)	(5.74)
(248.15282)	(4.16)	(5.69)
(249.15575)	(5.63)	(6.20)
(250.16025)	(4.17)	(6.49)
(251.16360)	(5.25)	(6.68)
(252.16873)	(3.58)	(6.53)

Table 4 (Cont'd)

Elements and Masses	Binding Energies (Mev)	
	En	Ep
96-Curium		
(236.12447)		(4.21)
237.12637	6.59	4.09
238.12691	7.86	4.19
239.12894	6.47	4.57
240.12994	7.43	4.86
241.13230	6.16	5.32
242.13382	6.95	5.28
243.13665	5.72	5.53
244.13850	6.64	5.86
245.14138	5.68	6.40
246.14348	6.41	6.27
(247.14672)	(5.34)	(6.85)
(248.14930)	(5.96)	(6.66)
(249.15282)	(5.08)	(7.58)
(250.15599)	(5.41)	(7.36)
(251.16027)	(4.38)	(7.57)
(252.16355)	(5.30)	(7.62)
(253.16818)	(4.05)	(8.09)
(254.17153)	(5.24)	
(255.17633)	(3.90)	

Table 4 (Cont'd)

Elements and Masses	Binding Energies (Mev)	
	En	Ep
97-Berkelium		
(240.13445)		(2.45)
(241.13488)	(7.96)	(2.98)
242.13712	(6.28)	3.10
243.13822	7.33	3.48
244.14087	5.90	3.66
245.14213	7.18	4.20
246.14499	5.71	4.23
(247.14690)	(6.57)	(4.39)
248.14998	(5.50)	(4.55)
249.15186	6.61	(5.20)
250.15599	4.51	(4.63)
(251.15843)	(6.09)	(5.31)
(252.16276)	(4.33)	(5.26)
(253.16550)	(5.81)	(5.77)
(254.16980)	(4.36)	(6.08)
(255.17294)	(5.43)	(6.27)
(256.17787)	(3.77)	(6.14)
98-Californium		
(241.13870)		(3.62)
(242.13903)	(8.06)	(3.72)
243.14084	(6.67)	4.11
244.14162	7.64	4.42

Table 4 (Cont'd)

Elements and Masses	Binding Energies (Mev)	
	En	Ep
245.14375	6.37	4.89
246.14506	7.15	4.86
247.14762	5.97	5.12
248.14920	6.89	(5.44)
249.15180	5.94	5.88
250.15395	6.36	5.63
(251.15725)	(5.29)	(6.41)
(252.15988)	(5.91)	(6.23)
(253.16321)	(5.26)	(7.16)
(254.16618)	(5.60)	(6.95)
(255.17025)	(4.57)	(7.16)
(256.17332)	(5.50)	(7.23)
(257.17774)	(4.24)	(7.70)
(258.18088)	(5.44)	
(259.18547)	(4.09)	
99-		
(244.14699)		(1.86)
(245.14720)	(8.16)	(2.38)
(246.14921)	(6.49)	(2.50)
(247.15011)	(7.52)	(2.87)
(248.15246)	(6.18)	(3.08)
(249.15341)	(7.47)	(3.66)
(250.15595)	(6.00)	(3.72)

Table 4 (Cont'd)

Elements and Masses	Binding Energies (Mev)	
	En	Ep
99 (Cont'd)		
(251.15791)	(6.53)	(3.89)
252.16103	(5.46)	4.06
253.16296	6.56	4.71
254.16688	4.71	(4.16)
(255.16918)	(6.22)	(4.78)
(256.17332)	(4.51)	(4.72)
(257.17584)	(6.01)	(5.23)
(258.17993)	(4.56)	(5.55)
(259.18286)	(5.63)	(5.74)
(260.18757)	(3.97)	(5.62)
100		
(245.15183)		(3.07)
(246.15193)	(8.27)	(3.18)
(247.15352)	(6.88)	(3.57)
(248.15406)	(7.86)	(3.91)
(249.15597)	(6.58)	(4.31)
(250.15697)	(7.43)	(4.27)
(251.15922)	(6.26)	(4.53)
(252.16086)	(6.84)	(4.84)
253.16350	(5.90)	5.28
254.16570	6.31	5.03
255.16886	5.42	5.74

Table 4 (Cont'd)

Elements and Masses	Binding Energies (Mev)	
	En	Ep
100 (Cont'd)		
(256.17128)	(6.11)	(5.63)
(257.17441)	(5.45)	(6.57)
(258.17716)	(5.80)	(6.36)
(259.18101)	(4.77)	(6.57)
(260.18387)	(5.70)	(6.64)
(261.18810)	(4.42)	(7.09)
(262.19102)	(5.64)	
(263.19539)	(4.29)	
101		
(251.16264)		(2.30)
(252.16466)	(6.48)	(2.52)
(253.16566)	(7.43)	(3.11)
(254.16825)	(5.95)	(3.16)
(255.17027)	(6.48)	(3.33)
(256.17220)	(5.63)	(3.54)
(257.17494)	(6.74)	(4.17)
(258.17865)	(4.91)	(3.63)
(259.18073)	(6.42)	(4.25)
(260.18467)	(4.69)	(4.17)
(261.18698)	(6.21)	(4.68)
(262.19086)	(4.75)	(5.01)
(263.19357)	(5.84)	(5.21)
(264.19807)	(4.17)	(5.09)

Table 4 (Cont'd)

Elements and Masses	Binding Energies (Mev)	
	En	Ep
102		
(255.17212)		(3.98)
(256.17379)	(6.80)	(4.30)
(257.17624)	(6.08)	(4.75)
(258.17825)	(6.49)	(4.50)
(259.18119)	(5.62)	(5.21)
(260.18341)	(6.30)	(5.09)
(261.18633)	(5.64)	(6.04)
(262.18886)	(6.00)	(5.83)
(263.19251)	(4.97)	(6.05)
(264.19515)	(5.90)	(6.11)
(265.19917)	(4.62)	(6.56)
(266.20188)	(5.83)	
(267.20604)	(4.49)	
103		
(264.19680)		(3.58)
(265.19889)	(6.42)	(4.10)
(266.20255)	(4.95)	(4.43)
(267.20504)	(6.04)	(4.64)

from their adjustment of atomic constants. Once the atomic masses of Pb^{206}, Pb^{207}, Pb^{208}, and Pb^{209} were fixed and therefore the connections between the four radioactive series established, the masses of the nuclides in the cycles were calculated from the cycle decay energies. The mass of He^4 employed to calculate mass differences between nuclei separated by an alpha particle was 4.00387, which corresponds to the reported[78] value of 4.003873 ± 0.000015. Proton binding energies and additional neutron binding energies were calculated from the cycle energies and lead neutron binding energies using the additional information (for the calculation of proton binding energies) that the difference ${}_0n^1 - {}_1H^1$ is equal to 0.78 Mev.[78] An optional procedure for calculating the binding energies would have been to calculate them from the masses. The use of parentheses to distinguish uncertain masses and binding energies was discussed previously in connection with the closed cycle energies.

The calculated masses and neutron binding energies have been compared with measured values in Table 5. The values of the unadjusted masses reported by the various authors have been tabulated because the calculated masses themselves in the present work constitute a basis for adjustment of measured values with the exception of the case of the Pb^{208} mass. The fact that the two measured values for the mass of Pb^{208} agree quite well is an indication that the absolute masses calculated relative to this value may have a fair degree of accuracy. It can be noted that the calculated masses of Th^{232} and U^{234} agree with the measured values within their limits of error while the calculated masses for Bi^{209}

and U^{238} are at the limits of error for the corresponding measured values. On the other hand the calculated mass for Pb^{207} is just outside the limit of error for the measured value. In this case the calculated value is probably to be preferred since it depends on the masses of Pb^{208} and its neutron binding energy, which has been determined precisely.

In the same way the calculated neutron binding energies agree with the measured values with the exception of the Bi^{210} neutron binding energy, although the calculated energy for U^{239} is slightly outside of the limit of error for the measured value.

Table 5

Measured Masses and Neutron Binding Energies
Masses (in atomic mass units)

Nuclide	Measured	Calculated
Pb^{207}	$207.0429 \pm 0.0016^{(80)}$	207.03995
Pb^{208}	$208.0409 \pm 0.0013^{(80)}$	208.04100
Pb^{208}	$208.0410 \pm 0.0015^{(75)}$	208.04100[a]
Bi^{209}	$209.0471 \pm 0.0015^{(75)}$	209.04514
Th^{232}	$232.1092 \pm 0.0010^{(80)}$	232.11001
U^{234}	$234.1133 \pm 0.0011^{(80)}$	234.11341
U^{238}	$238.1234 \pm 0.0010^{(80)}$	238.12454

[a] Measured value accepted.

(Table 5 continued on the following page)

Table 5 (Cont'd)

Measured Neutron Binding Energies in the Trans-Thallium Region

Nuclide	Upper limit (γ, n)	Lower limit	Value accepted
$Tl^{202-203}$	8.80 ± 0.20[86]		8.80[a]
$Tl^{203-204}$		6.42 ± 0.15[d(88)]	6.42[a]
$Tl^{204-205}$	7.3 ± 0.25[81]	7.7 ± 0.2[b(77)]	7.48[a]
	7.48 ± 0.15[84]		
	7.55 ± 0.20[86]		
$Tl^{205-206}$		6.23 ± 0.05[c(76)]	6.23[a]
		6.16 ± 0.15[d(88)]	
$Pb^{205-206}$	8.25 ± 0.10[85]	8.10 ± 0.10[b(77)]	8.18[a]
$Pb^{206-207}$	6.9 ± 0.1[81]	6.70 ± 0.05[b(77)]	6.73[a]
	6.95 ± 0.10[85]	6.734 ± 0.008[c(76)]	
	6.75 ± 0.20[86]	6.71 ± 0.03[d(77)]	
$Pb^{207-208}$	8.1 ± 0.3[82]	7.37 ± 0.03[b(77)]	7.38[a]
	7.44 ± 0.10[85]	7.380 ± 0.008[c(76)]	
	7.30 ± 0.20[86]	7.37 ± 0.03[d(77)]	
$Pb^{208-209}$		3.87 ± 0.05[d(77)]	3.87[a]
$Bi^{208-209}$	7.2 ± 0.1[81]	7.44 ± 0.05[b(77)]	7.44[a]
	7.45 ± 0.2[83]		
	7.40 ± 0.20[86]		
$Bi^{209-210}$		4.170 ± 0.015[c(76)]	4.65
		4.14 ± 0.03[d(77)]	
$Th^{231-232}$	6.0 ± 0.15[81]		6.31
	6.35 ± 0.1[87]		

Table 5 (Cont'd)

Nuclide	Upper limit (γ, n)	Lower limit	Value accepted
$Th^{232-233}$		4.9 ± 0.2[d(77)]	5.06
$U^{237-238}$	5.8 ± 0.15[(81)]	5.9 ± 0.2[b(77)]	5.99
	5.97 ± 0.1[(87)]		
$U^{238-239}$		4.63 ± 0.15[d(77)]	4.83

[a] Measured value accepted.

[b] (d, t) reaction.

[c] (n, γ) reaction.

[d] (d, p) reaction.

The measured values for the Bi^{210} neutron binding energy have been discussed in detail by various authors[21, 23] and the conclusion reached that the measured values are low and merely represent a lower limit. The same conclusion was reached in the present investigation. It will be noted that upper and lower limits for the neutron binding energies of Tl^{205}, Pb^{206}, Pb^{207}, Pb^{208}, Bi^{209}, and U^{238} have been determined which enhances the reliability of these binding energies considerably.

The neutron and proton binding energies listed in Table 4 have been plotted against mass number and points for each element connected in Figs. 10 and 11, respectively. The neutron binding energies for the even neutron and odd neutron isotopes of each element decrease regularly with increasing mass number, indicating that as the more neutrons are added their binding energies are

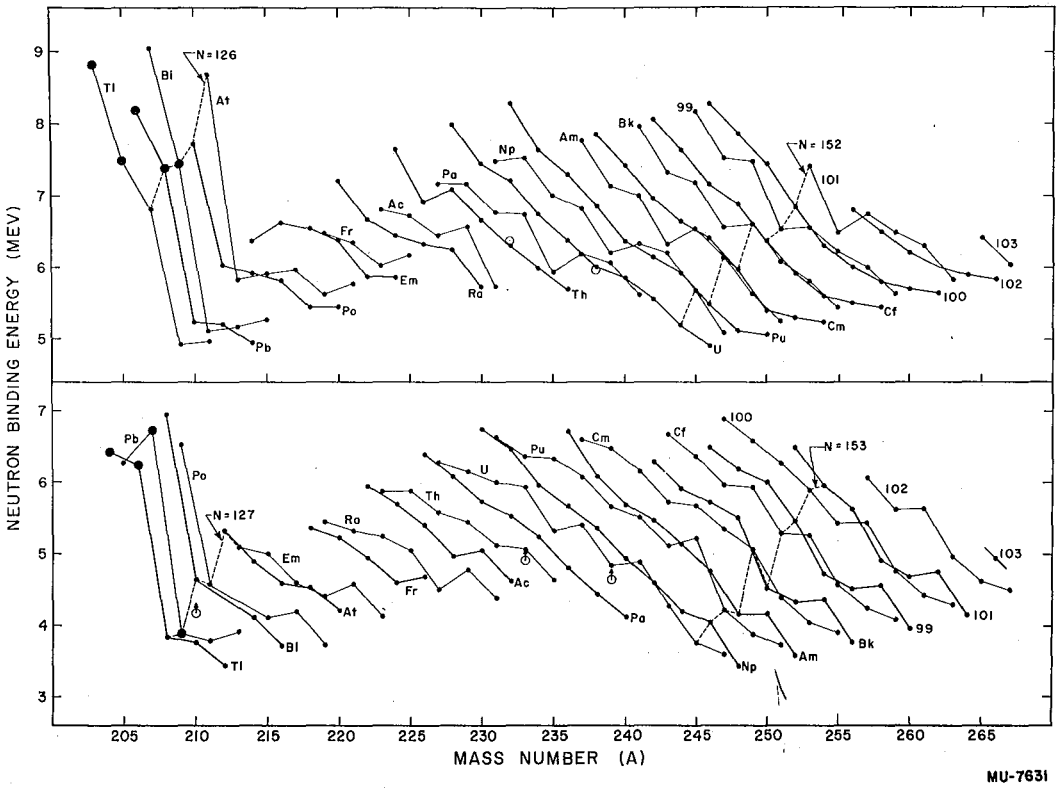

Fig. 10. Neutron binding energies for the isotopes of the elements above mercury as a function of mass number: o, experimental energies; ●, calculated energies.

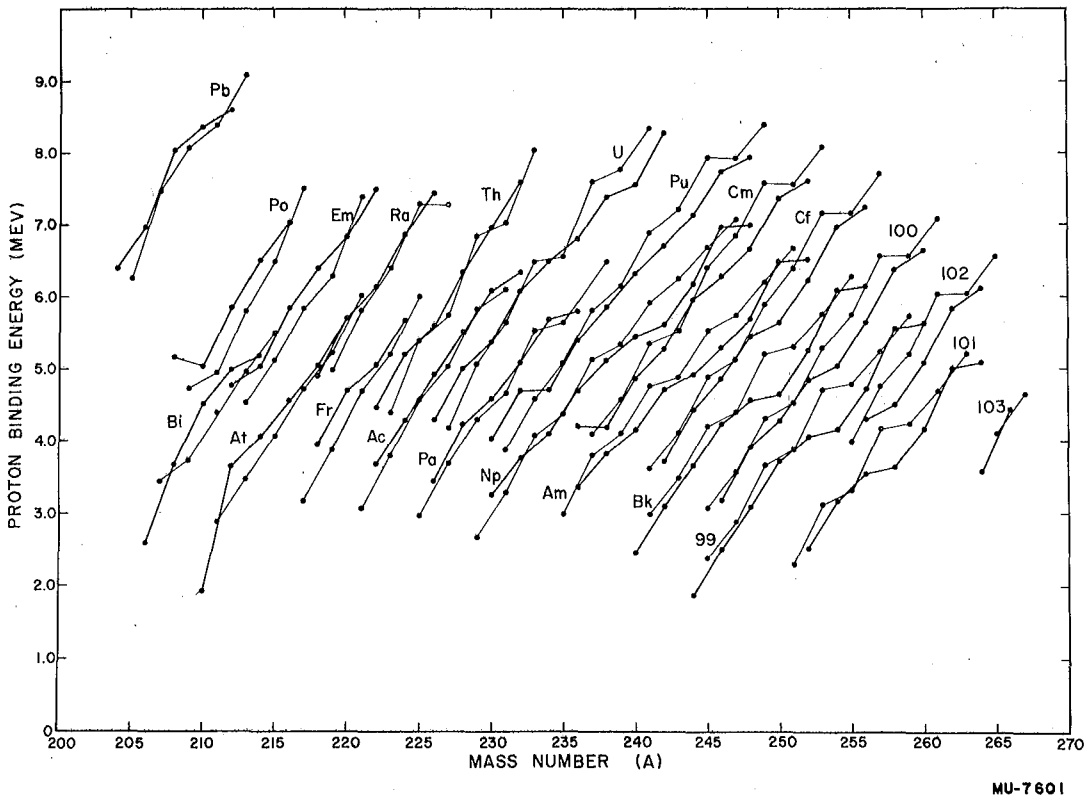

Fig. 11. Proton binding energies for the isotopes of the elements above thallium as a function of mass number: ● , calculated energies.

smaller. As expected, the binding energies for nuclides with an even number of neutrons are higher than those for nuclides with an odd number. As in the alpha and beta energy systematics many of the irregularities in the lines are probably due to cumulative errors in decay energies. The sudden decrease of neutron binding energies after the 126 neutron closed shell, however, is a real and striking effect. On the other hand, no noticeable effect can be observed in the 152 neutron region, but in this case the nuclides are far removed from the lead isotopes whose neutron binding energies have been used as a basis for the calculations. The fact that the lines for the elements cross over in the region above mass number 136 is another effect probably due to cumulative errors. It will be noted that the calculated neutron binding energies for Pa^{237}, Np^{241}, Am^{245}, Bk^{249}, 99^{253}, and 101^{257} all appear to be high. These values are all based on the accumulative decay energy in the 4n + 1 series and more particularly on the beta$^-$ energy connecting the alpha chain between 101^{257} and Pa^{237} to the rest of the cycles. This suggests that the beta$^-$ energy of Bk^{249} may be too low. At the same time this isotope has a one year half-life and a low beta$^-$ energy is expected. The problem is at present unresolved. The high binding energies for the isotopes just cited are reflected in low values on the odd neutron number graph for the Np^{242}, Am^{246}, etc., binding energies indicating that the masses of Pa^{237}, Np^{241}, and the other corresponding nuclides may be too low. This problem illustrates just one of the many regions of nuclides where further experimental data are needed. Determinations of the beta$^-$ energies of Pa^{237} and Np^{241} would help clarify the situation just outlined.

The proton binding energies increase regularly with increasing mass number for each element indicating that as more neutrons are added the proton binding energy of the last proton is greater. For both the neutron and proton binding energies, as either type particles tend to become in relative excess their binding energies decrease. In other words the nucleus prefers a balance of neutrons and protons. The proton binding energies for each element, contrary to the neutron binding energies, lie almost on one line. The explanation lies in the nuclear types of the isotopes connected by the proton binding energies. Proton binding energies for nuclides with even numbers of neutrons connect even-even and odd-even nuclear types whereas proton binding energies for nuclides with odd numbers of neutrons connect even-odd and odd-odd nuclear types. In both cases since the energy surfaces spanned have about the same energy separation, a continuous change in proton binding energies is observed.

A number of authors have recently calculated masses[21, 90] and nucleon binding energies[21, 23] in the region of the heaviest elements. The present paper, however, represents the most extensive treatment of all aspects of the energy systematics in the region of the heaviest elements yet reported.

2. Chemical atomic weights. -- The masses tabulated in Table 4 were also used to calculate chemical atomic weights with the aid of isotopic abundances from the Table of Isotopes.[41] It was necessary to convert the Table 4 masses from the physical scale based on the mass of O^{16} set at 16 to the chemical based on the mass of the naturally occurring mixture of O^{16}, O^{17}, and O^{18}

set at 16. This was done by dividing the values on the physical scale by the conversion factor 1.000275.[91] The results are given in Table 6. The values[91] adopted by the commission on Atomic Weights of the International Union of Pure and Applied Chemistry at its meeting in September 1951, are also included in the table.

Table 6

Chemical Atomic Weight

Element	This paper	I. U. C. values (1951)
Thallium	204.39	204.39
Lead	207.18	207.21
Bismuth	208.99	209.00
Radium[a]	226.03	226.05
Thorium	232.05	232.12
Uranium	238.04	238.07

[a] $Radium^{226}$ is in almost 100 percent abundance.

The values from the masses reported in this paper should not be in error by more than 0.01 atomic weight unit and probably are much better. It can be seen then that small changes in the atomic weights of the elements listed, particularly thorium, will be necessary. Although it has been the increasing tendency in recent years to adjust atomic weights according to isotopic mass determinations[91] there are still elements in the periodic table which have not been adjusted until complete agreement is obtained.

D. Bohr-Wheeler Parameters

This part of the paper is concerned with the calculation of the parameters of the semi-empirical mass equation developed by Weizsäcker,[92] Fermi,[5] and Bohr and Wheeler[4] among others. The equation is commonly employed in two forms: the Fermi-Weizsäcker form and the Bohr-Wheeler form. The factors affecting nuclear stability are more readily seen from the Fermi-Weizsäcker form which can be written as follows:[5]

$$M_{(Z^A)} = NM_n + ZM_H - a_1A + a_2A^{2/3} + a_3\frac{(A/2 - Z)^2}{A}$$

$$+ 0.000627\,\frac{Z^2}{A^{1/3}} + \begin{cases} 0 & A \text{ odd} \\ -1/2\,\delta A & A \text{ even, } Z \text{ even} \\ +1/2\delta A & A \text{ even, } Z \text{ odd} \end{cases}$$

The sum of the first two terms is approximately the mass that the nucleus would have if it were merely a mixture of unbound neutrons and protons. The next term (volume term) corrects the mass for the fact that the nucleus has a binding energy that is roughly proportional to the number of nucleons (saturated nuclear forces). The following term (surface term) corrects the volume term for the fact that the nucleons on the surface do not have as great binding energy as those in the center. Since the surface area of a sphere is proportional to the square of the radius and the radius in turn is proportional to $A^{1/3}$ this term is expressed by $a_2A^{2/3}$. The term associated with the constant a_3 compensates for the increase in mass with increasing neutron excess. The next term (coulomb term) corrects for the increase of mass due to coulombic repulsion in the nucleus, and becomes relatively more important as the ratio

of protons to neutrons becomes greater. The δ_A term corrects for odd even effects and will be discussed in detail farther on. The constants in the mass equation have been evaluated for known masses of stable elements. The final equation given by Fermi[5] is as follows:

$$M_{(Z^A)} = 0.99391A - 0.00085Z + 0.14A^{2/3} + 0.083\frac{(A/2 - Z)^2}{A} + 0.000627\frac{Z^2}{A^{1/3}},$$

$$\begin{cases} 0 & A \text{ odd} \\ -0.036A^{3/4} & A \text{ even, } Z \text{ even} \\ +0.036A^{3/4} & A \text{ even, } Z \text{ odd.} \end{cases}$$

The Bohr-Wheeler form of the mass equation can be written as follows:[4]

$$M_{(Z^A)} = MZ_A + 1/2B_A(Z - Z_A)^2 + \begin{cases} 0 & A \text{ odd} \\ -1/2\delta A & A \text{ even, } Z \text{ even} \\ +1/2\delta A & A \text{ even, } Z \text{ odd.} \end{cases}$$

The equation has been formulated to indicate mass relations between isobars, and emphasizes the parabolic shape[7, 8] of the energy surface along lines of constant A. In the equation, Z_A is the most stable value of Z for a given A (bottom of the parabola) and M_A is the associated mass. An expression for beta energies can be readily derived from this equation:

$$E_{\beta^-} = M_{(Z^A)} - M_{(Z+1)^A}$$

$$= B_A[\,|Z_A - Z| - 1/2\,] + \begin{cases} 0 & A \text{ odd} \\ -\delta A & A \text{ even, } Z \text{ even} \\ +\delta A & A \text{ even, } Z \text{ odd.} \end{cases}$$

It is the three parameters of this equation, Z_A, B_A, and δ_A, that have been evaluated from closed cycle beta decay energies in this paper. In addition, the Fermi form of the mass equation can be used to calculate theoretical values for the parameters. The para-

meter Z_A can be derived by differentiation of the equation holding A constant and the following expression obtained:

$$Z_A = \frac{A}{1.981 + 0.015A^{2/3}}$$

Likewise, an expression for B_A can be derived:

$$B_A = 2\left(\frac{0.083}{A} + \frac{0.000627}{A^{1/3}}\right).$$

In addition, the δ_A term can be evaluated directly from the expression

$\delta_A = 0$	A odd
$-0.072A^{3/4}$	A even, Z even
$+0.072A^{3/4}$	A even, Z odd.

The values of the parameters determined from the closed cycles and those calculated from the mass equation are compared in this section.

The δ_A term is in reality not equal to zero for odd A nuclides; in fact there are different energy surfaces composed of odd neutron and odd proton nuclides. The designation δ_{AO} will be used to refer to the energy difference between these two surfaces. At the same time δ_{AE} will be used in place of the former δ_A. Thus there are two correction terms to the Bohr-Wheeler equation: δ_{AE}, for use with nuclides with even mass numbers and δ_{AO}, for use with nuclides with odd mass numbers. The attempts to evaluate the three parameters of the equation have recently been reviewed by Coryell[18]. In that paper the symbol $\epsilon_A = \pi - \upsilon$ is used to designate δ_{AE}.

Since for any given A there are three parameters in the Bohr-Wheeler beta energy equation: Z_A, B_A, and δ_{AE} or δ_{AO}, three beta decay energies serve to define their values. The parameters have been evaluated for each set of three successive beta decay energies, both beta$^-$ and electron capture, in the cycles for the four radioactive series. Although there are a number of cases in which non-successive beta decay energies can be used to calculate further values for the parameters, the treatment has been restricted to the successive beta chains because these illustrate the calculations adequately. The same approach has been used in these calculations that was used in the previously described systematics; that is, values for the parameters have been calculated in all possible cases, even those subject to considerable uncertainty, in order to make the analysis complete. In this way the values calculated from uncertain decay energies can be compared with the more certain values to point out possible errors in the decay energies involved. Three simple formulas have been used for the actual calculation of the parameters. If β_1, β_2, and β_3 are three successive beta decay energies connecting the isotopes Z, Z + 1, Z + 2, and Z + 3, the values for δ_{AE} and δ_{AO} can be calculated from the following formula:

$$\delta_A \text{ (Mev)} = \frac{\beta_1 - 2\beta_2 + \beta_3}{4} .$$

If a value of β is an electron capture decay energy a negative sign is affixed to it. In addition, in order to insure that a positive value of δ_A is obtained, the right hand side of the equation is multiplied by -1 if Z_1 is an even number. The formula used to

calculate B_A is as follows:

$$B_A \text{ (Mev)} = \frac{\beta_1 - \beta_3}{2} .$$

If β_1 is a beta$^-$ decay energy and β_3 an electron capture decay energy the numerator is $\beta_1 + \beta_3$. In all other cases the formula is used as given. The formula for Z_A is as follows:

$$Z_A = Z_1 + 1/2 + \frac{\beta_1 - \delta_A}{B_A} .$$

If Z_1 is an even number, δ_A is added to β_1. In addition, if β_1 is an electron capture decay energy a negative sign is affixed to it.

The calculated values of the parameters are tabulated in Table 7 and are presented in Figs. 12 (δ_A), 13(B_A), and 14(Z_A). The values calculated from the Fermi mass equation are indicated by dashed lines in the figures. Average values of δ_{AE}, δ_{AO}, and B_A have also been calculated for the more certain values of the parameters (those not included in parentheses in Table 7). The average value of δ_{AE} calculated for mass numbers between 214 and 244 is 1.44 Mev with an average deviation of 0.14 Mev. This indicates that the even-even energy surface is an average of 1.44 Mev lower in energy than the odd-odd surface. At the same time the average value of δ_{AO} is 0.16 Mev for mass numbers between 213 and 245 with an average deviation of 0.07 Mev. In this case the indication is that the even-odd energy surface is an average of 0.16 Mev lower in energy than the odd-even surface. The average value of B_A between mass numbers 213 and 245 for both even and odd mass numbers is 1.14 Mev with an average deviation of 0.09 Mev.

Table 7

Bohr-Wheeler Parameters

A	Z to Z	δ_{AE}	δ_{AO}	B_A	Z_A
208	81 84	2.46		3.00	82.34
209	81 84		0.18	2.93	82.78
210	81 84	1.61		2.11	83.29
210	82 85	(1.83)		(2.55)	(83.24)
211	81 84		(0.51)	(1.80)	(83.55)
211	82 85		0.18	1.15	83.87
212	81 84	(1.77)		(1.86)	(83.48)
212	82 85	(1.38)		(1.08)	(84.31)
212	83 86	(1.41)		(1.02)	(84.32)
213	82 85		0.25	0.95	84.70
213	83 86		(0.25)	(0.96)	(84.69)
214	82 85	1.59		1.04	85.01
214	83 86	1.55		1.13	84.93
215	83 86		0.13	1.01	85.36
216	83 86	1.76		1.03	85.76
217	84 87		0.16	0.97	86.02
218	84 87	1.69		1.10	86.38
218	85 88	1.65		1.18	86.36
219	84 87		0.09	1.01	86.85
219	85 88		0.06	1.08	86.79
220	84 87	(1.77)		(0.97)	(87.40)
220	85 88	1.66		1.17	87.17
221	85 88		(0.22)	(1.09)	(87.51)

Table 7 (Cont'd)

A	Z to Z	δ_{AE}	δ_{AO}	B_A	Z_A
221	86 89		0.26	1.18	87.47
222	86 89	1.55		1.09	87.89
222	87 90	1.43		1.34	87.91
223	86 89		0.29	1.25	88.22
223	87 90		0.21	1.41	88.20
224	86 89	(1.72)		(1.00)	(88.82)
224	87 90	1.53		1.37	88.60
225	87 90		(0.18)	(1.23)	(88.90)
225	88 91		0.19	1.23	88.91
226	87 90	(1.45)		(1.29)	(89.13)
226	88 91	1.31		1.03	89.16
226	89 92	(1.26)		(1.14)	(89.25)
227	88 91		-0.02	1.20	89.58
227	89 92		0.01	1.14	89.56
228	88 91	1.60		1.06	90.05
228	89 92	1.51		1.24	90.04
229	88 91		0.17	1.10	90.31
229	89 92		0.13	1.18	90.29
229	90 93		(0.12)	(1.17)	(90.29)
230	88 91	(1.39)		(1.23)	(90.56)
230	89 92	(1.44)		(1.13)	(90.61)
230	90 93	1.40		1.05	90.58
230	91 94	(1.33)		(1.18)	(90.74)
231	88 91		(0.33)	(1.09)	(91.10)

Table 7 (Cont'd)

A	Z	to Z	δ_{AE}	δ_{AO}	B_A	Z_A
231	89	92		(0.27)	(1.21)	(90.99)
231	90	93		0.23	1.12	90.99
231	91	94		0.17	1.24	91.09
232	89	92	(1.50)		(1.22)	(91.35)
232	90	93	1.45		1.11	91.40
232	91	94	1.42		1.16	91.42
233	90	93		0.23	1.16	91.76
233	91	94		0.14	1.34	91.79
234	90	93	1.36		1.17	92.06
234	91	94	1.32		1.25	92.07
235	90	93		0.30	0.97	92.63
235	91	94		0.15	1.27	92.49
235	92	95		(0.12)	(1.20)	(92.46)
236	90	93	(1.49)		(0.90)	(93.14)
236	91	94	1.33		1.23	92.84
236	92	95	1.29		1.13	92.84
236	93	96	(1.28)		(1.12)	(92.82)
237	91	94		(0.23)	(1.21)	(93.11)
237	92	95		0.13	1.00	93.15
237	93	96		-0.04	1.33	93.36
238	91	94	(1.30)		(1.22)	(93.48)
238	92	95	1.23		1.08	93.55
238	93	96	1.17		1.20	93.58
239	91	94		(0.16)	(0.89)	(94.12)

Table 7 (Cont'd)

A	Z to Z	δ_{AE}	δ_{AO}	B_A	Z_A
239	92 95		0.23	1.03	93.97
239	93 96		0.12	1.25	93.98
240	91 94	(1.42)		(1.04)	(94.20)
240	92 95	1.36		0.91	94.39
240	93 96	1.26		1.10	94.32
240	94 97	(1.38)		(1.37)	(93.90)
241	91 94		(0.31)	(1.08)	(94.45)
241	92 95		(0.22)	(0.89)	(94.77)
241	93 96		(0.10)	(1.12)	(94.61)
241	94 97		(0.15)	(1.21)	(94.64)
241	95 98		(0.09)	(1.33)	(94.76)
242	92 95	(1.40)		(0.74)	(95.51)
242	93 96	(1.20)		(1.15)	(94.97)
242	94 97	1.23		1.21	94.98
242	95 98	(1.24)		(1.19)	(94.95)
243	92 95		(0.07)	(1.10)	(95.06)
243	93 96		(0.17)	(0.90)	(95.30)
243	94 97		0.23	1.01	95.28
243	95 98		0.12	1.22	95.40
244	92 95	(1.36)		(1.00)	(95.64)
244	93 96	(1.36)		(1.00)	(95.64)
244	94 97	1.36		1.21	95.44
244	95 98	1.30		1.10	95.68
244	96 99	(1.45)		(1.40)	(95.96)

Table 7 (Cont'd)

A	Z to Z	δ_{AE}	δ_{AO}	B_A	Z_A
245	92 95		(0.31)	(1.31)	(95.58)
245	93 96		(0.37)	(1.20)	(95.72)
245	94 97		(0.22)	(0.90)	(95.97)
245	95 98		0.13	1.08	95.97
245	96 99		(0.22)	(1.26)	(96.12)
245	97 100		(0.15)	(1.40)	(96.31)
246	92 95	(1.44)		(1.24)	(95.96)
246	93 96	(1.51)		(1.10)	(96.21)
246	94 97	(1.40)		(0.89)	(96.49)
246	95 98	(1.26)		(1.18)	(96.37)
246	96 99	(1.28)		(1.24)	(96.40)
246	97 100	(1.29)		(1.23)	(96.39)
247	92 95		(0.13)	(1.03)	(96.86)
247	93 96		(0.12)	(1.06)	(96.78)
247	94 97		(0.21)	(1.24)	(96.53)
247	95 98		(0.29)	(1.08)	(96.60)
247	96 99		(0.29)	(1.08)	(96.61)
247	97 100		(0.20)	(1.25)	(96.80)
248	93 96	(1.47)		(1.01)	(97.29)
248	94 97	(1.46)		(0.99)	(97.34)
248	95 98	(1.32)		(1.28)	(97.03)
248	96 99	(1.28)		(1.20)	(97.04)
248	97 100	(1.32)		(1.11)	(96.96)
249	94 97		(0.36)	(1.10)	(97.65)

Table 7 (Cont'd)

A	Z	to Z	δ_{AE}	δ_{AO}	B_A	Z_A
249	95	98		(0.25)	(1.34)	(97.35)
249	96	99		(0.18)	(1.20)	(97.40)
249	97	100		(0.17)	(1.22)	(97.40)
250	94	97	(1.43)		(1.11)	(97.78)
250	95	98	(1.47)		(1.04)	(97.90)
250	96	99	(1.42)		(0.93)	(98.03)
250	97	100	(1.17)		(1.42)	(98.01)
251	94	97		(0.19)	(1.01)	(98.38)
251	95	98		(0.20)	(1.00)	(98.40)
251	96	99		(0.28)	(1.17)	(98.20)
251	97	100		(0.28)	(1.16)	(98.21)
251	98	101		(0.34)	(1.28)	(98.28)
252	95	98	(1.50)		(1.07)	(98.60)
252	96	99	(1.42)		(0.91)	(98.87)
252	97	100	(1.25)		(1.26)	(98.63)
252	98	101	(1.23)		(1.24)	(98.63)
253	96	99		(0.38)	(1.14)	(99.03)
253	97	100		(0.29)	(1.31)	(98.90)
253	98	101		(0.20)	(1.12)	(98.88)
254	96	99	(1.45)		(1.14)	(99.19)
254	97	100	(1.45)		(1.14)	(99.18)
254	98	101	(1.31)		(0.86)	(99.26)
255	96	99		(0.22)	(1.08)	(99.62)
255	97	100		(0.21)	(1.11)	(99.57)

Table 7 (Cont'd)

A	Z to Z	δ_{AE}	δ_{AO}	B_A	Z_A
255	98 101		(0.23)	(1.15)	(99.56)
255	99 102		(0.30)	(1.01)	(99.50)
256	97 100	(1.53)		(1.17)	(99.82)
256	98 101	(1.40)		(0.90)	(100.06)
256	99 102	(1.23)		(1.22)	(100.05)
257	98 101		(0.35)	(1.14)	(100.36)
257	99 102		(0.28)	(1.27)	(100.33)
258	98 101	(1.42)		(1.14)	(100.53)
258	99 102	(1.43)		(1.11)	(100.54)
259	98 101		(0.19)	(1.09)	(100.90)
259	99 102		(0.19)	(1.08)	(100.92)
260	99 102	(1.53)		(1.14)	(101.18)

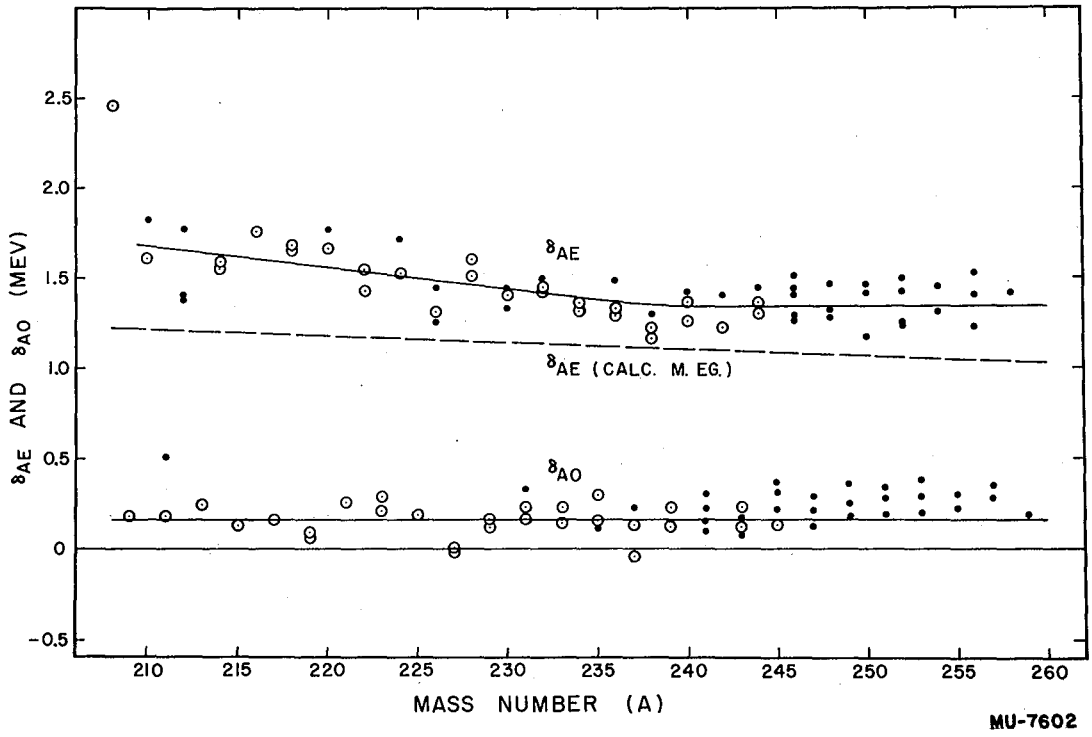

Fig. 12. Bohr-Wheeler parameters, δ_{AE} and δ_{AO}, as a function of mass number: ○, reliable values; ●, uncertain values.

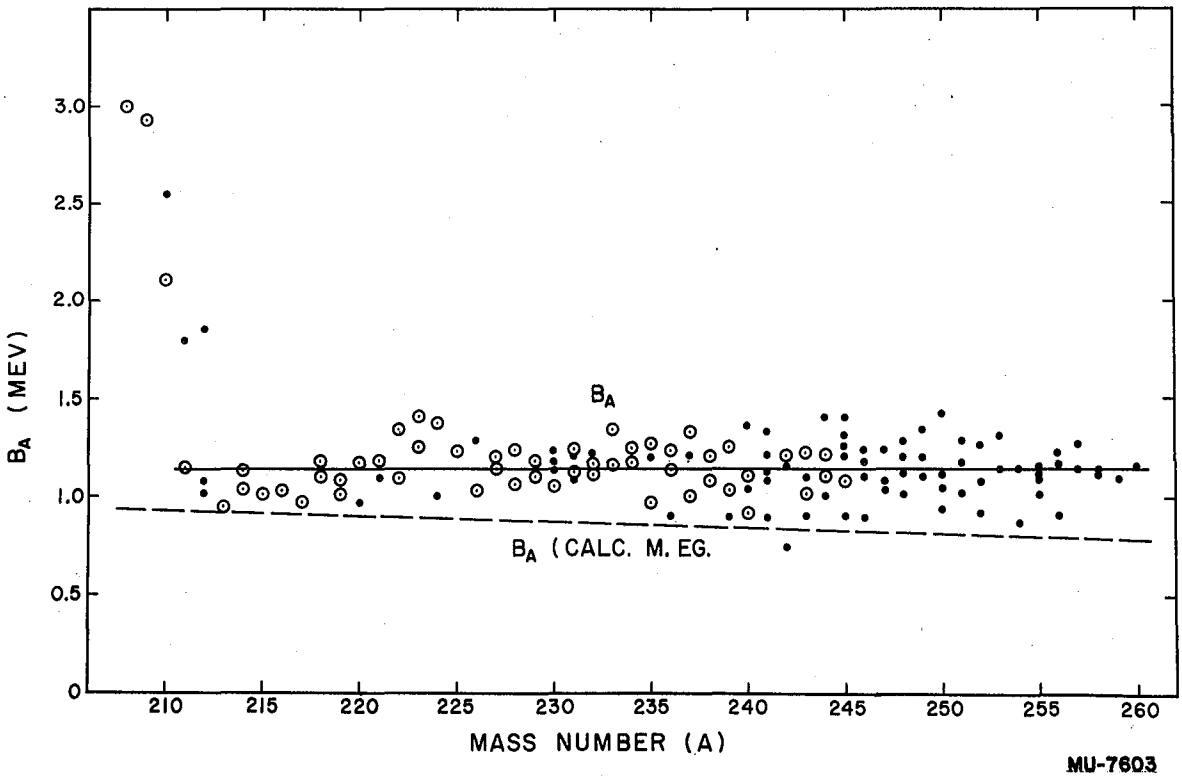

Fig. 13. Bohr-Wheeler parameter, B_A, as a function of mass number: ⊙, reliable values; ●, uncertain values.

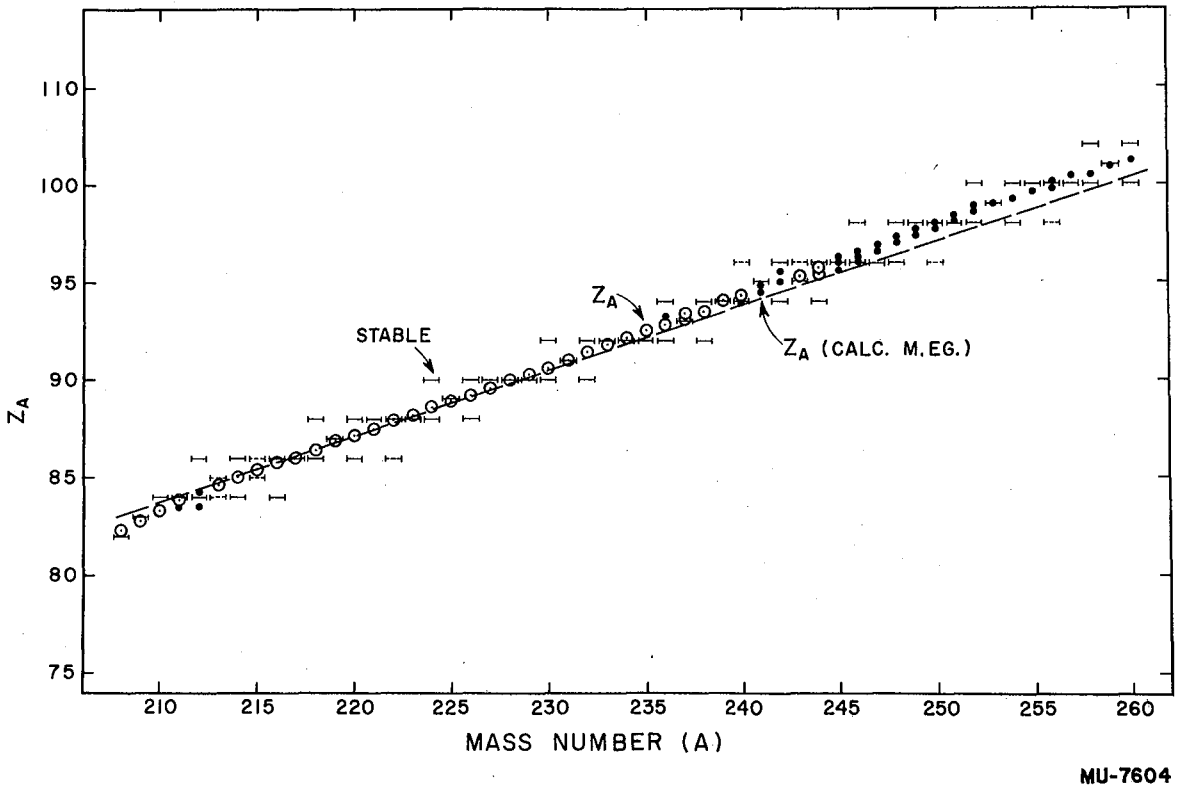

Fig. 14. Bohr-Wheeler parameter, Z_A, as a function of mass number: o , reliable values; ● , uncertain values.

It will be noted that δ_{AE} has a relatively high value in the low mass number region of Fig. 12 and decreases slightly with increasing mass number over the first half of the graph. This may be due to higher pairing energies of neutron and proton pairs in the region just beyond the 126 neutron and 82 proton closed shells where high nucleon spins and hence coupling energies are expected.[93] As more nucleons are added, the values of the spin assignments are smaller and hence the coupling energy and δ_{AE} is smaller also. No such effect is noted among the δ_{AO} points, which may be due to the fact that in all odd A nuclides either the neutrons or protons are all paired. In both the δ_{AE} and δ_{AO} graphs there is a considerable scatter of points which is probably due in some degree to accumulative errors in the cycles. The example of the two low δ_{AO} values for mass number 227 can be used to illustrate the type of reasoning employed to apply effects on the δ_A plots to cycle energies. The fact that both δ_A values are low must be due to the fact that either the beta$^-$ energy of Ac^{227} or the electron capture energy of Pa^{227} is too small, since these are the two energies used in both calculations. If the small values for δ_{AO} are due to incorrect decay energies, and indeed it may be that the values actually are low, it is unlikely that the beta$^-$ decay energy of Ac^{227} is low by very much, so that the electron capture energy of Pa^{227} must be too high, which would tend to indicate that there is energy missing in the alpha chain connecting Pa^{227} and Bi^{211}. An inspection of the beta energy versus mass number graph (Fig. 7), however, reveals that the electron capture energy of Pa^{227} may already be a little small, so it is difficult to reach a conclusion on this point.

The graph of B_A versus mass number again shows a large scatter of points. The values of B_A are interpreted as the curvatures of the Bohr-Wheeler parabolas. One way of looking at this is that if B_A has a high value the energy surface has rather steep sides at the given value of A. Although the high values of B_A around mass number 209 are of doubtful significance due to the discontinuities in the energy surface at the 126 neutron and 82 proton closed shells, which tend to invalidate the treatment of beta decay in terms of parabolas, it is interesting that B_A has a very high value for mass number 208. This indicates that the energy surface rises sharply along a line of constant A on both sides of Pb^{208}. As in the case of the δ_A graphs, the values of B_A calculated from closed cycle energies do not agree well with those calculated from the Fermi mass equation.

The calculated values for Z_A are shown in Fig. 14. In addition, the beta stable nuclides are also represented. It will be noted that essentially all of the values of Z_A for odd mass numbers satisfy the requirement that they lie within 0.5 charge unit of the beta stable element. In the cases of mass numbers 213 and 215 Z_A falls within 0.5 charge unit of astatine, which tends to indicate that At^{213} and At^{215} are both beta stable; however, the results are not of a great enough certainty to make the conclusion definite.

Possible actual Bohr-Wheeler parabolas are shown in Fig. 15. The average calculated values of B_A, δ_{AE}, and δ_{AO} have been used in their construction. Actual parabolas in the lighter element region have been constructed by Bochez, Robert and Tobailem.[94]

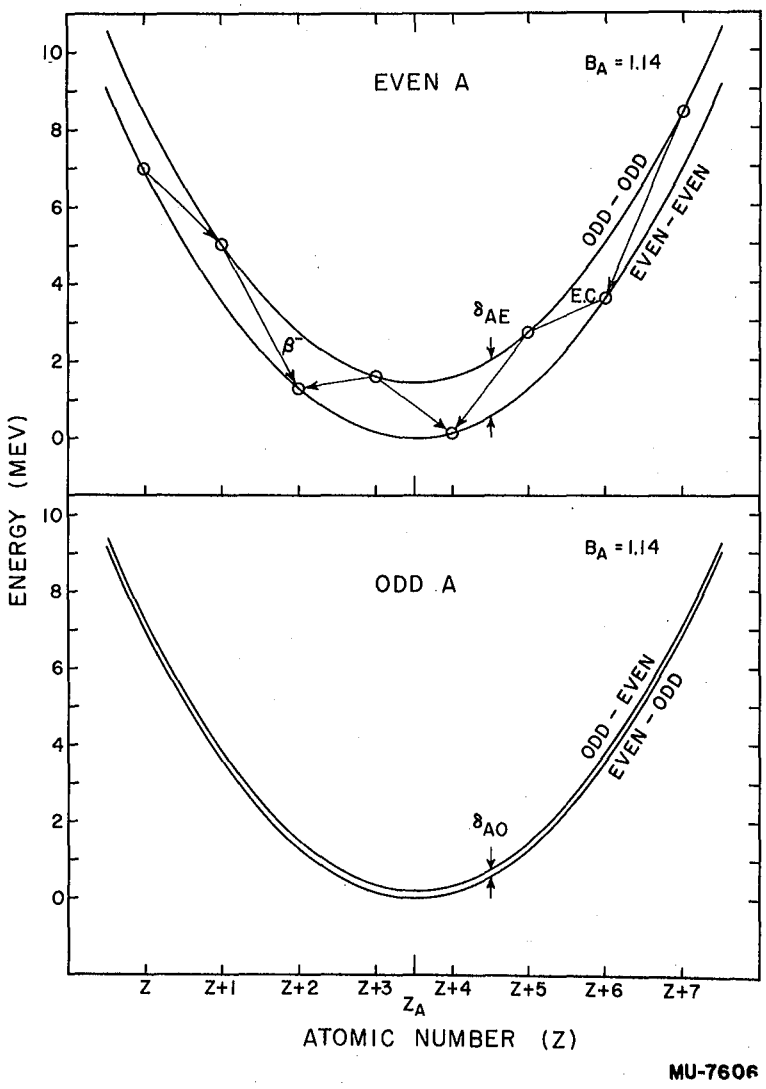

Fig. 15. Bohr-Wheeler parabolas constructed from average values of the parameters.

Finally, the interpretation of δ_{AO} in terms of neutron and proton pairing energies is illustrated in Fig. 16. The beta$^-$ decay of an odd proton nuclide results in the breaking of a neutron pair and formation of a proton pair. Since the nuclide with the proton pair is on the lower energy surface the conclusion is drawn that the proton pairing energy in the heaviest element region is greater than the neutron pairing energy. This observation has been made by a number of authors.[18] The first calculation of δ_{AO} in this region is attributed to Glueckauf.[95]

E. Half-Life Systematics

In addition to the energy surface regularities, half-life correlations are of considerable interest, particularly for the purpose of predicting these properties for unknown nuclides. Half-life energy relations are presented in this section for alpha, beta$^-$, and electron capture decay. In all three cases the general behavior that half-lives became shorter with increasing particle energies is observed. The half-life data employed that were not taken from the Table of Isotopes[4] are tabulated in Table 8.

1. Alpha half-lives. -- The alpha half-life energy relations have been thoroughly treated by Perlman, Ghiorso, and Seaborg.[9] Although new data have been collected since then, the interpretation of the regularities observed is essentially the same. The partial alpha half-lives for the alpha groups of even-even nuclei have been plotted against alpha disintegration energies in Fig. 17. Smooth lines connect the half-lives of the isotopes of each element. It will be noted that where information is available on fine structure groups these points also fall close to the lines. Although the lines

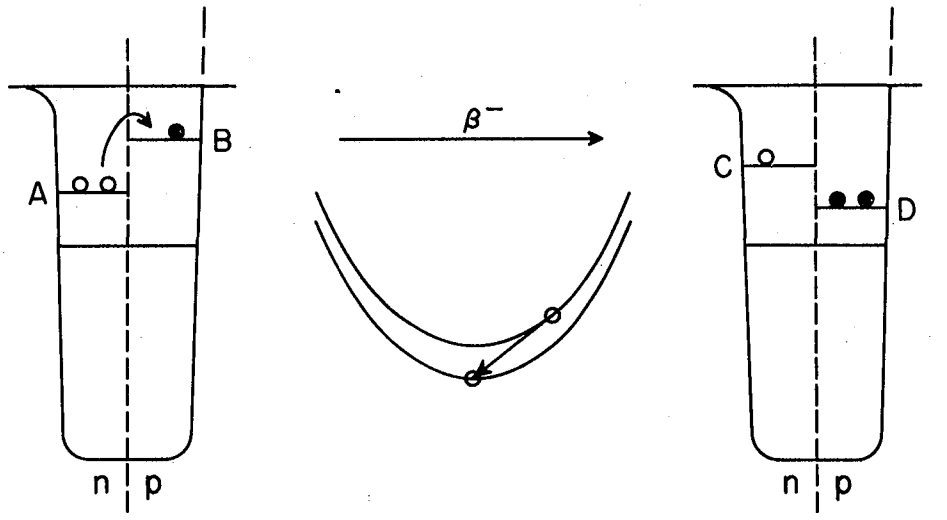

Fig. 16. Representation of the breaking of a neutron pair and forming of a proton pair in the beta⁻ decay of odd A nuclides.

Table 8

Half-Life Data not in the Table of Isotopes

Nuclide	Particle energy (Mev) (abundance)		Half-life of isotope
Alpha half-lives (even-even nuclides)			
U^{230}	5.99	(68%)[44]	
	5.92	(31%)	
U^{232}	5.41	(69%)[44]	
	5.35	(31%)	
Pu^{242}	4.98	(80%)[53]	
	4.94	(20%)	
Cf^{246}	6.86	(78%)[97]	
	6.81	(22%)	
Cf^{248}			225 d[50]
Cf^{250}			12 y[49]
Cf^{252}			~2 y[49]
100^{255}			3.2 h[55]
Alpha half-lives (odd nucleon nuclides)			
Pu^{241}	4.98	(75%)[53]	
Bk^{249}			10^5 y[54]
Cf^{249}	5.92	(90%)[49]	400 y[49]
99^{253}			20 d[55]
100^{255}			15 h[55]

Table 8 (Cont'd)

Nuclide	Particle energy (Mev) (abundance)	Half-life of isotope
Beta$^-$ half-lives		
Pu^{243}	0.56 (53%)[63]	4.98 h[63]
Bk^{250}		3.13 h[49]
Cf^{253}		20 d[55]
99^{254}		36 h[55]
99^{255}		~1 month[55]
Electron capture half-lives		
Bk^{246}		1.9 d[69]
Cf^{247}		~2.7 h[69]

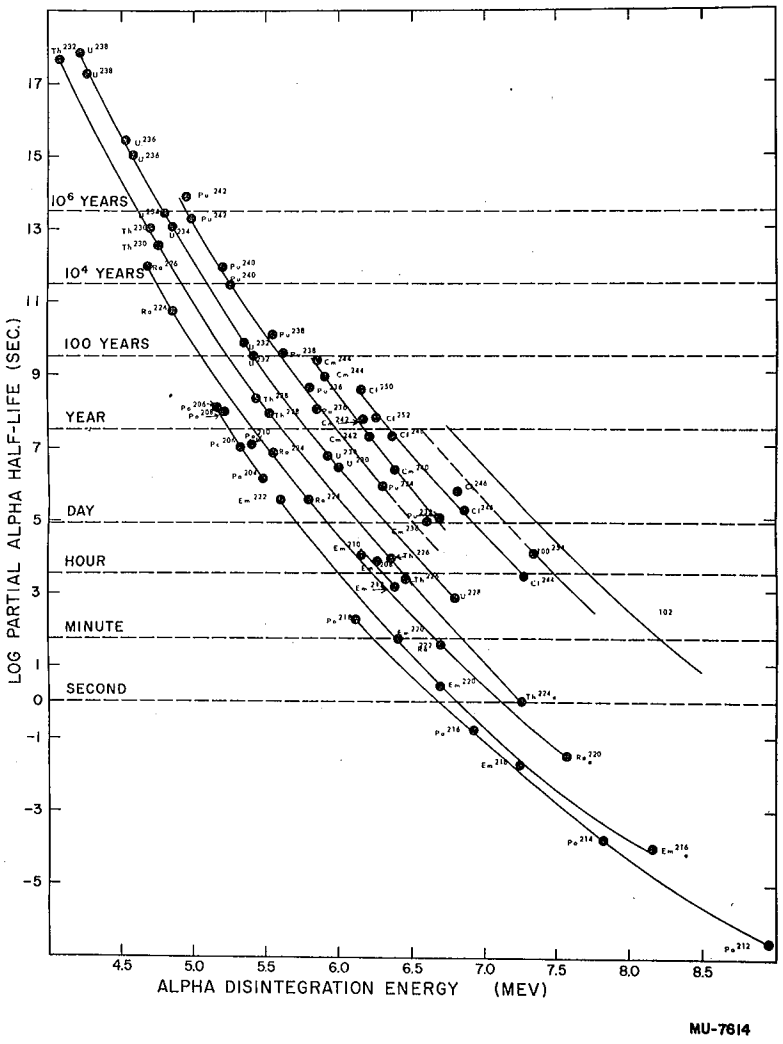

Fig. 17. Alpha half-lives of even-even nuclides as a function of their alpha disintegration energies.

for each element are in general continuous, the points for isotopes of polonium and emanation with less than 126 neutrons lie above the extensions of their respective lines for heavier isotopes, indicating that their decay is being hindered. This effect can be interpreted in terms of a radius shrinkage just below the closed shell.[96] At the same time there are reasonable explanations for the few other irregularities in the alpha lines. The half-lives of Em^{216}, Ra^{220}, and Th^{224} have been estimated by previous authors[41] and can readily be changed. The former two should probably be lowered slightly. In addition, with regard to the high Pu^{232} point, it appears certain that the alpha branching ratio of this isotope is indeed much greater than 2 percent,[42] in fact 17 percent would be a more reasonable value. For another example, the alpha branching ratio of Cm^{238} is more likely to be 5 percent than greater than 10 percent,[41] if this point is to lie on the line formed by the even-even curium alpha emitters. In general, because of the regular trends on the alpha half-life versus energy plot, the alpha half-lives can be predicted with a fair degree of confidence from a knowledge of the estimated alpha energy.

The half-life relationships for nuclides with one or two odd nucleons are much less regular than those for even-even nuclei as can be seen from an inspection of the plot of the partial half-life of the alpha group in major abundance for each nuclide versus the disintegration energy of the group (see Fig. 18). The solid lines have been transposed from the curve for even-even alpha emitters to act as guide lines. Dashed lines between these indicate the

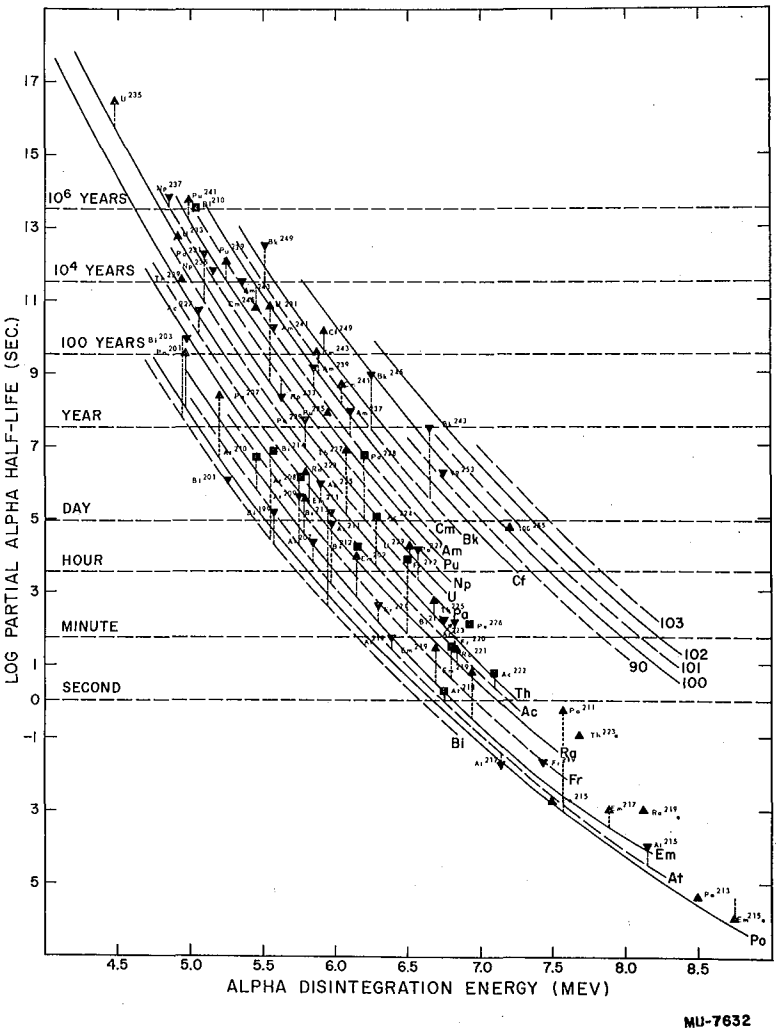

Fig. 18. Alpha half-lives of odd nucleon nuclides as a function of their alpha disintegration energies.

points for odd element isotopes to lie if their alpha decay were not hindered. Departure factors (hindrance factors) for the alpha decay half-lives range from about 1 to 10^4. It will be noted that although Am^{237}, Am^{241}, and Am^{243} do not appear to have large departure factors, the berkelium isotopes, Bk^{243}, Bk^{245}, and Bk^{249} do. Going one step further, 99^{253} again has a small departure factor. In connection with this latter case, it is interesting to note that 100^{255} as well as 99^{253} has a departure factor of about unity. The alpha half-life predictions presented later on were made from this graph. Where predictions were made that extended beyond the measured values in the region of californium, lines parallel to the polonium line were drawn. Because of the lack of hindrance in the decay of 99^{253} and 100^{255} the half-lives were estimated from the lines themselves and therefore really represent lower limits.

2. Beta$^-$ half-lives. -- Beta$^-$ half-lives can also be correlated with particle energies. Graphs of log $t_{1/2}$ (or log λ) versus log E, first used by Sargent,[98] have long been used to show the decrease in half-life with increase in beta$^-$ energy. Attempts to distinguish lines associated with various forbiddenness factors and section rules have met with little success. A more quantitative method of classifying beta decay according to ft values is more generally used to indicate applicable selection rules.[99] The log of the partial beta half-life for the beta particle in greatest abundance has been plotted against the log of the beta particle energy for the heavy elements in Fig. 19. Two solid lines have been included which are hypothetical allowed and first forbidden lines. The lower line was constructed according to the assumption that 5.1 was a fair average value for log ft

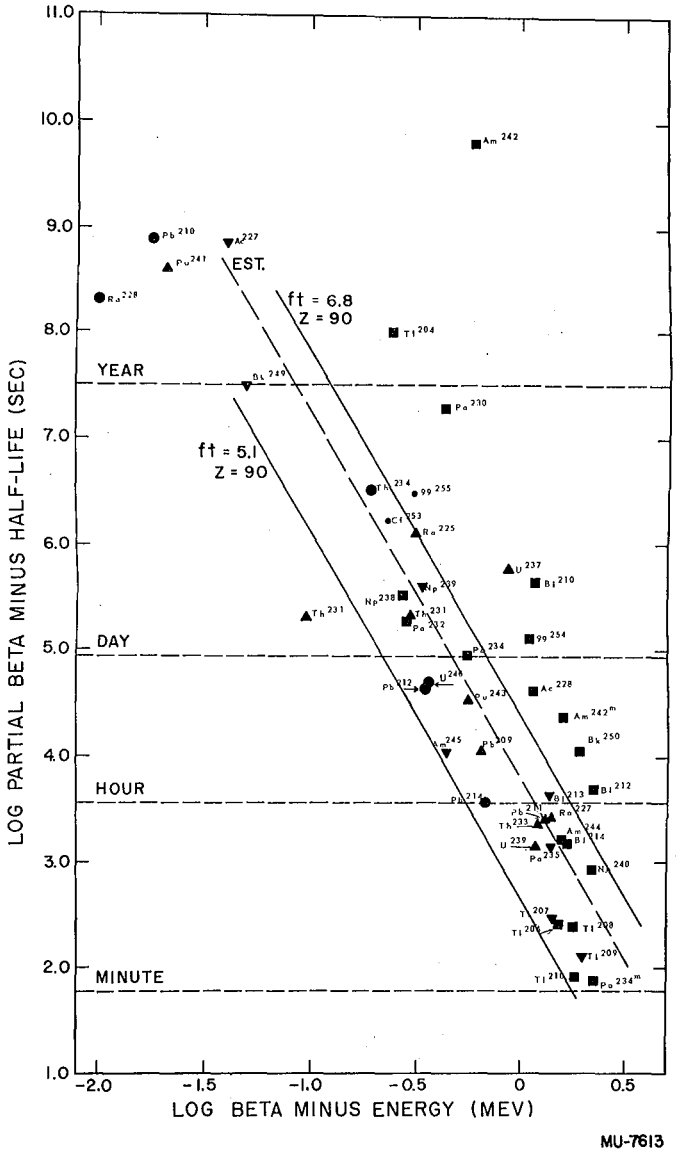

Fig. 19. Beta$^-$ half-lives as a function of beta particle energies.

for allowed transitions ($\Delta I = 0, 1$ no) and with the use of Moszkowski's beta decay graphs.[100] The upper line was constructed from data taken from the same graphs with the assumption that 6.8 was a fair average value for log ft for first forbidden transitions ($\Delta I = 0, 1$ yes type). An atomic number of 90 was employed in both cases. It will be seen that the lines do not actually pass through those areas with greatest density of points although most of the beta energies appear to lie between these lines for allowed and first forbidden transitions. Another interesting observation is that only points for odd-odd nuclei lie above the upper line with the exception of the one for U^{237}. Although no theoretical significance is claimed for this phenomenon, it seems to be true for electron capture as well as beta$^-$ decay. The beta$^-$ half-life predictions reported further on were made from the dashed line between the two solid lines on the graph.

Even though there is a large scatter of points in Fig. 19 there are certain features which stand out. First, the very high forbiddenness in the decay of Am^{242} makes its case analogous to that of K^{40}. At the other extreme Ra^{228} and the 0.094 Mev beta group in Th^{231} may be superallowed, however, in these examples experimental errors are possible.

3. Electron capture half-lives. -- Figure 20 is a graph of log electron capture half-life versus log decay energy exactly like that for beta$^-$ decay. The electron capture energies were obtained from the closed cycles and data on gamma energies.[41] In addition, the information on Cm^{241} and Am^{240} from this paper is included.

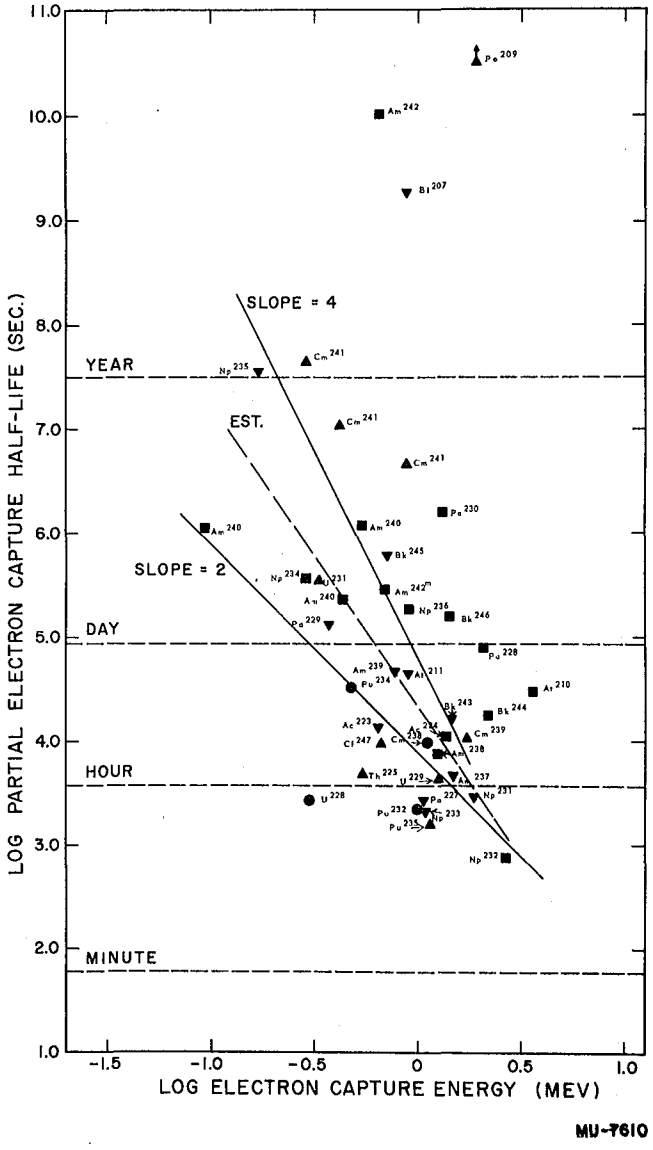

Fig. 20. Electron capture half-lives as a function of electron capture energies.

The features of this type of plot have been rather thoroughly discussed by Hoff[36] and will not be gone into in detail in this report. A number of points for nuclides with less than 126 neutrons were not in Hoff's thesis but have been included in Fig. 20, i.e., Bi^{207}, Po^{209}, and At^{210}. In all three of these cases long half-lives are associated with high electron capture energies, which appear to be a characteristic of this region.

Predictions of electron capture half-lives are very difficult because, among other things, both K and L capture are possible in most cases and these have different rates. Lines with slopes of 2 and 4 have been included in Fig. 20 to correspond to allowed and first forbidden electron capture decay.[36] The actual predictions that were made were taken from the dashed line between the two solid lines.

In view of the limited number of decay schemes that have been worked out, it is evident that much more work is needed in the field of electron capture isotopes. Until such time Sargent diagrams such as those presented by Thompson,[35] Hoff,[36] and Feather[101] will be of limited value.

4. Predictions of nuclear properties. --One of the tests of any systematics is in the ability to predict unknown properties with its use. Predictions of the energies and half-lives for undiscovered isotopes of elements 99-103 are tabulated in Table 9. Alpha energies have been estimated from Fig. 8 and beta energies have been estimated from Fig. 9. All additional energies are calculated values from the closed cycles, Figs. 2-5. The half-

lives were estimated from Figs. 18 (alpha), 19 (beta$^-$), and 20 (electron capture). Nuclides are included which will be produced both by heavy ion bombardments and neutron irradiations of target materials.

Table 9
Predicted Properties for Isotopes of Elements 99-103

Nuclide	α		EC or β^-	
	Energy (Mev)	Half-life	Energy (Mev)	Half-life
99^{245}	7.87	50 s	3.21 EC	10 m
99^{246}	7.66	4 m	3.87 EC	7 m
99^{248}	7.19	4 h	3.03 EC	20 m
99^{249}	6.90	3 d	1.50 EC	2 h
99^{250}	6.61	60 d	1.86 EC	1 h
99^{251}	6.65	40 d	0.62 EC	1 d
99^{252}	6.69	20 d	1.07 EC	5 h
99^{256}			1.90 β^-	10 m
99^{257}			1.34 β^-	40 m
100^{246}	8.41	3 s	2.53 EC	30 m
100^{247}	8.20	10 s	3.17 EC	10 m
100^{248}	7.98	1 m	1.49 EC	2 h
100^{249}	7.77	5 m	2.38 EC	30 m
100^{250}	7.49	50 m	0.95 EC	7 h
100^{251}	7.20	10 h	1.22 EC	3 h
100^{252}	7.25	8 h		
100^{253}	7.29	5 h	0.50 EC	2 d
100^{256}	7.01	3 d		
100^{257}	6.82	20 d		

Table 9 (Cont'd)

Nuclide	α		EC or β^-	
	Energy (Mev)	Half-life	Energy (Mev)	Half-life
100^{258}	6.62	160 d		
100^{259}	6.42	4 y	0.26 β^-	8 d
100^{260}	6.22	40 y		
100^{261}	6.04	400 y	1.04 β^-	3 h
100^{262}	5.84	4,000 y	0.15 β^-	50 d
101^{251}	8.06	1 m	3.18 EC	10 m
101^{252}	7.76	20 m	3.54 EC	10 m
101^{253}	7.80	10 m	2.01 EC	50 m
101^{254}	7.85	7 m	2.37 EC	30 m
101^{255}	7.90	4 m	1.31 EC	3 h
101^{256}	7.73	20 m	1.79 EC	1 h
101^{257}	7.55	1 h	0.50 EC	2 d
101^{258}	7.35	9 h	1.39 EC	2 h
101^{259}	7.15	2 d		
101^{260}	6.97	10 d	1.18 β^-	1 h
101^{261}	6.77	100 d	0.61 β^-	9 h
101^{262}			1.86 β^-	10 m
101^{263}			0.99 β^-	2 h
102^{255}	8.40	20 s	1.72 EC	1 h
102^{256}	8.44	10 s	0.55 EC	2 d
102^{257}	8.26	50 s	1.21 EC	4 h
102^{258}	8.08	3 m		
102^{259}	7.88	20 m	0.43 EC	3 d

Table 9 (Cont'd)

Nuclide	α		EC or β^-	
	Energy (Mev)	Half-life	Energy (Mev)	Half-life
102^{260}	7.69	1 h		
102^{261}	7.50	7 h		
102^{262}	7.30	2 d		
102^{263}	7.10	10 d		
102^{264}	6.90	90 d		
102^{265}	6.70	2 y	0.26 β^-	8 d
102^{266}	6.51	20 y		
102^{267}	6.31	200 y	0.93 β^-	2 h
103^{264}	7.69	3 h	1.54 EC	2 h
103^{265}	7.48	20 h		
103^{266}	7.28	6 d	0.62 EC	1 h
103^{267}	7.08	40 d		

V. ACKNOWLEDGMENTS

The three nuclear investigations described in this dissertation were suggested by Professor Glenn T. Seaborg and were performed under his direction. His interest and patient guidance are gratefully acknowledged.

Appreciation is also expressed to K. Street, Jr., for guidance in the chelating agent studies.

The cross section investigations were performed with the generous help of J. W. Cobble, whose broad experience in many phases of physical and inorganic chemistry aided in the solution of many of the problems connected with the investigations. Appreciation is also expressed to S. G. Thompson and A. Ghiorso for many helpful discussions. The help of M. J. LaSalle and F. S. Stephens in some of the experimental aspects of the problem is gratefully acknowledged as is the counting help of T. K. Pionteki. Appreciation is also expressed to Professor J. G. Hamilton, G. B. Rossi, W. B. Jones and the staff of the 60-inch cyclotron for the alpha particle bombardments. The aid of the Health Chemistry group under N. Garden in handling the high levels of plutonium alpha activity is appreciated.

Appreciation is expressed to A. Ghiorso, F. Asaro, T. O. Passell, and H. Jaffe for supplying some of the energies used in the nuclear systematics section.

This work was performed under the auspices of the United States Atomic Energy Commission.

VI. REFERENCES

Section II

1. E. R. Tompkins, J. X. Khym, and W. E. Cohn, J. Am. Chem. Soc. 69, 2769 (1947).
2. D. H. Harris and E. R. Tompkins, ibid., 2792.
3. B. H. Ketelle and G. E. Boyd, ibid., 2800.
4. G. E. Boyd, J. Schubert, and A. W. Adamson, ibid., 2818.
5. E. R. Tompkins and S. W. Mayer, ibid., 2859.
6. S. W. Mayer and E. R. Tompkins, ibid., 2866.
7. S. G. Thompson, A. Ghiorso, and G. T. Seaborg, Phys. Rev. 77, 838 (1950).
8. S. G. Thompson, K. Street, Jr., A. Ghiorso, and G. T. Seaborg, ibid., 78, 298 (1950).
9. S. G. Thompson, A. Ghiorso, and G. T. Seaborg, ibid., 80, 781 (1950).
10. K. Street, Jr., S. G. Thompson, and G. T. Seaborg, J. Am. Chem. Soc. 72, 4832 (1950).
11. J. Schubert, "Ion Exchange", F. C. Nachod, editor, (Academic Press, Inc., New York, 1949) p. 167.
12. G. E. Boyd, Ann. Rev. Phys. Chem. 2, 309 (1951).
13. A. E. Martell and M. Calvin, "Chemistry of the Metal Chelate Compounds", (Prentice-Hall, Inc., New York, N. Y., 1952).
14. S. G. Thompson, A. Ghiorso, B. G. Harvey, and G. R. Choppin, Phys. Rev. 93, 1129 (1954).
15. G. Schwarzenbach and H. Ackermann, Helv. Chim. Acta 31, 1029 (1948).
16. The Dow Chemical Company, Midland, Michigan.

17. S. W. Mayer and E. C. Freiling, J. Am. Chem. Soc. 75, 5647 (1953).

18. F. H. Spedding, J. E. Powell, and E. J. Wheelwright, ibid., 76, 612 (1954).

19. International Critical Tables, VI, (McGraw-Hill Book Company, Inc., New York, N. Y., 1929) p. 264.

20. E. C. Freiling and L. R. Bunney, J. Am. Chem. Soc. 76, 1021 (1954).

21. H. Ley, Ber. deut. chem. Ges. 42, 354 (1909).

Section III

1. R. Serber, Phys. Rev. 72, 1114 (1947).

2. E. P. Steinberg and M. S. Freedman, "Radiochemical Studies of the Fission Products," (McGraw-Hill Book Company, Inc., New York, N. Y., 1951), National Nuclear Energy Series, Vol. 9, p. 1378.

3. R. W. Spence and G. P. Ford, Ann. Rev. Nuc. Sci. 2, 399 (1953).

4. D. H. Templeton, ibid., 93.

5. N. Bohr, Nature, 137, 344 (1936).

6. N. Bohr and J. A. Wheeler, Phys. Rev. 56, 426 (1939).

7. R. H. Goeckermann and I. Perlman, ibid., 76, 628 (1949).

8. R. E. Batzel, D. R. Miller, and G. T. Seaborg, ibid., 84, 671 (1951).

9. R. E. Batzel and G. T. Seaborg, ibid., 82, 607.

10. G. Rudstam, P. C. Stevenson, and R. L. Folger, ibid., 87, 358 (1952).

11. H. A. Tewes and R. A. James, ibid., 88, 860.

12. J. Jungerman, ibid., 79, 632 (1950).

13. A. S. Newton, ibid., 75, 17 (1949).

14. K. Street, Jr., Ph. D. thesis, University of California Unclassified Report UCRL-301 (March 1949).

15. G. T. Seaborg, Phys. Rev. 85, 157 (1952).

16. S. G. Thompson, A. Ghiorso, and G. T. Seaborg, ibid., 80, 781 (1950).

17. G. B. Rossi and W. B. Jones, private communication (October 1953).

18. K. D. Jenkins, Crocker Laboratory, 60-inch cyclotron report (60-68) (April 3, 1950).

19. E. L. Kelly and E. Segre, Phys. Rev. 75, 999 (1949).

20. G. T. Seaborg, private communication (1953).

21. D. L. Hufford and B. F. Scott, "The Transuranium Elements: Research Papers," (McGraw-Hill Book Company, Inc., New York, N. Y., 1949), National Nuclear Energy Series, Plutonium Project Record, Vol. 14B, p. 1149.

22. M. S. Freedman, R. P. Metcalf, and N. Sugarman, "Radiochemical Studies: The Fission Products," (McGraw-Hill Book Company, Inc., New York, N. Y., 1951), National Nuclear Energy Series, Plutonium Project Record, Vol. 9, p. 459.

23. H. W. Miller and R. J. Brouns, Anal. Chem. 24, 536 (1952).

24. B. B. Cunningham, A. Ghiorso, and J. C. Hindman, Metallurgical Project Report CN-124 (A-1818), (January 5, 1944), p. 1.

25. J. C. Wallmann, Ph. D. thesis, University of California Radiation Laboratory Classified Report UCRL-1255 (April 1951).

26. W. A. Aron, B. G. Hoffman, and F. C. Williams, U. S. Atomic Energy Commission Unclassified Document AECU-663 (May 28, 1951).

27. W. W. Meinke, University of California Radiation Laboratory Declassified Report UCRL-432, Addenda 1 and 2 (August 30, 1949).

28. C. D. Coryell and N. Sugarman, "Radiochemical Studies: The Fission Products," (McGraw-Hill Book Company, Inc., New York, N. Y. 1951), National Nuclear Energy Series, Plutonium Project Record, Vol. 9.

29. N. Garden and co-workers (unpublished data).

30. J. M. Hollander, I. Perlman, and G. T. Seaborg, Revs. Modern Phys. 25, 469 (1953).

31. Dow Chemical Company, Midland, Michigan.

32. H. G. Hicks, R. S. Gilbert, P. C. Stevenson, and W. H. Hutchin, California Research and Development Company Report LRL-65 (1953).

33. H. G. Hicks, P. C. Stevenson, and R. S. Gilbert, unpublished data (1953).

34. K. Street, Jr. and G. T. Seaborg, J. Am. Chem. Soc. 72, 2790 (1950).

35. K. Street, Jr., unpublished data (1950); K. R. Chapman, G. R. Choppin, S. G. Thompson, and B. G. Harvey, unpublished data (1953).

36. A. Ghiorso, A. H. Jaffey, H. P. Robinson, and B. B. Weissbourd, "The Transuranium Elements: Research Papers," (McGraw-Hill Book Company, Inc., New York, N. Y., 1949), National Nuclear Energy Series, Plutonium Project Record, Vol. 14B, p. 1226.

37. Radiation Counter Laboratories, Skokie, Illinois.

38. G. H. Higgins, Ph. D. thesis, University of California Radiation Laboratory Unclassified Report UCRL-1796 (June 1952).

39. E. K. Hulet, Ph. D. thesis, University of California Radiation Laboratory Unclassified Report UCRL-2283 (July 1953).

40. A. Ghiorso, unpublished data (1954).

41. H. P. Robinson and E. G. Potter, private communication (1953).

42. W. E. Nervik and P. C. Stevenson, Nucleonics 10, 18 (1952).

43. L. R. Zumwalt, U. S. Atomic Energy Commission Declassified Document MDDC-1346 (September 18, 1947).

44. R. G. Baker and L. Katz, Nucleonics, 11, 14 (1953).

45. D. W. Osborne, R. C. Thompson, Q. Van Winkle, "The Transuranium Elements: Research Papers," (McGraw-Hill Book Company, Inc., New York, N. Y., 1949), National Nuclear Energy Series, Plutonium Project Record, Vol. 14B, p. 1397.

46. E. K. Hulet, unpublished data (1953).

47. R. M. Lessler, unpublished data (1954).

48. A. Ghiorso, G. B. Rossi, B. G. Harvey, and S. G. Thompson, Phys. Rev. 93, 257 (1954).

49. J. W. Cobble, private communication (1954).

50. F. Asaro, private communication (1954).

51. H. Jaffe, private communication (1954).

52. P. M. McLaughlin and G. D. O'Kelley, California Research and Development Company Report MTA-40 (1953).

53. J. D. Knight, M. E. Bunker, B. Warren, and J. W. Starner, Phys. Rev. 91, 889 (August 15, 1953).

54. H. Slätis, J. O. Rasmussen, Jr., and H. Atterling, ibid., 93, 646 (1954).

55. R. W. Hoff, Ph. D. thesis, University of California Radiation Laboratory Unclassified Report UCRL-2325 (September 1953).

Section IV

1. G. Gamow, Zeits. f. Phys. 51, 204 (1928); "Structure of Atomic Nuclei and Nuclear Transformations," Oxford University Press, London, 1937; E. U. Condon and R. W. Gurney, Phys. Rev. 33, 127 (1929); H. A. Bethe, Revs. Modern Phys. 9, 121 (1937); M. A. Preston, Phys. Rev. 71, 865 (1947).

2. E. Fermi, Z. Phys. 88, 161 (1934); H. A. Bethe and R. F. Bacher, Revs. Modern Phys. 8, 82 (1936); G. Gamow and E. Teller, Phys. Rev. 49, 895 (1936).

3. R.E. Marshak, ibid., 61, 431 (1942).

4. N. Bohr and J A. Wheeler, ibid., 56, 426 (1939).

5. E. Fermi, "Nuclear Physics," notes by J. Orear, A. H. Rosenfeld, and R. A. Schluter, University of Chicago Press, Chicago, Illinois, 1949.

6. N. Metropolis and G. Reitwiesner, Atomic Energy Commission Document NP-1980 (1950).

7. W. Heisenberg, Z. Physik, 78, 156 (1932).

8. G. Gamow, ibid., 89, 592 (1934).

9. I. Perlman, A. Ghiorso, and G. T. Seaborg, Phys. Rev. 77, 26 (1950).

10. G. S. Stanford, H. E. Duckworth, B. G. Hogg, and J. S. Geiger, ibid., 85, 1039 (1952).

11. H. Palevsky and A. O. Hanson, ibid., 79, 242 (1950).

12. J. Schintlmeister, Wien. Chem. Zeits. 46, 106 (1943).

13. K. Way and W. Wood, Phys. Rev. (to be published).

14. H. E. Suess and J. H. D. Jensen, Arkiv för Fysik 3, 577 (1951).

15. R. A. Brightsen, M.S. thesis, Massachusetts Institute of Technology, Cambridge, Massachusetts (1950).

16. C. D. Coryell, R. A. Brightsen, and A. C. Pappas, Phys. Rev. 85, 732 (1952).

17. T. P. Kohman, ibid., 530.

18. C. D. Coryell, Ann. Rev. Nuclear Sci. 2, 305 (1953).

19. N. Feather, Phil. Mag. 43, 133 (1952); Proc. Roy. Soc. (Edinburgh) (A) 63, 242 (1952).

20. J. A. Harvey, Phys. Rev. 81, 353 (1951); Can. J. Phys. 31, 278 (1953).

21. J. R. Huizenga and L. B. Magnusson, Argonne National Laboratory Unclassified Report ANL-5158 (November 1953).

22. A. H. Wapstra, Physica 17, 628 (1951).

23. A. H. Wapstra, Ph. D. thesis, University of Amsterdam, published by G. Van Soest, Amsterdam, 1953.

24. V. A. Kravtsov, Dablay Academy Nauk SSR, 78, 43 (1951).

25. S. Sengupta, Phys. Rev. 87, 1136 (1952).

26. A. R. Edmonds, Proc. Phys. Soc. (London) 66, 796 (1953).

27. B. Karlick, Ariz. Akad. Wiss. Wien. 217 (1953).

28. B. C. Hogg and H. E. Duckworth, Phys. Rev. 91, 1289 (1953); Can. J. Phys. 32, 65 (1954).

29. W. W. Meinke, A. Ghiorso, and G. T. Seaborg, Phys. Rev. 75, 314 (1949).

30. Ibid., 81, 782 (1951).

31. W. W. Meinke and G. T. Seaborg, ibid., 78, 475 (1950).

32. S. G. Thompson, A. Ghiorso, B. G. Harvey, and G. R. Choppin, ibid., 93, 908 (1954).

33. I. Perlman, A. Ghiorso, and G. T. Seaborg, ibid., 74, 1730 (1948).

34. Ibid., 75, 1096 (1949).

35. S. G. Thompson, ibid., 76, 319 (1949).

36. R. W. Hoff, Ph. D. thesis, University of California Radiation Laboratory Unclassified Report UCRL-2325 (September 1953).

37. G. T. Seaborg, Third Annual Lecture Series of Phi Lambda Upsilon, Ohio State University (March 1952).

38. B. G. Harvey, unpublished data (1953).

39. G. T. Seaborg, Phys. Rev. 88, 1429 (1952).

40. J. R. Huizenga and R. B. Duffield, ibid., 88, 959 (1952).

41. J. M. Hollander, I. Perlman, and G. T. Seaborg, Revs. Modern Phys. 25, 469 (1953).

42. The alpha disintegration energy for the 8.776 Mev alpha particle listed in the Table of Isotopes is in error by one kev.

43. G. Bastin-Scoffier, J. Santana-Dionisio, Compt. rend. 236, 1016 (1953).

44. L. M. Slater, F. Asaro, and I. Perlman, unpublished data (1953).

45. B. G. Harvey, unpublished data (1953).

46. T. O. Passell, unpublished data (1954).

47. See Section III, this paper.

48. J. D. Knight, M. E Bunker, B. Warren, and J. W. Starner, Phys. Rev. 91, 889 (1953).

49. A. Ghiorso, S. G. Thompson, G. R. Choppin, and B. G. Harvey, to be published, Phys. Rev. (May 15, 1954).

50. A. Ghiorso, G. B. Rossi, B. G. Harvey, and S. G. Thompson, Phys. Rev. 93, 257 (1954).

51. S. G. Thompson, A. Ghiorso, B. G. Harvey, and G. R. Choppin, ibid., 908.

52. F. Wagner, Jr., M. S. Freedman, D. W. Engelkemeier, and J. R. Huizenga, ibid., 89, 502 (1953).

53. F. Asaro, Ph. D. thesis, University of California Radiation Laboratory Unclassified Report UCRL-2180 (June 1953).

54. A. Ghiorso, S. G. Thompson, G. R. Choppin, and B. G. Harvey, unpublished data (1954).

55. G. R. Choppin, S. G. Thompson, A Ghiorso, and B. G. Harvey, to be published, Phys. Rev. (May 15, 1954).

56. E. E. Berlovich, Izvest. Akad. Nauk. Ser. Fiz. SSR 16, 314 (1953).

57. O. P. Hok and G. J. Sizoo, Physica 19, 1208 (1953).

58. E. F. De Haan, G. J. Sizoo, and P. Kramer, ibid., 1205.

59. The isomeric transition energy of Pa^{234m} was calculated to be 0.28 Mev by subtraction of the 2.03 Mev Pa^{234} decay energy

from Ref. 57 from the 2.31 Mev beta energy of Pa^{234m} from Ref. 58.

60. The value 8.64 corresponding to the alpha particle energy listed first in the Table of Isotopes, which is the standard for Asaro's measurement, would have been better to use.

61. E. K. Hyde, unpublished data (1954).

62. J. P. Butler and J. S. Adam, Phys. Rev. 91, 1219 (1953).

63. D. W. Engelkemeier, P. R. Fields, J. R. Huizenga, ibid., 90, 6 (1953).

64. M. H. Studier and E. K. Hyde, ibid., 74, 591 (1948).

65. W. A. Jenkins and G. T. Seaborg, ibid., 85, 758 (1952).

66. G. T. Seaborg and J. J. Katz, "The Actinide Elements," (McGraw-Hill Book Company, Inc., New York, N. Y., 1954), National Nuclear Energy Series, Plutonium Project Record, Vol. 14A.

67. G. T. Seaborg, Phys. Rev. 92, 1074 (1954).

68. G. H. Higgins, Ph. D. thesis, University of California Radiation Laboratory Unclassified Report UCRL-1796 (June 1952).

69. E. K. Hulet, Ph. D. thesis, University of California Radiation Laboratory Unclassified Report UCRL-2283 (July 1953).

70. P. H. Stoker, M. Heershap, and O. P. Hok, Physica, 19, 433 (1953).

71. A. Ghiorso, S. G. Thompson, G. H. Higgins, B. G. Harvey, and G. T. Seaborg, to be published.

72. H. Faraggi and A. Berthelot, Compt. rend. 232, 2093 (1951).

73. W. Riezler, W. Porschen, Z. Naturforsch, 7a, 634 (1952).

74. E. P. Hincks and C. H. Millar, Abstract 106, June Meeting, Roy. Soc. (Canada) (1952).

75. P. I. Richards, E. E. Hays, and S. A. Goudsmit, Phys. Rev. 85, 630 (1952).

76. B. B. Kinsey, G. A. Bartholomew, and W. H. Walker, ibid., 82, 380 (1951).

77. J. A. Harvey, ibid., 81, 353.

78. F. Ajzenberg and T. Lauritsen, Revs. Modern Phys. 24, 321 (1952).

79. J. W. DuMond and E. R. Cohen, ibid., 25, 691 (1953).

80. G. S. Stanford, H. E Duckworth, B. C. Hogg, and J. S. Geiger, Phys. Rev. 85, 1039 (1952).

81. R. W. Parsons and C. H. Collie, Proc. Phys. Soc. (London) 63, 839 (1950).

82. R. W. Parsons, D. J. Lees, and C. H. Collie, ibid., 915.

83. J. McEhinney, A. O. Hanson, R. A. Becker, R. B. Duffield, and B. C. Diven, Phys. Rev. 75, 542 (1949).

84. A. O. Hanson, R. B. Duffield, B. C. Diven, and H. Palevsky, ibid., 76, 578.

85. H. Palevsky and A. O. Hanson, ibid., 79, 242 (1950).

86. R. Sher, J. Halpern, and A. K. Mann, ibid., 84, 387 (1951).

87. J. R. Huizenga, L. B. Magnusson, M. S. Freedman, and F. Wagner, ibid., 1264.

88. J. A. Harvey, private communication to A. H. Wapstra, Physica, 17, 628 (1951).

89. A. H. Wapstra, Phys. Rev. 86, 562 (1952).

90. M. O. Stern, Revs. Modern Phys. 21, 316 (1949).

91. E. Wichers, J. Am. Chem. Soc. 74, 2447 (1952).

92. C. F. von Weizsäcker, Z. Physik, 96, 431 (1935).

93. M. G. Mayer, Phys. Rev. 75, 1969 (1949); ibid., 78, 1622 (1950).

94. R. Bouchez, J. Robert, and J. Tobailem, Institute of Radium Curie Laboratory Report (January 1953).

95. E. Glueckauf, Proc. Phys. Soc. (London) 61, 21 (1948).

96. I. Perlman and T. J. Ypsilantis, Phys. Rev. 79, 30 (1950).

97. F. Asaro and J. Hummel, unpublished data (1954).

98. B. W. Sargent, Proc. Roy. Soc. (London) 139A, 659 (1933).

99. M. G. Mayer, S. A. Moszkowski, and L. W. Nordheim, Revs. Modern Phys. 23, 316 (1951); ibid., 322.

100. S. A. Moszkowski, Phys. Rev. 82, 35 (1951).

101. N. Feather, Physica, 18, 1023 (1952).